STRUCTURAL, FUNCTIONAL AND EVOLUTIONARY

STUDIES ON PROLYL-HYDROXYLASES

A thesis submitted to the Board of the Faculty of Physical Sciences of the University of Oxford in partial fulfilment of the requirements for the degree of Doctor of Philosophy

John S. Scotti
The Queen's College, Oxford
Trinity Term, 2014

ABSTRACT

John S. Scotti D. Phil
The Queen's College Trinity Term, 2014

Structural, Functional and Evolutionary Studies on Prolyl-Hydroxylases

The role of prolyl-hydroxylation was first identified in collagen, wherein hydroxyproline was found to stabilise the collagen triple helix. In the 1960s, the presence of hydroxyproline in collagen was found to be a result of enzyme catalysed protein modification. An enzyme, now known as collagen prolyl-4-hydroxylase (CP4H), was found to be completely dependent on Fe(II), 2-oxoglutarate (2OG) and molecular oxygen for catalysis, and was the inaugural member of enzyme family known as the Fe(II) and 2OG-dependent oxygenases (2OG oxygenases), the members of which have since expanded dramatically – more than 60 2OG oxygenases are predicted to exist in humans alone.

It was not until the 21st century that hydroxyproline was found to play roles in human biology beyond its well-characterised role in collagen stabilisation. In animals, cells adapt to low oxygen conditions (hypoxia) via the upregulation of hundreds of target genes as governed by the hypoxia-inducible transcription factor (HIF). The mammalian hypoxic sensing system was discovered to be regulated by a conserved family of hypoxia-inducible factor prolyl-hydroxylases (PHDs or EGLNs), which catalyse the prolyl-4-hydroxylation of a conserved proline residue in HIF-α under normoxic conditions, so targeting HIF-α for proteasomal degradation via the von Hippel-Lindau (pVHL) E3 ubiquitin ligase pathway. As a result, the PHDs are current therapeutic targets for the treatment of anemia and ischemia-related diseases. Thus, hydroxyproline also plays a critical role in mammalian oxygen sensing. However, the discovery also raised the question of the evolutionary origin of these enzymes and what roles, if any, they may play in other organisms.

This thesis begins by describing the identification and biochemical characterisation of the first homologue of the human PHDs in prokaryotes, specifically, in *Pseudomonas* species, which contains pathogens such as *P. aeruginosa*. *Pseudomonas* PHD (PPHD) was discovered to catalyse the prolyl-hydroxylation of a conserved region of elongation factor Tu (EF-Tu), a translational GTPase universally conserved in prokaryotes and known for its critical role in bacterial translation. A crystal structure of PPHD, the first of a prokaryotic prolyl-hydroxylase, was then determined, revealing a striking structural homology of PPHD to the human PHDs. The further determination of crystal structures of *Pseudomonas* EF-Tu and a PPHD:EF-Tu protein-protein complex, the first of any 2OG oxygenase in complex with its full-length protein substrate, provides important insights into the substrate recognition mechanisms of both the CP4Hs and the PHDs and reveals an evolutionarily conserved pathway of substrate recognition that extends to prokaryotes and will be useful in the design of selective inhibitors of the PHDs.

Differences were investigated between the PHDs and a recently discovered subfamily of eukaryotic prolyl-3-hydroxylases, which catalyse the hydroxylation of a conserved proline residue in the small ribosomal subunit S23 (RPS23) and have been implicated in translation accuracy and the stress response. Crystal structures of the RPS23 hydroxylases human OGFOD1 and yeast Tpa1 in complex with 2OG-mimetic inhibitors provide insight into their evolutionary origins. Analyses of the structures will be useful for targeting either OGFOD1 or the PHDs for human therapy.

The thesis then describes work on human CP4H, a 240 kDa $\alpha_2\beta_2$ heterotetramer. A novel expression and purification protocol is described for the CP4H complex in addition to the first known reports of its crystallisation and diffraction. Further, the foundations of a high-throughput inhibition assay of the human CP4Hs is presented and will be of immediate interest for assaying inhibitors of the human PHDs in clinical trials, some of which are also predicted to inhibit the CP4Hs.

In closing, the thesis attempts to synthesise the results presented in order to provide further insight into the question of the ancestral origins of the prolyl-hydroxylases, a family of enzymes whose range of functions and biological roles likely will continue to expand.

Acknowledgments

First and foremost, I would like to thank my supervisor, Professor Christopher J. Schofield, for giving me the wonderful opportunity to pursue a D.Phil in his laboratory and for his guidance and ideas over the years.

I would also like to thank the following people for their greatly appreciated help and contributions: Dr. Wei Ge, for introducing me to the world of experimental biochemistry and for mentoring me those first few months; Dr. Armin Thalhammer, for his ideas and assistance with the functional aspect of my project; Dr. Mukram Mackeen and Dr. Lingzhi Gong, for explaining to me the intricacies of MS/MS; Dr. Michael McDonough, for teaching me all there is to know about X-ray crystallography and for being an amazing mentor; Dr. Rok Sekirnik, for welcoming me to the laboratory and for all those lunches at St. Catherine's College; Dr. Wei Shen Aik, for his willingness to undertake the CP4H project with me and for cheering me up when I needed it; Dr. Hwanho Choi and Dr. Shoichiro Horita, for helping me when I needed it and for all the great conversations over tea; Herminio Manso Jubier, for helping my experiments go quickly; Wendy Sobey and Dr. Adam Hardy, for generally helping all my experiments go more smoothly and providing a great work environment; and all the members of the CJS group, past and present, for all their help and support during my D.Phil.

I would like to thank The Rhodes Trust and all members of Rhodes House for providing me the opportunity of a lifetime, for being such an integral part of my Oxford experience, and for always being there for support when I needed it.

Finally, and most importantly, I would like to express my most sincere thanks to my wife, Lisa, and our families for their constant loving support, without which I would not be the person I am today.

Table of contents

Abbreviations

2,4-PDCA	pyridine 2,4-dicarboxylic acid
2OG	2-oxoglutarate
aa-tRNA	aminoacyl transfer ribonucleic acid
ADP	adenosine diphosphate
ASC	sodium ascorbate
ATP	adenosine triphosphate
bHLH	basic helix-loop-helix
Bis-tris	2-[bis(2-hydroxyethyl)amino]-2-(hydroxymethyl)-1,3-propanediol
BSA	bovine serum albumin
CAPS	3-(cyclohexylamino)-1-propanesulfonic acid
CAPSO	2-hydroxypropane-3-(cyclohexylamino)-1-sulfonic acid
CBP	cAMP response element binding protein
CF	cystic fibrosis
CHES	2-(cyclohexylamino)ethanesulfonic acid
CODD	*C*-terminal oxygen degradation domain
CP3H	collagen prolyl-3-hydroxylase
CP4H	collagen prolyl-4-hydroxylase
CPH	collagen prolyl hydroxylase
CrP4H	*Chlamydomonas reinhardtii* prolyl-4-hydroxylase
Cul2	cullin box 2 protein
CV	column volume
DLS	dynamic light scattering
DMOG	dimethyloxalylglycine
DNA	deoxyribonucleic acid
DSBH	double-stranded β-helix
DSF (T_m shift)	differential scanning fluorimetry
DTT	dithiothreitol
EDTA	ethylenediaminetetraacetic acid
EF-Ts	elongation factor Ts
EF-Tu	elongation factor Tu
EGLN	egg-laying-defective nine (otherwise known as the PHDs)
ER	endoplasmic reticulum
FIH	factor-inhibiting hypoxia-inducible factor
FTO	fat mass and obesity-associated protein
GDP	guanosine diphosphate
GTP	guanosine triphosphate
HEPES	2-[4-(2-hydroxyethyl)piperazin-1-yl]ethanesulfonic acid
HIF	hypoxia-inducible factor
Hyp	hydroxyproline
IC50	half maximal inhibitory concentration
IPTG	isopropyl β-d-1-thiogalactopyranoside
kDa	kilodalton
LC-MS	liquid chromatography mass spectrometry
LC-MS/MS	liquid chromatography tandem mass spectrometry
MALDI-TOF-MS	matrix -assisted laser desorption/ionization time-of-flight mass spectrometry
MCS	multiple cloning site
MES	2-(*N*-morpholino)ethanesulfonic acid
MINA53	MYC-induced nuclear antigen 53
MOPSO	2-hydroxy-3-morpholinopropanesulfonic acid

mRNA	messenger RNA
MS	mass spectrometry
NMR	nuclear magnetic resonance
NO66	nucleolar protein 66
NODD	*N*-terminal oxygen degradation domain
NOG	*N*-oxalylglycine
ODD	oxygen degradation domain
OE-PCR	overlap extension-polymerase chain reaction
Ofd1	*Schizosaccharomyces pombe* 2-oxoglutarate and iron-dependent oxygenase domain-containing protein 1
OGFOD1	2-oxoglutarate and iron-dependent oxygenase domain containing 1
otOGFOD1	*Ostreococcus tauri* 2-oxoglutarate and iron-dependent oxygenase domain-containing protein 1
P4H	prolyl-4-hydroxylase
PAGE	polyacrylamide gel electrophoresis
PAS	**P**eriod circadian protein, **A**ryl hydrocarbon receptor nuclear translocator protein, **S**ingle-minded protein domain
PCR	polymerase chain reaction
PDI	protein disulfide isomerase
PHD	prolyl-hydroxylase domain-containing protein
PHD2	prolyl-hydroxylase domain-containing protein 2
PIPES	piperazine-1,4-bis(2-ethanesulfonic acid)
PPHD	*Pseudomonas* prolyl-hydroxylase domain-containing protein
PPP	synthetic polypeptide: H_2N-IVEFDKIDSAPEEKARGITI-$CONH_2$
PSB	peptide-substrate-binding domain
pVHL	von Hippel-Lindau protein
qRT-PCR	quantitative real-time polymerase chain reaction
Rbx1	RING box protein 1
RNA	ribonucleic acid
ROS	reactive oxygen species
ROX	ribosomal oxygenases
RPS23	ribosomal protein S23
rRNA	ribosomal RNA
SAD	single-wavelength anomalous dispersion
SAXS	small-angle X-ray scattering
SDS-PAGE	sodium dodecyl sulfate polyacrylamide gel electrophoresis
SeMet	selenomethionine
Skp1	component of the SCF (Skp1-cullin-F box protein complex) ubiquitin ligases
Sud1	Sudestada1
TCEP	tris(2-carboxyethyl)phosphine
TES	2-[[1,3-dihydroxy-2-(hydroxymethyl)propan-2-yl]amino]ethanesulfonic acid
TMED	tetramethylethylenediamine
Tpa1	termination and polyadenylation associated protein 1
Tris	2-amino-2-hydroxymethyl-propane-1,3-diol
tRNA	transfer RNA
VEGF	vascular endothelial growth factor
X-gal	5-bromo-4-chloro-indolyl-β-d-galactopyranoside

Standard abbreviations for amino acids are used throughout this thesis.

1 Introduction

1.1 The collagen prolyl-4-hydroxylases

1.1.1 Scurvy, collagen, and the discovery of 2OG oxygenases

First identified by Hippocrates (c. 400 BC) and prevalent among sailors well into the early 20th century, scurvy is a potentially fatal disease caused by defective collagen fibrillogenesis, which produces characteristic symptoms including skin spots and abnormal bleeding (*1*). In 1747, in what has been referred to as the first clinical trial, Scottish physician James Lind conclusively showed that scurvy could be cured by the administration of citrus fruits (*2*). However, it was not until 1927 that Hungarian biochemist Albert Szent-Györgyi isolated a compound called 'hexuronic acid', which was later shown to have anti-scorbutic properties, and therefore named ascorbic acid, or vitamin C (*1*). At the time, the molecular mechanism underlying the anti-scorbutic properties of ascorbic acid was unknown (*1*).

Collagen is subjected to various post-translational modifications including lysyl-hydroxylation, prolyl-3- and prolyl-4-hydroxylation (*3*). In 1955, Ramachandran and Kartha used X-ray diffraction data to determine the collagen triple helical structure, prompting numerous studies on the nature of collagen stability (*4*). The critical role of 4-hydroxyproline was well-known [typically a rare amino acid yet composes ~10% of the residues in mammalian collagen (*5*)] in stabilising the collagen triple helix, in that unhydroxylated pro-collagen chains do not form collagen fibrils *in vivo* (*6*). Initially, the 4-hydroxyl group was thought to form hydrogen bonds with the carbonyl oxygen of a neighbouring

chain. A more recent high-resolution X-ray crystal structure of a collagen-like peptide revealed that the hydroxyl groups of 4-hydroxyprolines are positioned to form hydrogen bonds to water molecules in a closed cylinder of hydration around the peptide triple helix (*7*). However, neither of these theories was revealed to be correct. Further studies on fluoroproline containing peptides revealed that 4-hydroxyproline stabilises human collagen via operation of the gauche effect, in that the electron-withdrawing hydroxyl group preorganises the pyrrolidine ring pucker thereby resulting in adoption of torsion angles characteristic of a collagen triple helix (*8*).

Shortly after Ramachandran related his findings, in 1967, Hutton et al. reported that the enzyme-catalysed formation of 4-hydroxyproline in collagen was stimulated by ascorbate (*9*), directly linking the anti-scorbutic properties of vitamin C to the defective collagen fibrillogenesis observed in scurvy patients. In addition to ascorbate, the enzyme, called collagen prolyl-4-hydroxylase (CP4H), was found to be dependent on Fe(II), 2-oxoglutarate (2OG), and molecular oxygen (Figure 1.1).

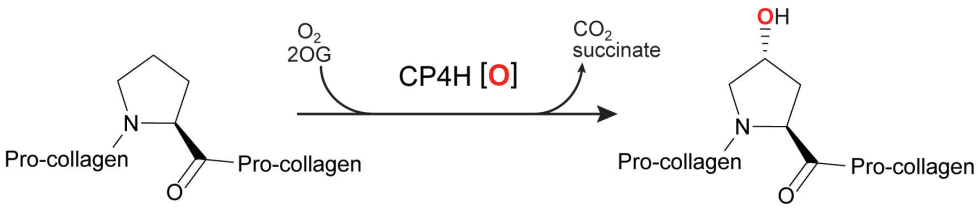

Figure 1.1. CP4H catalyses the prolyl-4-hydroxylation of collagen substrates. CP4H couples the oxidation of C-4 of prolyl residues to the oxidative decarboxylation of 2OG into succinate.

1.1.2 CP4H is a member of the 2OG oxygenase superfamily

CP4H represents the inaugural member in what has since been revealed to be a large superfamily of enzymes known as the 2OG oxygenases, of which

there are more than 60 members in humans that catalyse a range of reactions including desaturation, epimerisation, ring closure, and chlorination (*10, 11*). All characterised 2OG oxygenases are characterised by a complete dependence on Fe(II), 2OG, and molecular oxygen for catalysis (Figure 1.2). Structural studies have shown that 2OG coordinates Fe(II) in a bidentate manner through its 1-carboxylate and 2-oxo groups (*12*). 2OG oxygenase catalysis is proposed, at least in many cases, to proceed through a highly oxidising Fe(IV)=O (oxo) intermediate, which has been trapped and characterised spectroscopically (*12-15*). Although the exact role(s) of ascorbate in 2OG oxygenase catalysis is unknown, it is thought to reinitiate uncoupled reaction cycles via reduction to Fe(II), a proposal consistent with data suggesting ascorbate can be replaced by other reducing agents, such as β-mercaptoethanol to varying degrees of success (*9, 16*).

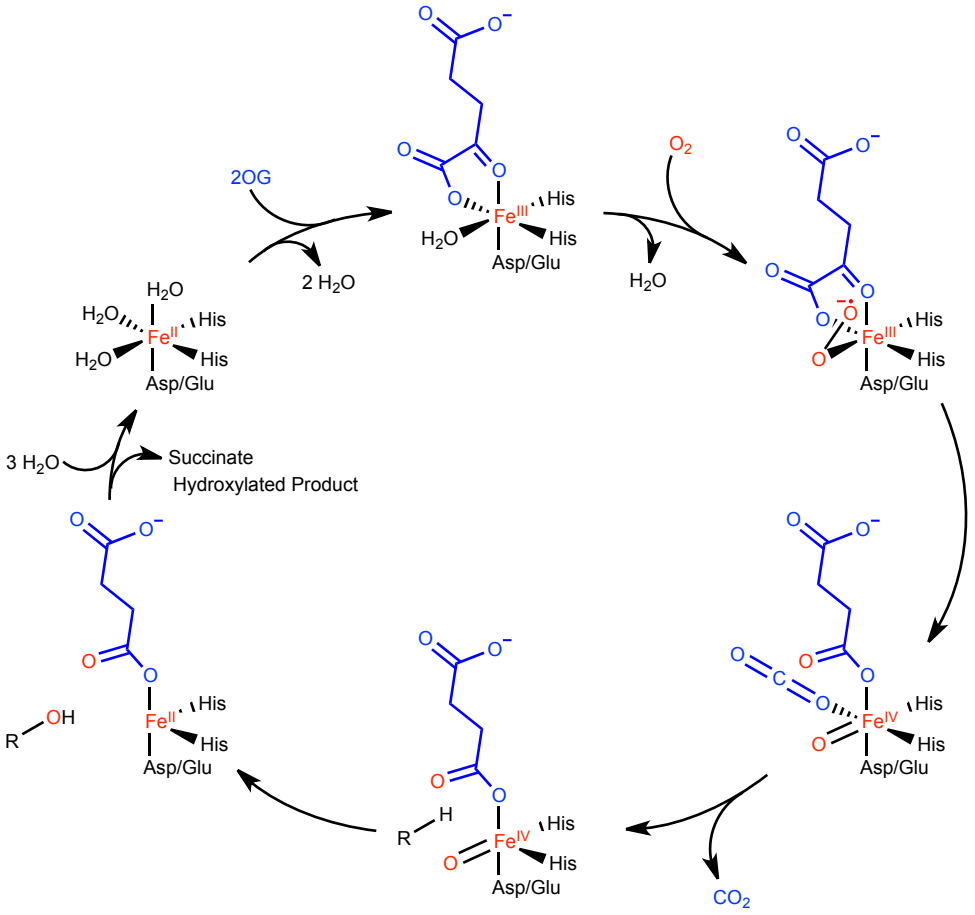

Figure 1.2. Outline of proposed catalytic mechanism for 2OG oxygenases.

1.1.3 CP4H is an $\alpha_2\beta_2$ heterotetramer

Human CP4H catalyses the hydroxylation of proline residues in X-Pro-Gly repeats of collagen polypeptides (*6, 17*). Further studies led to its identification as a 240 kDa heterotetrameric enzyme composed of two α and two β subunits (Figure 1.3)(*6*). Three isoforms of the α subunit, α(I), α(II), and α(III) exist in humans (*6, 18, 19*). Coexpression in insect cells provides strong evidence against the formation of mixed tetramers (i.e. $\alpha(I)\alpha(II)\beta_2$) (*18*). The processed α(I) subunit [$\alpha(I)_2\beta_2$ tetramer henceforth referred to as CP4H in this thesis] consists of 517 residues and is synthesised in a form containing a *N*-terminal signal

peptide of 17 residues that targets CP4H to the lumen of the endoplasmic reticulum (ER)(*20*).

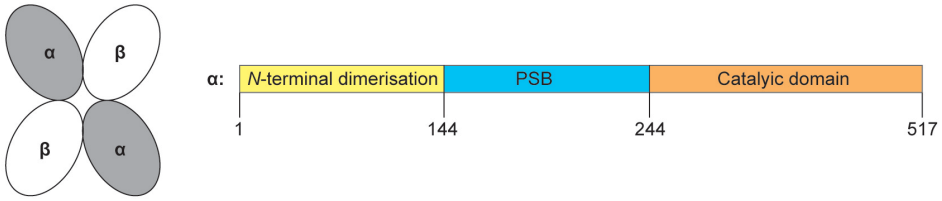

Figure 1.3. CP4H is an $\alpha_2\beta_2$ heterotetramer. The α subunit is composed of three domains: the *N*-terminal dimerisation domain, the PSB, and the catalytic domain, whereas the β subunit is identical to the polypeptide protein disulfide isomerase.

The α subunit contains the catalytic machinery and is itself composed of 3 domains: a *N*-terminal dimerisation domain (residues 1-144), a peptide-substrate-binding-domain (PSB)(residues 145-244)(*21, 22*), and a *C*-terminal 2OG oxygenase catalytic domain (residues 245-517)(Figure 1.3).

The β subunit is identical to protein disulfide isomerase (PDI) (*23*), a 55 kDa multifunctional enzyme important in many cellular processes, including lipid homeostasis, neurodegeneration, and virus entry (*24, 25*). PDI is a thiol-disulfide oxidoreductase located in the ER that catalyses the oxidation, reduction, and isomerisation of disulfide bonds and, more generally, assists in the correct folding of proteins. At least 21 PDI family members exist in humans (*26*), possibly having evolved to facilitate proper folding of a number of different proteins. The exact role of PDI in CP4H tetramer assembly is unknown, yet studies have revealed it to be necessary in preventing aggregation of the α subunit and maintaining its ER localisation (*27, 28*). Crystal structures of human PDI in its oxidised and reduced forms reveal it to contain four thioredoxin domains *a*, *b*, *b'*, and *a'* (in that order from *N* to *C*) of which the *a* and *a'* domains

are catalytically active and the *b* and *b'* domains contain a hydrophobic substrate binding pocket (Figure 1.4)(*29*). The PDI active site typically contains a CGHC motif positioned to form a disulfide bond that catalyses disulfide exchange with its variety of substrates.

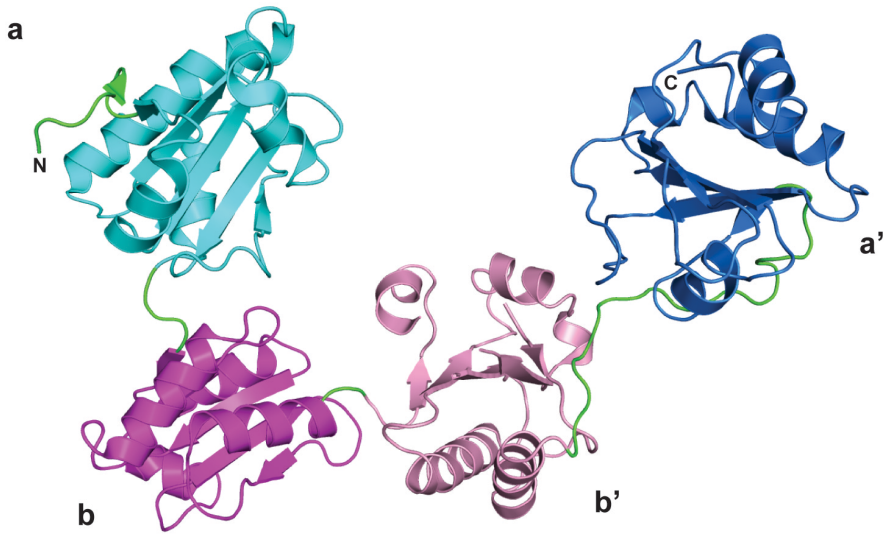

Figure 1.4. View from a crystal structure of the human PDI in its oxidised form. The structure consists of four thioredoxin domains in the following order: a (residues 26-133; cyan), b (residues 137-232; magenta), b' (residues 235-349; pink), and a' (residues 369-479; blue). Interdomain loops are coloured green. Domains a and a' each contain a CGHC motif. PDB ID: 4EL1 (*29*).

Despite decades of research, advances in the structural studies of mammalian collagen prolyl-4-hydroxylases have been slowed by difficulties inherent in their purification. *In vitro* assembly of the $\alpha_2\beta_2$ tetramer has remained unsuccessful. Initial successful attempts to produce an active CP4H $\alpha_2\beta_2$ heterotetramer involved coexpression of the α and β subunits in insect cells (*27, 30*) and yeast (*31*). In the last decade, however, successful expression of the CP4H tetramer in *E. coli* has been achieved through the use of the *E. coli* Origami 2 expression strain, which maintains an oxidising cytosolic environment due to

engineered mutations in both the thioredoxin reductase (*trxB*) and glutathione reductase (*gor*) genes (*32*).

Site-directed mutagenesis studies on human CP4H have shown that tetramer formation is, at least in part, mediated by two sets of intrachain disulfide bonds in the α subunit (Cys276:Cys293 and Cys486:Cys511) (*33, 34*). In addition, the α subunit also possesses two asparagine residues (Asn92 and Asn242) for the post-translational attachment of oligosaccharides (*34*). Although mutagenesis studies have shown these residues do not affect tetramer formation, the presence of disordered and heterogeneous post-translational modifications likely render crystallographic experiments on CP4H tetramer even more challenging.

As a result of the difficulty in producing homogeneous CP4H tetramer, no structures of the α subunit catalytic domain or the $\alpha_2\beta_2$ heterotetramer are available. However, a crystal structure of the *N*-terminal dimerisation domain and PSB of human CP4H in complex with collagen-like peptide substrate [$(PPG)_3$] has been reported (*35*). The overall structure resembles a Z-shape and reveals that dimerisation is indeed mediated by the *N* domain, in which an α-helical bundle (4 helices; α1-α4, residues 8-103) packs onto that of an adjacent domain to result in a dimerisation interface of 4,000 $Å^2$ (Figure 1.5*A*). The *N*-terminal dimerisation domain and PSB are connected by a linker region (residues 104-143) consisting of two α-helices (α5-α6) and a loop *C*-terminal to α6. The $(PPG)_3$ peptide binds to a groove in the PSB lined by 6 tyrosine residues (Tyr158, Tyr193, Tyr196, Tyr199, Tyr230, and Tyr233), the aromatic surface of which forms van der Waals interactions with prolyl residues in the collagen-like

peptide, and by Asn227, Phe231, and a salt bridge between Asp192 and Arg223 (Figure 1.5*B*).

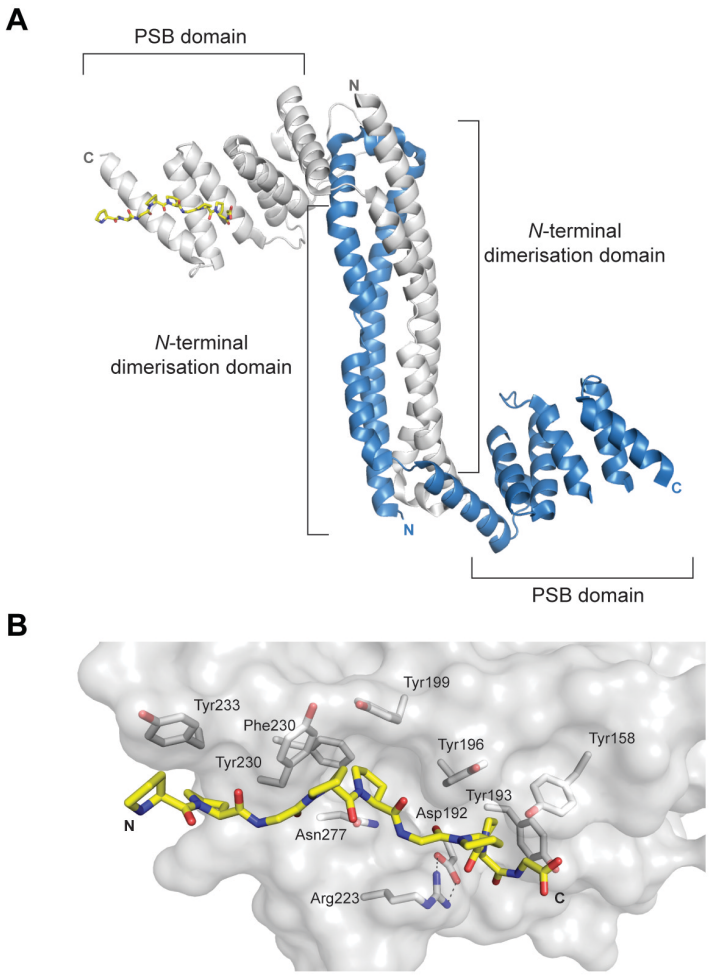

Figure 1.5. View from a crystal structure of the *N*-terminal dimerisation domain and PSB of human CP4H. (**A**) Overall structure (chain A, grey; chain B, blue) of the *N* domain and the PSB domain reveals that dimerisation is mediated by the α-helical bundle of the *N* domain and collagen-like peptide substrate [sequence: $(PPG)_3$] is bound to the PSB domain. (**B**) Close-up of the peptide binding site reveals a groove lined primarily by hydrophobic residues. PDB ID: 4BTA (*35*).

1.2 The role of prolyl-hydroxylation in mammalian oxygen sensing

1.2.1 Hypoxia-inducible factor and the hypoxic response

Recently, the roles for prolyl-hydroxylation have expanded beyond collagen stabilisation. Aerobic organisms have a constant and absolute requirement for oxygen for survival and have evolved complex respiratory and circulatory systems to ensure the sufficient delivery of oxygen to cells and tissues. Mammalian cells adapt to low oxygen levels (hypoxia) by upregulating a host of target genes, including those involved in angiogenesis [e.g. vascular endothelial growth factor (VEGF)], erythropoiesis (e.g. erythropoetin), and glucose metabolism [e.g. glucose transporters 1 and 3 (GLUT1 and GLUT3, respectively)], and glycolytic enzymes aldolase A and phosphoglycerate kinase 1, a conserved process mediated by a DNA-binding transcription factor called hypoxia-inducible factor (HIF)(*36, 37*). In its transcriptionally active form, HIF is a heterodimer composed of α and β subunits, both of which are basic helix-loop-helix PAS domain proteins (PAS domain: **P**eriod circadian protein, **A**ryl hydrocarbon receptor nuclear translocator protein, **S**ingle-minded protein domain) (*38*). The human genome contains three HIF-α genes, HIF-1α, HIF-2α, and HIF-3α, of which HIF-1α is the most thoroughly studied (*39*). HIF-β belongs to the family of aryl hydrocarbon receptor nuclear translocators (ARNTs) (*40*). In hypoxic conditions, HIF-1α dimerises with HIF-1β and translocates to the nucleus where it then recruits the p300/CBP (CBP: cAMP response element binding protein) coactivator proteins (*41-43*), which are also required for transcriptional activity of numerous different transcription factors including p53 (*44*), and upregulates a plethora of target genes in the hypoxic response (Figure 1.6).

In contrast, in well-oxygenated conditions (normoxia), an absence of intracellular HIF-1α levels (HIF-1β levels remain constitutive) results in its inability to recruit HIF-1β and form a transcriptionally active complex (*45*).

Subsequent studies revealed that HIF-1α was targeted for oxygen-dependent proteasomal degradation in normoxia by the von Hippel-Lindau tumour suppressor protein (pVHL) E3 ubiquitin ligase complex (*46-48*). Hereditary mutations in *VHL* can cause VHL disease, which is associated with increased risk of cancer characterised by highly vascular tumours that overproduce HIF target genes (*39*). pVHL binds HIF-1α in a complex of elongin B and elongin C proteins and targets HIF-1α for polyubiquitination with Cul2 (Cullin box 2) and Rbx1 (RING box protein 1) as part of an E3 ubiquitin ligase complex (Figure 1.6)(*49, 50*).

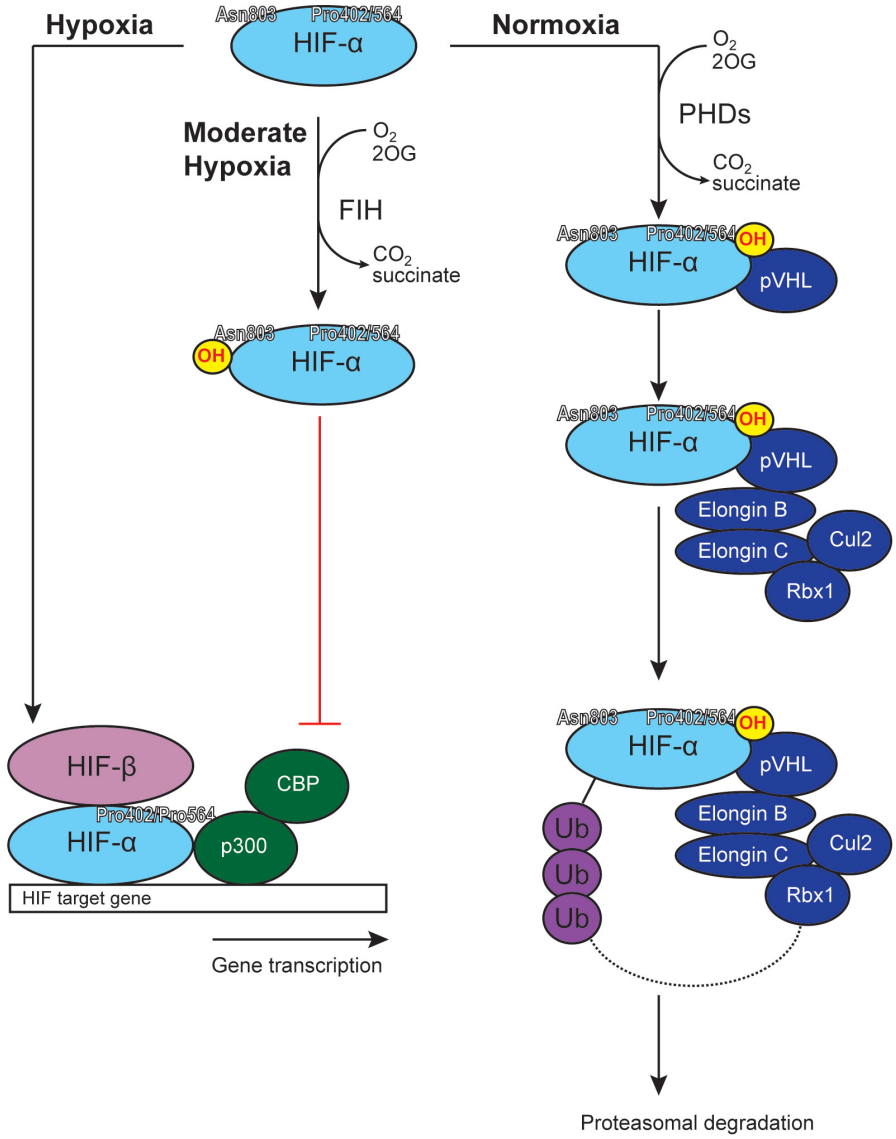

Figure 1.6. The human hypoxic response. In normoxia, HIF-α residues Pro402/Pro564 are prolyl-hydroxylated as catalysed by the PHDs, so signalling HIF-α for proteasomal degradation by the pVHL E3 ubiquitin ligase complex. In moderate hypoxia, FIH, which has a lower requirement for oxygen than the PHDs, hydroxylates HIF-α at a conserved asparagine residue, Asn803, introducing a steric clash and preventing HIF-α from associating with coactivator proteins p300/CBP. In hypoxia, HIF-α is not subject to oxygen-dependent post-translational modification and translocated to the nucleus where it dimerises with HIF-β and along with p300/CBP induces transcription of genes critical for the human hypoxic response.

1.2.2 The HIF prolyl-hydroxylases and metazoan oxygen sensing

Studies had shown that intracellular HIF-1α levels are low in normoxia and become elevated in hypoxia, but the exact mechanism by which high oxygen

levels result in the recruitment of pVHL and subsequent destruction of HIF-1α had yet to be determined. However, important observations remained unexplained: i) iron chelators or cobalt chloride stabilise HIF and result in transcriptional activation of its target genes (*51, 52*), and ii) pVHL only binds to HIF produced in oxygenated mammalian cells and not in *E. coli*. It was thus clear that pVHL recognition of HIF is due to a factor only present in mammalian cells that is both iron and oxygen dependent (*53, 54*).

The HIF prolyl-hydroxylases (PHDs or EGLNs) catalyse the *trans*-4 prolyl-hydroxylation of conserved proline residues, Pro402 and Pro564, in the HIF-1α *N*-terminal and *C*-terminal oxygen degradation domains (NODD and CODD, respectively)(*37, 53-55*). This post-translational modification alone is sufficient, at least under many conditions, to target HIF-1α for proteasomal degradation via the pVHL E3 ligase complex (Figure 1.6). The PHDs consist of three different enzymes in humans, PHD1, PHD2, and PHD3. PHD2 is primarily localised in the cytosol and PHD1 in the nucleus, yet PHD3 is found in both compartments (*56*). PHD1, PHD2, and PHD3 are composed of 407, 426, and 237 residues, respectively, and PHD2 has been shown to be the dominant enzyme (*57, 58*). PHD2 possesses a K_m for oxygen of ~200 μM, which renders PHD2 sensitive to changes in oxygen over a physiologically relevant range (*55, 59, 60*). Therefore, PHD2 acts as an oxygen sensor in human cells.

The PHDs, like the collagen prolyl-4-hydroxylases, are members of the Fe(II)- and 2OG-dependent oxygenase superfamily (*6*). Importantly, the PHDs and CP4Hs do not share similar substrates; CP4Hs do not catalyse the prolyl-hydroxylation of HIF-1α ODDs (*54*). Therefore, at the time of their discovery, the PHDs represented an unknown family of HIF-specific prolyl-4-hydroxylases (*57*).

1.2.3 Factor-inhibiting hypoxia-inducible factor

In addition to PHD-catalysed prolyl-hydroxylation, the ability of HIF-1α to initiate transcription is also governed by a pVHL-independent hydroxylation of an asparaginyl residue (Asn803) in the *C*-terminal transactivation domain (CTAD) as catalysed by factor-inhibiting hypoxia-inducible factor (FIH) (*41, 61, 62*). Unlike in the case of HIF-1α regulation by the PHDs, regulation by FIH is independent of pVHL. Hydroxylation at the β-carbon of Asn803 introduces a steric clash that prevents HIF-1α interaction with p300/CBP coactivator proteins (Figure 1.6)(*63, 64*). The catalytic properties of FIH are different from those of the PHDs, in that FIH is active at lower oxygen concentrations (*65*). Accordingly, FIH is predicted to provide a second layer of HIF-α regulation in moderate hypoxia (*37*).

1.2.4 Structural basis for oxygen-dependent HIF-1α binding to pVHL

Crystal structures of the VBC complex (pVHL, elongin B, elongin C) bound to hydroxylated HIF-1α CODD peptide revealed the structural basis for the oxygen-dependent mechanism of HIF-1α recognition by pVHL (*66, 67*). The structure showed that Hyp564 (hydroxyproline: Hyp) is buried in a cleft in the β domain of pVHL and makes several contacts with surrounding residues (Figure 1.7). The pyrrolidine ring is positioned in a hydrophobic core in pVHL and makes van der Waals contacts with Trp88, Tyr98, and Trp117. The hydroxyl group of Hyp564 is positioned to form two hydrogen bonds to the hydroxyl group of Ser111 and the Nδ His115. All five of the pVHL residues that contact Hyp564 have reported missense mutations in VHL disease (*68*). Further analyses revealed that the drastic difference in binding affinity (~1,000 fold) between

unhydroxylated and hydroxylated CODD amounts to 4 kcal mol^{-1}, which is roughly equivalent to two normal hydrogen bonds.

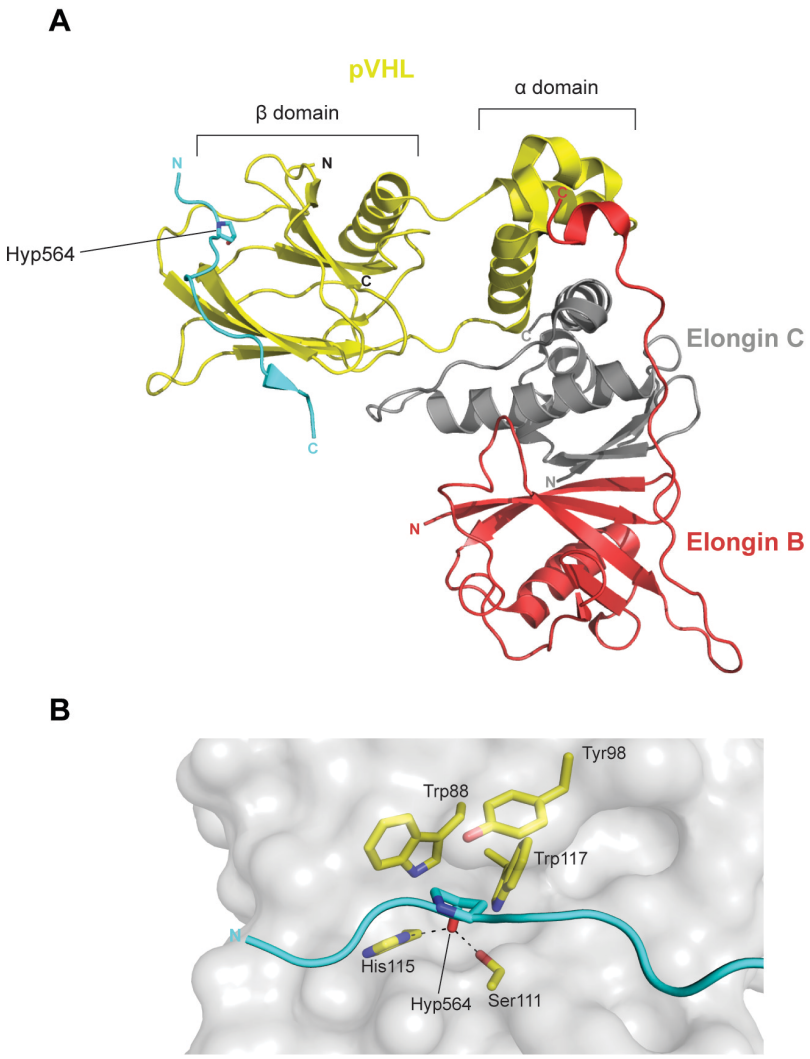

Figure 1.7. View from a crystal structure of the VBC complex bound to hydroxylated (Hyp564) HIF-1α CODD peptide. (**A**) HIF-1α CODD (residues 561-575 modelled in the structure) is bound to the β-domain of pVHL in the VBC complex, consisting of pVHL, elongin B, and elongin C. (**B**) Hyp564 is positioned in a hydrophobic cleft buried from solvent, making van der Waals contacts with Trp88, Trp117, Tyr98 and positioned to form hydrogen bonds to Ser111 and His115. PDB ID: 1LM8 (*66*).

Inspection of the *apo* (ligand-absent) structure of the VBC complex revealed the presence of a water molecule that forms hydrogen bonds to Ser111 and His115 (*69*). This water molecule is displaced by hydroxyproline in the

CODD-bound structure. Although unhydroxylated proline could fit into the hydroxyproline binding site, the displacement of bound water to pVHL would not be energetically balanced by the formation of two additional hydrogen bonds, rendering binding of unhydroxylated CODD to pVHL energetically unfavourable, and revealing the structural basis for a role of hydroxyproline in signalling (*67*).

1.2.5 PHD homologues in other organisms

The discovery of PHDs and their critical role in metazoan oxygen sensing prompted the search for PHD homologues in other organisms, especially those that lack HIF-α. A human HIF-α prolyl-4-hydroxylase homologue was identified in the slime-mould *Dictyostelium discoideum*, a soil amoeba and unicellular eukaryote (*70*). *D. discoideum* prolyl-4-hydroxylase (DdP4H) was found to hydroxylate Pro143 of Skp1, a component of the SCF (Skp1-cullin-F box protein complex) ubiquitin ligases, which are implicated in the ubiquitination of selected proteins for proteasomal degradation and resemble the VBC complex in humans (*39, 70, 71*). Like the PHDs, DdP4H was found to be dependent on molecular oxygen, 2OG, Fe(II), and ascorbate and to be inhibited by metal ions such as $CoCl_2$ (*70*).

In *D. discoideum*, prolyl-4-hydroxylation of Skp1 Pro143 does not target it for proteasomal degradation as does HIF-1α Pro564 hydroxylation. Rather, the Pro143 hydroxyl group presents a target for further post-translational elaboration via glycosylation by (Skp1 protein)-hydroxyproline α-*N*-acetyl-D-glucosaminyltransferase (GnT1) (*70*). Full development of *Dictyostelium* is regulated by molecular oxygen, requiring levels greater than 10% (*72*). Studies

have shown that *D. discoideum* prolyl-4-hydroxylase activity is critical for full development of *Dictyostelium* and that DdP4H knockout cells have a much higher oxygen requirement for development (*73*). The results reveal that PHD-like prolyl-4-hydroxylases exist in unicellular eukaryotes and provide support for the presence of oxygen sensing prolyl-4-hydroxylases in unicellular organisms.

1.3 Prolyl-hydroxylases as potential regulators of translation

1.3.1 Discovery of the RPS23 hydroxylases

Recent work has expanded the roles of prolyl-hydroxylases to include potential regulation of translation as well as transcription and collagen stabilisation. It has been reported that eukaryotic ribosomes undergo prolyl-hydroxylation at Pro62 (human numbering) of the small ribosomal subunit protein S23 (RPS23) as catalysed by 2OG- and Fe(II)-dependent oxygenase domain containing protein (OGFOD1) in humans, termination and polyadenylation protein 1 (Tpa1) in baker's yeast *Saccharomyces cerevisiae*, Sudestada1 (Sud1) in *Drosophila melanogaster*, 2OG- and Fe(II)-dependent oxygenase domain containing protein (Ofd1) in fission yeast *Schizosaccharomyces pombe*, and otOGFOD1 in the green algae *Ostreococcus tauri* (Figure 1.8)(*74-76*). Whereas OGFOD1 and Sud1 catalyse monohydroxylation, Tpa1, Ofd1, and otOGFOD1 were revealed to catalyse an unprecedented dihydroxylation likely at the C-3 and C-4 positions (*74-76*). Interestingly, and in contrast to HIF-α *trans*-4 prolyl-hydroxylation (*77*), OGFOD1 has been shown to catalyse the *trans*-3 prolyl-hydroxylation of RPS23 Pro62 (*74*).

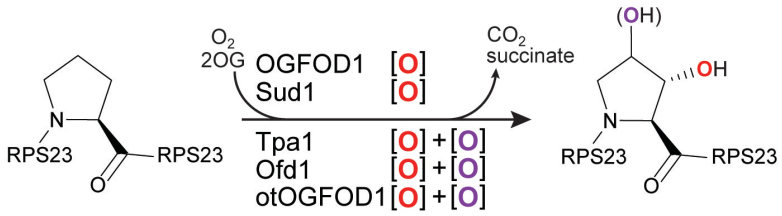

Figure 1.8. OGFOD1 and homologues catalyse the post-translational hydroxylation of a conserved Pro62 (human numbering) in RPS23 in eukaryotic ribosomes. OGFOD1 in humans and Sud1 in *D. melanogaster* catalyse monohydroxylation. Tpa1 in *S. cerevisiae*, Ofd1 in *S. pombe*, and otOGFOD1 in *O. tauri* catalyse 3,4-dihydroxylation.

Crystal structures of the ribosome reveal that the hydroxylated prolyl residue is located at the apex of a loop projecting into the mRNA-tRNA codon-anticodon recognition site, specifically at the third codon, otherwise known as the 'wobble' position as variation does not often alter the identity of the encoded amino acid (Figure 1.9)(*78*). Post-translational *trans*-3 prolyl-hydroxylation at this position may position the hydroxyl group to contact the phosphate backbone of 3' mRNA, and, therefore, may affect ribosomal processivity, translation rate, or translation accuracy.

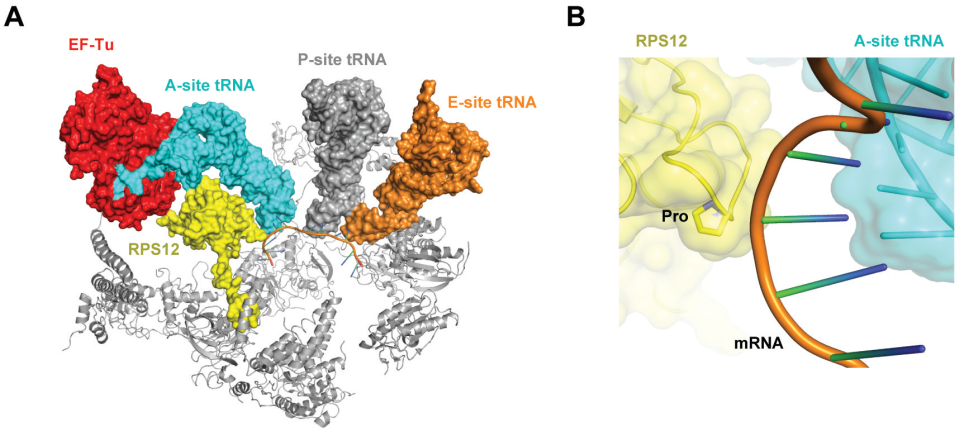

Figure 1.9. RPS23 is located at the heart of the ribosome. (**A**) View from the crystal structure of the *T. thermophilus* small ribosomal subunit bound to elongation factor Tu (EF-Tu) and tRNA reveals that RPS12 (prokaryotic homologue of RPS23) is positioned at the centre of the ribosome. (**B**) Pro62 (human numbering) is positioned at the apex of a loop adjacent to the mRNA-tRNA codon-anticodon recognition site. Ribosomal RNA is not shown. Except for RPS23, all ribosomal proteins are shown in grey. Note that this is a structure of the prokaryotic ribosome, which is not subject to hydroxylation.

1.3.2 Insights into the functional role of RPS23 hydroxylases

Although studies to elucidate the functional role of RPS23 prolyl-hydroxylation are ongoing, preliminary results suggest that OGFOD1 and homologues may play a role in the regulation of translation, among other cellular pathways. In *S. pombe*, Ofd1 has been implicated in the oxygen-dependent degradation of sterol regulatory element binding protein 1 (Sre1), which upregulates the expression of genes required for growth in low oxygen (*79, 80*). In *S. cerevisiae*, which does not contain a Sre1 homologue (*81*), *tpa1* deletion was found to affect translation termination up to ~10-fold in a sequence-dependent manner (*75*). In addition *tpa1* deletion has shown to result in increased stop-codon readthrough, mRNA half-lives, and poly(A) tail length (*82*). In *D. melanogaster*, Sud1 is involved in proper organ growth, as shown by RNAi-mediated knockdown of *sud1* (*76*). Finally, experiments on shRNA-mediated knockdown of *OGFOD1* in human cells have shown that OGFOD1 likely plays a role in stress granule formation and translational arrest (*74*). Taken together, the results reveal that the RPS23 prolyl-hydroxylases likely share a conserved role in the translation-mediated stress response, yet more biochemical evidence is needed to establish a connection, if any, between RPS23 hydroxylation and observed phenotypes.

1.4 Structural studies on prolyl-hydroxylases

1.4.1 Crystal structures of human PHD2 and an algal P4H reveal substrate binding is mediated by induced fit

In 2006, McDonough et al. reported a structure of human PHD2 bound to a bicyclic 2OG-mimetic inhibitor [*N*-(4-hydroxy-8-iodoisoquinolin-3-yl)carbonylglycine], which at the time was the first reported structure of a prolyl-hydroxylase (*83*). Shortly thereafter, bioinformatic analyses revealed the presence of a CP4H homologue in the algae *Chlamydomonas reinhardtii* (*84*). Crystal structures of *C. reinhardtii* P4H (CrP4H) and human PHD2 in its *apo* (no-substrate bound) and substrate-bound forms reveal the structural mechanisms underlying P4H catalysis (*83, 85-87*).

As do all reported structures of 2OG oxygenases (*88*), CrP4H and PHD2 each contain a double-stranded β-helix (DSBH) core, consisting of eight β-strands (I-VIII) that fold into major and minor β-sheets (Figure 1.10, *A* and *B*). The active site is positioned in between the major and minor β-sheets and is composed of an HxD/E…H metal-binding motif, which along with the 2OG 2-oxo and 1 carboxylate groups complete octahedral coordination of the metal [Fe(II) is required for catalysis, yet other metals such as Zn(II) or Mn(II) are often used as a surrogate for Fe(II) in crystallisation]. *N*-oxalylglycine (NOG) and other non-reactive 2OG-mimetic inhibitors, so called 2OG-mimetic because they contain the 2OG core, are often substituted for 2OG to stabilise the protein and promote crystallisation. The 2OG C-5 carboxylate (or analogous inhibitor carboxylate) is positioned to form a salt bridge with an arginine ($Arg383_{PHD2}$) or lysine ($Lys237_{CrP4H}$) that extends from strand VIII.

Structures of CrP4H and PHD2 in complex with proline-rich peptide and CODD peptide fragment, respectively, provide insights into the structural basis of prolyl-hydroxylase catalysis (Figure 1.10, *A* and *B*) (*86, 87*). In both CrP4H and PHD2, the conformationally flexible β2-β3 finger loop, which occupies a partially disordered, 'open' position in their respective *apo* structures, undergoes a substantial conformational change upon substrate binding, so positioned to enclose substrate in the active site for catalysis (Figure 1.10, *A* and *B*). The structures provided the first evidence that prolyl-hydroxylase, and perhaps more broadly, 2OG oxygenase, catalysis involves an induced fit mechanism.

The determination of the structure of human PHD2 in complex with HIF-1α CODD peptide fragment provides insights into the structural mechanism underlying HIF-1α prolyl-hydroxylation and is useful in the design of selective PHD2 inhibitors. In the structure, Pro564 is positioned in the PHD2 active site in a C-4 *endo* conformation in *pro trans*-4 stereochemistry, in contrast to the C-4 *exo* conformation of Hyp564 observed in the pVHL:CODD(Hyp564) structure (*66, 67*).

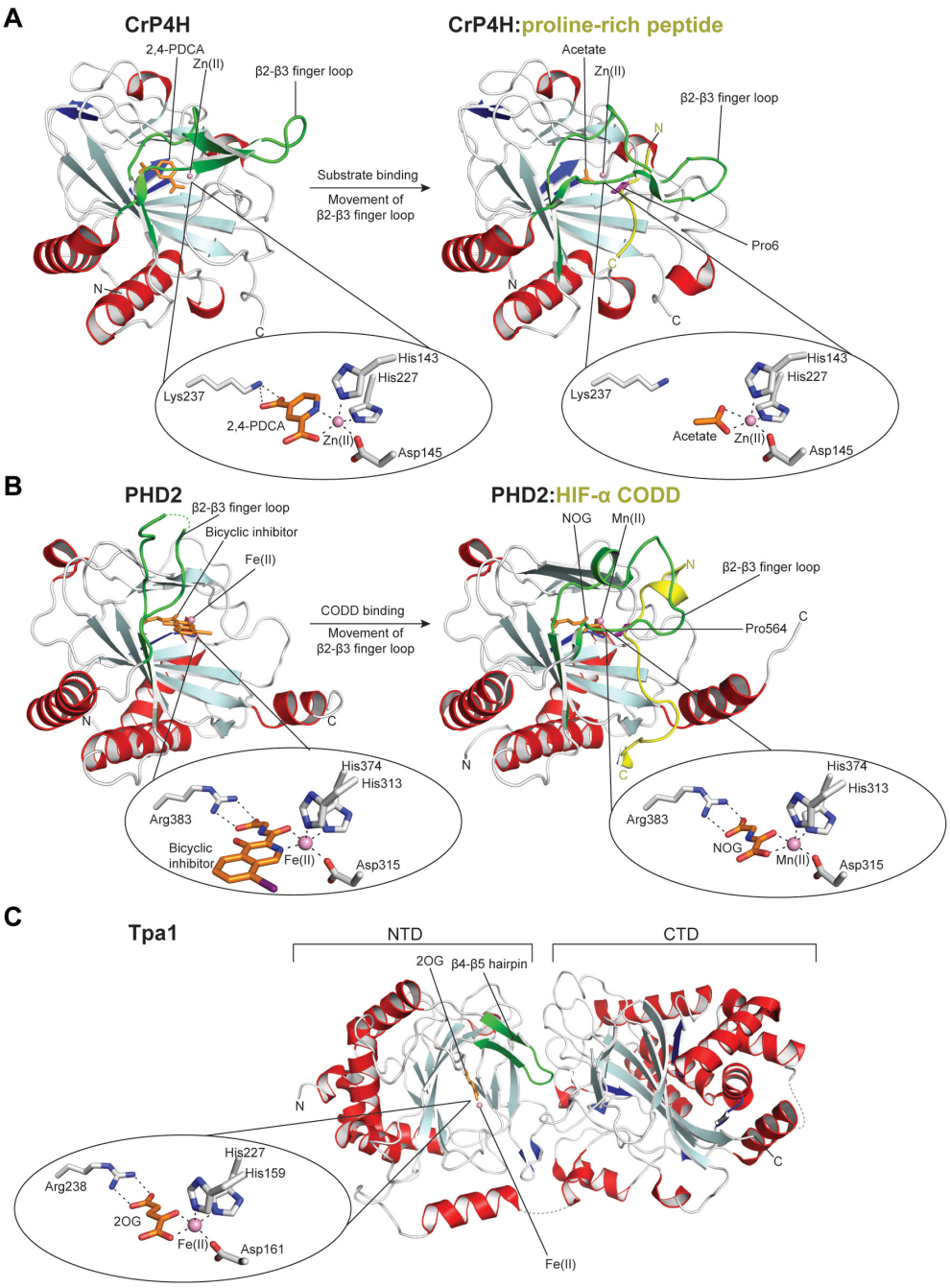

Figure 1.10. Structural overview of collagen, HIF, and RPS23 prolyl-hydroxylases. View from crystal structures of (**A**) *C. reinhardtii* P4H (CrP4H) in its *apo* form (left)(PDB ID: 2JIG)(*85*) and when complexed with proline-rich peptide substrate [sequence: $(PS)_5$](right)(PDB ID: 3GZE)(*87*), and of (**B**) human PHD2 in its *apo* form (left)(PDB ID: 2G1M)(*83*) and when complexed to CODD peptide fragment (right)(PDB ID: 3HQR)(*86*) reveal a conserved mechanism of substrate binding involving conformational changes in the β2-β3 finger loop. (**C**) Crystal structure of *S. cerevisiae* Tpa1 (PDB ID: 3KT7)(*89*) reveals two DSBH containing domains, the *N*-terminal domain (NTD) and *C*-terminal domain (CTD), of which only the NTD contains the catalytic machinery and bound metal. In all structures, DBSH-containing strands are shown in cyan, non-DBSH associated strands in blue, helices in red, loops in white, and β2-β3 finger loop (or β4-β5 hairpin in the case of Tpa1) in green.

1.4.2 Crystal structures of Tpa1 highlight differences between RPS23 hydroxylases and prolyl-4-hydroxylases

The RPS23 hydroxylases, of which structures have only been reported for Tpa1 (*89, 90*), are the only known subfamily of 2OG oxygenases to contain two DSBH domains in tandem (Figure 1.10*C*) (but there are other tandem DSBH enzymes, e.g. quercitin 2,3-dioxygenase) (*91*). However, only the *N*-terminal domain (NTD) contains the catalytic machinery, whereas the *C*-terminal domain (CTD) lacks an HxD/E…H metal binding motif. The β4-β5 hairpin of Tpa1 is structurally equivalent to the β2-β3 finger loop of CrP4H and PHD2 (Figure 1.10*C*). However, in contrast to the β2-β3 finger loops of CrP4H and PHD2, the Tpa1 β4-β5 hairpin is ordered in its *apo* form, and, therefore, not predicted to undergo an analogous conformational change upon substrate binding. Crystal structures of Tpa1, or other RPS23 hydroxylases, in complex with substrate will provide insights into the structural basis for RPS23 hydroxylation and allow for more informed comparisons with the prolyl-4-hydroxylases.

1.5 Therapeutic potential of prolyl-hydroxylases

1.5.1 Collagen prolyl-hydroxylases

Collagen plays a central role in fibrotic diseases, which are characterised by an accumulation of fibrous tissue in any organ or tissue (*92, 93*). Given the importance of 4-hydroxyproline in collagen stabilisation, the CP4Hs are appealing targets for anti-fibrotic treatment and were the earliest 2OG oxygenases to be the targets of inhibition studies (*92*). However, these studies did not produce therapeutically viable inhibitors, possibly due to difficulties inherent in the recombinant expression and purification of CP4H and the

resulting lack of structural information about the CP4H catalytic domain, and thus accurate SARs.

Recent work has shown that hypoxia-mediated HIF-1 upregulation of CP4H regulates metastasis of breast cancer tumours along collagen fibers and that *CP4H* knockdown reduces cancer cell intravasation (*94*). The results open the door to new avenues in breast cancer therapy, especially in triple negative breast cancers [minimal expression of estrogen receptor, progesterone receptor, and human epidermal growth factor receptor-2 (HER2)] that exhibit strong HIF-1 activation but do not respond well to current therapies (*95, 96*).

1.5.2 HIF prolyl-hydroxylases

Since their discovery as regulators of the pleiotropic nature of HIF, the HIF prolyl-hydroxylases have been the subject of intense interest for the treatment of anemia and ischemic-related diseases characterised by constitutive hypoxia, with some compounds in phase III clinical trials (*6, 97*). Inhibitors of the PHDs act as HIF agonists by precluding its proteasomal degradation in normoxia, thus leading to the stabilisation of HIF and promoting expression of HIF target genes. For example, PHD inhibition by small molecules stimulates production of erythropoietin (EPO), which is commonly used in the treatment of anemia (*98*).

Renal carcinomas, hemagioblastomas, and other highly vascular solid tumours in patients with VHL disease are characterised by an upregulation of VEGF, a HIF target gene (*99*). As a result, HIF antagonists are currently being pursued as anti-cancer agents (*37, 39, 100*).

1.5.3 Ribosomal prolyl-hydroxylases

In contrast to the PHDs, investigation into the potential functional roles of human OGFOD1 and its eukaryotic homologues is still in its infancy. As a result, their viability as therapeutic targets has not yet been fully characterised. However, given the recently established link between the ribosomal prolyl-hydroxylases and translation termination/accuracy, there is the possibility that inhibition of OGFOD1 may provide therapeutic benefit to diseases caused by nonsense readthrough, which is characterised by the errant inclusion of a stop codon within an mRNA open reading frame, thus preventing translation of full-length protein (*74, 75, 101, 102*). Diseases characterised by nonsense readthrough include Duchenne muscular dystrophy, the symptoms of which are currently treated via the chronic use of corticosteroids (*102*).

1.6 Aims of this thesis

Broadly, work described in this thesis aims to study the collagen, HIF, and RPS23 prolyl-hydroxylase subfamilies through the following: i) the identification, biochemical, and structural characterisation of a PHD homologue in prokaryotes (Chapters 2 and 3), ii) biochemical and structural analyses of OGFOD1 and Tpa1 (Chapter 4), and iii) expression, purification, and crystallisation/diffraction of human CP4H (Chapter 5). The results presented in this thesis aim to expand the knowledge of prolyl-hydroxylases as a whole and, in closing, propose insights into their ancestral origins.

1.7 References

1. K. J. Carpenter, *The history of scurvy and vitamin C*. (Cambridge University Press, Cambridge, 1986), pp. viii, 288 p.
2. J. Lind, C. P. Stewart, D. Guthrie, *Lind's Treatise on scurvy : a bicentenary volume containing a reprint of the first edition of A treatise of the scurvy*. (University Press, Edinburgh, 1953), pp. xi, 440 p.
3. J. Myllyharju, K. I. Kivirikko, Collagens and collagen-related diseases. *Annals of Medicine.* **33**, 7-21 (2001).
4. G. N. Ramachandran, G. Kartha, Structure of collagen. *Nature.* **176**, 593-595 (1955).
5. P. Szpak, Fish bone chemistry and ultrastructure: implications for taphonomy and stable isotope analysis. *J Archaeol Sci.* **38**, 3358-3372 (2011).
6. J. Myllyharju, Prolyl 4-hydroxylases, key enzymes in the synthesis of collagens and regulation of the response to hypoxia, and their roles as treatment targets. *Ann Med.* **40**, 402-417 (2008).
7. J. Bella, M. Eaton, B. Brodsky, H. M. Berman, Crystal-Structure and Molecular-Structure of a Collagen-Like Peptide at 1.9-Angstrom Resolution. *Science.* **266**, 75-81 (1994).
8. C. L. Jenkins, R. T. Raines, Insights on the conformational stability of collagen. *Nat Prod Rep.* **19**, 49-59 (2002).
9. J. J. Hutton, Jr., A. L. Trappel, S. Udenfriend, Requirements for alpha-ketoglutarate, ferrous ion and ascorbate by collagen proline hydroxylase. *Biochem Biophys Res Commun.* **24**, 179-184 (1966).
10. C. Loenarz, C. J. Schofield, Expanding chemical biology of 2-oxoglutarate oxygenases. *Nat Chem Biol.* **4**, 152-156 (2008).
11. C. Loenarz, C. J. Schofield, Physiological and biochemical aspects of hydroxylations and demethylations catalyzed by human 2-oxoglutarate oxygenases. *Trends Biochem Sci.* **36**, 7-18 (2011).
12. I. J. Clifton, M. A. McDonough, D. Ehrismann, N. J. Kershaw, N. Granatino, C. J. Schofield, Structural studies on 2-oxoglutarate oxygenases and related double-stranded beta-helix fold proteins. *J Inorg Biochem.* **100**, 644-669 (2006).
13. J. C. Price, E. W. Barr, B. Tirupati, J. M. Bollinger, Jr., C. Krebs, The first direct characterization of a high-valent iron intermediate in the reaction of an alpha-ketoglutarate-dependent dioxygenase: a high-spin FeIV complex in taurine/alpha-ketoglutarate dioxygenase (TauD) from Escherichia coli. *Biochemistry.* **42**, 7497-7508 (2003).
14. D. A. Proshlyakov, T. F. Henshaw, G. R. Monterosso, M. J. Ryle, R. P. Hausinger, Direct detection of oxygen intermediates in the non-heme Fe enzyme taurine/alpha-ketoglutarate dioxygenase. *J Am Chem Soc.* **126**, 1022-1023 (2004).
15. P. J. Riggs-Gelasco, J. C. Price, R. B. Guyer, J. H. Brehm, E. W. Barr, J. M. Bollinger, Jr., C. Krebs, EXAFS spectroscopic evidence for an Fe=O unit in the Fe(IV) intermediate observed during oxygen activation by taurine:alpha-ketoglutarate dioxygenase. *J Am Chem Soc.* **126**, 8108-8109 (2004).

16. E. Flashman, S. L. Davies, K. K. Yeoh, C. J. Schofield, Investigating the dependence of the hypoxia-inducible factor hydroxylases (factor inhibiting HIF and prolyl hydroxylase domain 2) on ascorbate and other reducing agents. *Biochem J.* **427**, 135-142 (2010).
17. J. Myllyharju, Prolyl 4-hydroxylases, the key enzymes of collagen biosynthesis. *Matrix Biol.* **22**, 15-24 (2003).
18. P. Annunen, T. Helaakoski, J. Myllyharju, J. Veijola, T. Pihlajaniemi, K. I. Kivirikko, Cloning of the human prolyl 4-hydroxylase alpha subunit isoform alpha(II) and characterization of the type II enzyme tetramer. The alpha(I) and alpha(II) subunits do not form a mixed alpha(I)alpha(II)beta2 tetramer. *J Biol Chem.* **272**, 17342-17348 (1997).
19. L. Kukkola, R. Hieta, K. I. Kivirikko, J. Myllyharju, Identification and characterization of a third human, rat, and mouse collagen prolyl 4-hydroxylase isoenzyme. *J Biol Chem.* **278**, 47685-47693 (2003).
20. T. Helaakoski, K. Vuori, R. Myllyla, K. I. Kivirikko, T. Pihlajaniemi, Molecular cloning of the alpha-subunit of human prolyl 4-hydroxylase: the complete cDNA-derived amino acid sequence and evidence for alternative splicing of RNA transcripts. *Proc Natl Acad Sci U S A.* **86**, 4392-4396 (1989).
21. J. Myllyharju, K. I. Kivirikko, Identification of a novel proline-rich peptide-binding domain in prolyl 4-hydroxylase. *EMBO J.* **18**, 306-312 (1999).
22. R. Hieta, L. Kukkola, P. Permi, P. Pirila, K. I. Kivirikko, I. Kilpelainen, J. Myllyharju, The peptide-substrate-binding domain of human collagen prolyl 4-hydroxylases. Backbone assignments, secondary structure, and binding of proline-rich peptides. *J Biol Chem.* **278**, 34966-34974 (2003).
23. J. Koivu, R. Myllyla, T. Helaakoski, T. Pihlajaniemi, K. Tasanen, K. I. Kivirikko, A Single Polypeptide Acts Both as the Beta-Subunit of Prolyl 4-Hydroxylase and as a Protein Disulfide-Isomerase. *Journal of Biological Chemistry.* **262**, 6447-6449 (1987).
24. C. Apperizeller-Herzog, L. Ellgaard, The human PDI family: Versatility packed into a single fold. *Bba-Mol Cell Res.* **1783**, 535-548 (2008).
25. A. M. Benham, The Protein Disulfide Isomerase Family: Key Players in Health and Disease. *Antioxid Redox Sign.* **16**, 781-789 (2012).
26. F. Hatahet, L. W. Ruddock, Protein Disulfide Isomerase: A Critical Evaluation of Its Function in Disulfide Bond Formation. *Antioxid Redox Sign.* **11**, 2807-2850 (2009).
27. K. Vuori, T. Pihlajaniemi, M. Marttila, K. I. Kivirikko, Characterization of the human prolyl 4-hydroxylase tetramer and its multifunctional protein disulfide-isomerase subunit synthesized in a baculovirus expression system. *Proc Natl Acad Sci U S A.* **89**, 7467-7470 (1992).
28. K. Vuori, T. Pihlajaniemi, R. Myllyla, K. I. Kivirikko, Site-directed mutagenesis of human protein disulphide isomerase: effect on the assembly, activity and endoplasmic reticulum retention of human prolyl 4-hydroxylase in Spodoptera frugiperda insect cells. *EMBO J.* **11**, 4213-4217 (1992).
29. C. Wang, W. Li, J. Q. Ren, J. Q. Fang, H. M. Ke, W. M. Gong, W. Feng, C. C. Wang, Structural Insights into the Redox-Regulated Dynamic Conformations of Human Protein Disulfide Isomerase. *Antioxid Redox Sign.* **19**, 44-53 (2013).

30. T. Helaakoski, P. Annunen, K. Vuori, I. A. MacNeil, T. Pihlajaniemi, K. I. Kivirikko, Cloning, baculovirus expression, and characterization of a second mouse prolyl 4-hydroxylase alpha-subunit isoform: formation of an alpha 2 beta 2 tetramer with the protein disulfide-isomerase/beta subunit. *Proc Natl Acad Sci U S A.* **92**, 4427-4431 (1995).
31. A. Vuorela, J. Myllyharju, R. Nissi, T. Pihlajaniemi, K. I. Kivirikko, Assembly of human prolyl 4-hydroxylase and type III collagen in the yeast Pichia pastoris: formation of a stable enzyme tetramer requires coexpression with collagen and assembly of a stable collagen requires coexpression with prolyl 4-hydroxylase. *Embo Journal.* **16**, 6702-6712 (1997).
32. A. Neubauer, P. Neubauer, J. Myllyharju, High-level production of human collagen prolyl 4-hydroxylase in Escherichia coli. *Matrix Biol.* **24**, 59-68 (2005).
33. D. C. John, N. J. Bulleid, Prolyl 4-hydroxylase: defective assembly of alpha-subunit mutants indicates that assembled alpha-subunits are intramolecularly disulfide bonded. *Biochemistry.* **33**, 14018-14025 (1994).
34. A. Lamberg, T. Pihlajaniemi, K. I. Kivirikko, Site-directed mutagenesis of the alpha subunit of human prolyl 4-hydroxylase. Identification of three histidine residues critical for catalytic activity. *J Biol Chem.* **270**, 9926-9931 (1995).
35. J. Anantharajan, M. K. Koski, P. Kursula, R. Hieta, U. Bergmann, J. Myllyharju, R. K. Wierenga, The structural motifs for substrate binding and dimerization of the alpha subunit of collagen prolyl 4-hydroxylase. *Structure.* **21**, 2107-2118 (2013).
36. G. L. Semenza, Hypoxia-inducible factor 1: master regulator of O-2 homeostasis. *Curr Opin Genet Dev.* **8**, 588-594 (1998).
37. W. G. Kaelin, P. J. Ratcliffe, Oxygen sensing by metazoans: The central role of the HIF hydroxylase pathway. *Molecular Cell.* **30**, 393-402 (2008).
38. G. L. Wang, B. H. Jiang, E. A. Rue, G. L. Semenza, Hypoxia-Inducible Factor-1 Is a Basic-Helix-Loop-Helix-Pas Heterodimer Regulated by Cellular O-2 Tension. *P Natl Acad Sci USA.* **92**, 5510-5514 (1995).
39. W. G. Kaelin, The von Hippel-Lindau protein, HIF hydroxylation, and oxygen sensing. *Biochem Bioph Res Co.* **338**, 627-638 (2005).
40. P. H. Maxwell, P. J. Ratcliffe, Oxygen sensors and angiogenesis. *Semin Cell Dev Biol.* **13**, 29-37 (2002).
41. N. L. Sang, J. Fang, V. Srinivas, I. Leshchinsky, J. Caro, Carboxyl-terminal transactivation activity of hypoxia-inducible factor 1 alpha is governed by a von Hippel-Lindau protein-independent, hydroxylation-regulated association with p300/CBP. *Molecular and Cellular Biology.* **22**, 2984-2992 (2002).
42. Z. Arany, L. E. Huang, R. Eckner, S. Bhattacharya, C. Jiang, M. A. Goldberg, H. F. Bunn, D. M. Livingston, An essential role for p300/CBP in the cellular response to hypoxia. *Proc Natl Acad Sci U S A.* **93**, 12969-12973 (1996).
43. P. Carrero, K. Okamoto, P. Coumailleau, S. O'Brien, H. Tanaka, L. Poellinger, Redox-regulated recruitment of the transcriptional coactivators CREB-binding protein and SRC-1 to hypoxia-inducible factor 1alpha. *Mol Cell Biol.* **20**, 402-415 (2000).

44. M. L. Avantaggiati, V. Ogryzko, K. Gardner, A. Giordano, A. S. Levine, K. Kelly, Recruitment of p300/CBP in p53-dependent signal pathways. *Cell.* **89**, 1175-1184 (1997).
45. G. L. Semenza, Regulation of mammalian O2 homeostasis by hypoxia-inducible factor 1. *Annu Rev Cell Dev Biol.* **15**, 551-578 (1999).
46. P. H. Maxwell, M. S. Wiesener, G. W. Chang, S. C. Clifford, E. C. Vaux, M. E. Cockman, C. C. Wykoff, C. W. Pugh, E. R. Maher, P. J. Ratcliffe, The tumour suppressor protein VHL targets hypoxia-inducible factors for oxygen-dependent proteolysis. *Nature.* **399**, 271-275 (1999).
47. K. Iwai, K. Yamanaka, T. Kamura, N. Minato, R. C. Conaway, J. W. Canaway, R. D. Klausner, A. Pause, Identification of the von Hippel-Lindau tumor-suppressor protein as part of an active E3 ubiquitin ligase complex. *P Natl Acad Sci USA.* **96**, 12436-12441 (1999).
48. M. E. Cockman, N. Masson, D. R. Mole, P. Jaakkola, G. W. Chang, S. C. Clifford, E. R. Maher, C. W. Pugh, P. J. Ratcliffe, P. H. Maxwell, Hypoxia inducible factor-alpha binding and ubiquitylation by the von Hippel-Lindau tumor suppressor protein. *Journal of Biological Chemistry.* **275**, 25733-25741 (2000).
49. C. E. Stebbins, W. G. Kaelin, Jr., N. P. Pavletich, Structure of the VHL-ElonginC-ElonginB complex: implications for VHL tumor suppressor function. *Science.* **284**, 455-461 (1999).
50. K. Tanimoto, Y. Makino, T. Pereira, L. Poellinger, Mechanism of regulation of the hypoxia-inducible factor-1 alpha by the von Hippel-Lindau tumor suppressor protein. *EMBO J.* **19**, 4298-4309 (2000).
51. G. L. Wang, G. L. Semenza, Desferrioxamine induces erythropoietin gene expression and hypoxia-inducible factor 1 DNA-binding activity: implications for models of hypoxia signal transduction. *Blood.* **82**, 3610-3615 (1993).
52. M. A. Goldberg, S. P. Dunning, H. F. Bunn, Regulation of the Erythropoietin Gene - Evidence That the Oxygen Sensor Is a Heme Protein. *Science.* **242**, 1412-1415 (1988).
53. M. Ivan, K. Kondo, H. Yang, W. Kim, J. Valiando, M. Ohh, A. Salic, J. M. Asara, W. S. Lane, W. G. Kaelin, Jr., HIFalpha targeted for VHL-mediated destruction by proline hydroxylation: implications for O2 sensing. *Science.* **292**, 464-468 (2001).
54. P. Jaakkola, D. R. Mole, Y. M. Tian, M. I. Wilson, J. Gielbert, S. J. Gaskell, A. von Kriegsheim, H. F. Hebestreit, M. Mukherji, C. J. Schofield, P. H. Maxwell, C. W. Pugh, P. J. Ratcliffe, Targeting of HIF-alpha to the von Hippel-Lindau ubiquitylation complex by O2-regulated prolyl hydroxylation. *Science.* **292**, 468-472 (2001).
55. A. C. R. Epstein, J. M. Gleadle, L. A. McNeill, K. S. Hewitson, J. O'Rourke, D. R. Mole, M. Mukherji, E. Metzen, M. I. Wilson, A. Dhanda, Y. M. Tian, N. Masson, D. L. Hamilton, P. Jaakkola, R. Barstead, J. Hodgkin, P. H. Maxwell, C. W. Pugh, C. J. Schofield, P. J. Ratcliffe, C-elegans EGL-9 and mammalian homologs define a family of dioxygenases that regulate HIF by prolyl hydroxylation. *Cell.* **107**, 43-54 (2001).
56. E. Metzen, U. Berchner-Pfannschmidt, P. Stengel, J. H. Marxsen, I. Stolze, M. Klinger, W. Q. Huang, C. Wotzlaw, T. Hellwig-Burgel, W. Jelkmann, H. Acker, J. Fandrey, Intracellular localisation of human HIF-1 alpha

hydroxylases: implications for oxygen sensing. *J Cell Sci.* **116**, 1319-1326 (2003).
57. R. K. Bruick, S. L. McKnight, A conserved family of prolyl-4-hydroxylases that modify HIF. *Science.* **294**, 1337-1340 (2001).
58. R. J. Appelhoff, Y. M. Tian, R. R. Raval, H. Turley, A. L. Harris, C. W. Pugh, P. J. Ratcliffe, J. M. Gleadle, Differential function of the prolyl hydroxylases PHD1, PHD2, and PHD3 in the regulation of hypoxia-inducible factor. *Journal of Biological Chemistry.* **279**, 38458-38465 (2004).
59. M. Hirsila, P. Koivunen, V. Gunzler, K. I. Kivirikko, J. Myllyharju, Characterization of the human prolyl 4-hydroxylases that modify the hypoxia-inducible factor. *Journal of Biological Chemistry.* **278**, 30772-30780 (2003).
60. D. Ehrismann, E. Flashman, D. N. Genn, N. Mathioudakis, K. S. Hewitson, P. J. Ratcliffe, C. J. Schofield, Studies on the activity of the hypoxia-inducible-factor hydroxylases using an oxygen consumption assay. *Biochem J.* **401**, 227-234 (2007).
61. P. C. Mahon, K. Hirota, G. L. Semenza, FIH-1: a novel protein that interacts with HIF-1 alpha and VHL to mediate repression of HIF-1 transcriptional activity. *Gene Dev.* **15**, 2675-2686 (2001).
62. D. Lando, D. J. Peet, J. J. Gorman, D. A. Whelan, M. L. Whitelaw, R. K. Bruick, FIH-1 is an asparaginyl hydroxylase enzyme that regulates the transcriptional activity of hypoxia-inducible factor. *Gene Dev.* **16**, 1466-1471 (2002).
63. W. G. Kaelin, Proline hydroxylation and gene expression. *Annu Rev Biochem.* **74**, 115-128 (2005).
64. L. A. McNeill, K. S. Hewitson, T. D. Claridge, J. F. Seibel, L. E. Horsfall, C. J. Schofield, Hypoxia-inducible factor asparaginyl hydroxylase (FIH-1) catalyses hydroxylation at the beta-carbon of asparagine-803. *Biochemical Journal.* **367**, 571-575 (2002).
65. P. Koivunen, M. Hirsila, V. Gunzler, K. I. Kivirikko, J. Myllyharju, Catalytic properties of the asparaginyl hydroxylase (FIH) in the oxygen sensing pathway are distinct from those of its prolyl 4-hydroxylases. *Journal of Biological Chemistry.* **279**, 9899-9904 (2004).
66. J. H. Min, H. Yang, M. Ivan, F. Gertler, W. G. Kaelin, Jr., N. P. Pavletich, Structure of an HIF-1alpha -pVHL complex: hydroxyproline recognition in signaling. *Science.* **296**, 1886-1889 (2002).
67. W. C. Hon, M. I. Wilson, K. Harlos, T. D. Claridge, C. J. Schofield, C. W. Pugh, P. H. Maxwell, P. J. Ratcliffe, D. I. Stuart, E. Y. Jones, Structural basis for the recognition of hydroxyproline in HIF-1 alpha by pVHL. *Nature.* **417**, 975-978 (2002).
68. C. Beroud, D. Joly, C. Gallou, F. Staroz, M. T. Orfanelli, C. Junien, Software and database for the analysis of mutations in the VHL gene. *Nucleic Acids Research.* **26**, 256-258 (1998).
69. C. E. Stebbins, W. G. Kaelin, N. P. Pavletich, Structure of the VHL-ElonginC-ElonginB complex: Implications for VHL tumor suppressor function. *Science.* **284**, 455-461 (1999).
70. H. van der Wel, A. Ercan, C. M. West, The Skp1 prolyl hydroxylase from Dictyostelium is related to the hypoxia-inducible factor-alpha class of animal prolyl 4-hydroxylases. *J Biol Chem.* **280**, 14645-14655 (2005).

71. T. Cardozo, M. Pagano, The SCF ubiquitin ligase: insights into a molecular machine. *Nat Rev Mol Cell Biol.* **5**, 739-751 (2004).
72. D. Sandona, S. Gastaldello, R. Rizzuto, R. Bisson, Expression of cytochrome c oxidase during growth and development of Dictyostelium. *J Biol Chem.* **270**, 5587-5593 (1995).
73. C. M. West, H. van der Wel, Z. A. Wang, Prolyl 4-hydroxylase-1 mediates O2 signaling during development of Dictyostelium. *Development.* **134**, 3349-3358 (2007).
74. R. S. Singleton, P. Liu-Yi, F. Formenti, W. Ge, R. Sekirnik, R. Fischer, J. Adam, P. J. Pollard, A. Wolf, A. Thalhammer, C. Loenarz, E. Flashman, A. Yamamoto, M. L. Coleman, B. M. Kessler, P. Wappner, C. J. Schofield, P. J. Ratcliffe, M. E. Cockman, OGFOD1 catalyzes prolyl hydroxylation of RPS23 and is involved in translation control and stress granule formation. *Proc Natl Acad Sci U S A.* **111**, 4031-4036 (2014).
75. C. Loenarz, R. Sekirnik, A. Thalhammer, W. Ge, E. Spivakovsky, M. M. Mackeen, M. A. McDonough, M. E. Cockman, B. M. Kessler, P. J. Ratcliffe, A. Wolf, C. J. Schofield, Hydroxylation of the eukaryotic ribosomal decoding center affects translational accuracy. *Proc Natl Acad Sci U S A.* **111**, 4019-4024 (2014).
76. M. J. Katz, J. M. Acevedo, C. Loenarz, D. Galagovsky, P. Liu-Yi, M. Perez-Pepe, A. Thalhammer, R. Sekirnik, W. Ge, M. Melani, M. G. Thomas, S. Simonetta, G. L. Boccaccio, C. J. Schofield, M. E. Cockman, P. J. Ratcliffe, P. Wappner, Sudestada1, a Drosophila ribosomal prolyl-hydroxylase required for mRNA translation, cell homeostasis, and organ growth. *Proc Natl Acad Sci U S A.* **111**, 4025-4030 (2014).
77. C. J. Schofield, P. J. Ratcliffe, Oxygen sensing by HIF hydroxylases. *Nat Rev Mol Cell Biol.* **5**, 343-354 (2004).
78. T. M. Schmeing, R. M. Voorhees, A. C. Kelley, Y. G. Gao, F. V. t. Murphy, J. R. Weir, V. Ramakrishnan, The crystal structure of the ribosome bound to EF-Tu and aminoacyl-tRNA. *Science.* **326**, 688-694 (2009).
79. B. T. Hughes, P. J. Espenshade, Oxygen-regulated degradation of fission yeast SREBP by Ofd1, a prolyl hydroxylase family member. *Embo Journal.* **27**, 1491-1501 (2008).
80. A. L. Hughes, B. L. Todd, P. J. Espenshade, SREBP pathway responds to sterols and functions as an oxygen sensor in fission yeast. *Cell.* **120**, 831-842 (2005).
81. C. M. Bien, P. J. Espenshade, Sterol Regulatory Element Binding Proteins in Fungi: Hypoxic Transcription Factors Linked to Pathogenesis. *Eukaryot Cell.* **9**, 352-359 (2010).
82. K. M. Keeling, J. Salas-Marco, L. Z. Osherovich, D. M. Bedwell, Tpa1p is part of an mRNP complex that influences translation termination, mRNA deadenylation, and mRNA turnover in Saccharomyces cerevisiae. *Molecular and Cellular Biology.* **26**, 5237-5248 (2006).
83. M. A. McDonough, V. Li, E. Flashman, R. Chowdhury, C. Mohr, B. M. Lienard, J. Zondlo, N. J. Oldham, I. J. Clifton, J. Lewis, L. A. McNeill, R. J. Kurzeja, K. S. Hewitson, E. Yang, S. Jordan, R. S. Syed, C. J. Schofield, Cellular oxygen sensing: Crystal structure of hypoxia-inducible factor prolyl hydroxylase (PHD2). *Proc Natl Acad Sci U S A.* **103**, 9814-9819 (2006).

84. K. Keskiaho, R. Hieta, R. Sormunen, J. Myllyharju, Chlamydomonas reinhardtii has multiple prolyl 4-hydroxylases, one of which is essential for proper cell wall assembly. *Plant Cell.* **19**, 256-269 (2007).
85. M. K. Koski, R. Hieta, C. Bollner, K. I. Kivirikko, J. Myllyharju, R. K. Wierenga, The active site of an algal prolyl 4-hydroxylase has a large structural plasticity. *Journal of Biological Chemistry.* **282**, 37112-37123 (2007).
86. R. Chowdhury, M. A. McDonough, J. Mecinovic, C. Loenarz, E. Flashman, K. S. Hewitson, C. Domene, C. J. Schofield, Structural basis for binding of hypoxia-inducible factor to the oxygen-sensing prolyl hydroxylases. *Structure.* **17**, 981-989 (2009).
87. M. K. Koski, R. Hieta, M. Hirsila, A. Ronka, J. Myllyharju, R. K. Wierenga, The crystal structure of an algal prolyl 4-hydroxylase complexed with a proline-rich peptide reveals a novel buried tripeptide binding motif. *J Biol Chem.* **284**, 25290-25301 (2009).
88. W. Aik, M. A. McDonough, A. Thalhammer, R. Chowdhury, C. J. Schofield, Role of the jelly-roll fold in substrate binding by 2-oxoglutarate oxygenases. *Curr Opin Struct Biol.* **22**, 691-700 (2012).
89. H. S. Kim, H. L. Kim, K. H. Kim, J. Kim do, S. J. Lee, J. Y. Yoon, H. J. Yoon, H. Y. Lee, S. B. Park, S. J. Kim, J. Y. Lee, S. W. Suh, Crystal structure of Tpa1 from Saccharomyces cerevisiae, a component of the messenger ribonucleoprotein complex. *Nucleic Acids Res.* **38**, 2099-2110 (2010).
90. J. Henri, D. Rispal, E. Bayart, H. van Tilbeurgh, B. Seraphin, M. Graille, Structural and Functional Insights into Saccharomyces cerevisiae Tpa1, a Putative Prolylhydroxylase Influencing Translation Termination and Transcription. *Journal of Biological Chemistry.* **285**, 30767-30778 (2010).
91. B. Gopal, L. L. Madan, S. F. Betz, A. A. Kossiakoff, The crystal structure of a quercetin 2,3-dioxygenase from Bacillus subtilis suggests modulation of enzyme activity by a change in the metal ion at the active site(s). *Biochemistry.* **44**, 193-201 (2005).
92. J. Myllyharju, K. I. Kivirikko, Collagens and collagen-related diseases. *Ann Med.* **33**, 7-21 (2001).
93. J. Myllyharju, Prolyl 4-hydroxylases, key enzymes in the synthesis of collagens and regulation of the response to hypoxia, and their roles as treatment targets. *Annals of Medicine.* **40**, 402-417 (2008).
94. D. M. Gilkes, P. Chaturvedi, S. Bajpai, C. C. Wong, H. Wei, S. Pitcairn, M. E. Hubbi, D. Wirtz, G. L. Semenza, Collagen prolyl hydroxylases are essential for breast cancer metastasis. *Cancer Res.* **73**, 3285-3296 (2013).
95. S. K. Pal, B. H. Childs, M. Pegram, Triple negative breast cancer: unmet medical needs. *Breast Cancer Res Tr.* **125**, 627-636 (2011).
96. D. C. Koboldt, R. S. Fulton, M. D. McLellan, H. Schmidt, J. Kalicki-Veizer, J. F. McMichael, L. L. Fulton, D. J. Dooling, L. Ding, E. R. Mardis, R. K. Wilson, A. Ally, M. Balasundaram, Y. S. N. Butterfield, R. Carlsen, C. Carter, A. Chu, E. Chuah, H. J. E. Chun, R. J. N. Coope, N. Dhalla, R. Guin, C. Hirst, M. Hirst, R. A. Holt, D. Lee, H. Y. I. Li, M. Mayo, R. A. Moore, A. J. Mungall, E. Pleasance, A. G. Robertson, J. E. Schein, A. Shafiei, P. Sipahimalani, J. R. Slobodan, D. Stoll, A. Tam, N. Thiessen, R. J. Varhol, N. Wye, T. Zeng, Y. J. Zhao, I. Birol, S. J. M. Jones, M. A. Marra, A. D. Cherniack, G. Saksena, R. C. Onofrio, N. H. Pho, S. L. Carter, S. E. Schumacher, B. Tabak, B. Hernandez, J. Gentry, H.

Nguyen, A. Crenshaw, K. Ardlie, R. Beroukhim, W. Winckler, G. Getz, S. B. Gabriel, M. Meyerson, L. Chin, P. J. Park, R. Kucherlapati, K. A. Hoadley, J. T. Auman, C. Fan, Y. J. Turman, Y. Shi, L. Li, M. D. Topal, X. P. He, H. H. Chao, A. Prat, G. O. Silva, M. D. Iglesia, W. Zhao, J. Usary, J. S. Berg, M. Adams, J. Booker, J. Y. Wu, A. Gulabani, T. Bodenheimer, A. P. Hoyle, J. V. Simons, M. G. Soloway, L. E. Mose, S. R. Jefferys, S. Balu, J. S. Parker, D. N. Hayes, C. M. Perou, S. Malik, S. Mahurkar, H. Shen, D. J. Weisenberger, T. Triche, P. H. Lai, M. S. Bootwalla, D. T. Maglinte, B. P. Berman, D. J. Van den Berg, S. B. Baylin, P. W. Laird, C. J. Creighton, L. A. Donehower, G. Getz, M. Noble, D. Voet, G. Saksena, N. Gehlenborg, D. DiCara, J. H. Zhang, H. L. Zhang, C. J. Wu, S. Y. Liu, M. S. Lawrence, L. H. Zou, A. Sivachenko, P. Lin, P. Stojanov, R. Jing, J. Cho, R. Sinha, R. W. Park, M. D. Nazaire, J. Robinson, H. Thorvaldsdottir, J. Mesirov, P. J. Park, L. Chin, S. Reynolds, R. B. Kreisberg, B. Bernard, R. Bressler, T. Erkkila, J. Lin, V. Thorsson, W. Zhang, I. Shmulevich, G. Ciriello, N. Weinhold, N. Schultz, J. J. Gao, E. Cerami, B. Gross, A. Jacobsen, R. Sinha, B. A. Aksoy, Y. Antipin, B. Reva, R. L. Shen, B. S. Taylor, M. Ladanyi, C. Sander, P. Anur, P. T. Spellman, Y. L. Lu, W. B. Liu, R. R. G. Verhaak, G. B. Mills, R. Akbani, N. X. Zhang, B. M. Broom, T. D. Casasent, C. Wakefield, A. K. Unruh, K. Baggerly, K. Coombes, J. N. Weinstein, D. Haussler, C. C. Benz, J. M. Stuart, S. C. Benz, J. C. Zhu, C. C. Szeto, G. K. Scott, C. Yau, E. O. Paul, D. Carlin, C. Wong, A. Sokolov, J. Thusberg, S. Mooney, S. Ng, T. C. Goldstein, K. Ellrott, M. Grifford, C. Wilks, S. Ma, B. Craft, C. H. Yan, Y. Hu, D. Meerzaman, J. M. Gastier-Foster, J. Bowen, N. C. Ramirez, A. D. Black, R. E. Pyatt, P. White, E. J. Zmuda, J. Frick, T. Lichtenberg, R. Brookens, M. M. George, M. A. Gerken, H. A. Harper, K. M. Leraas, L. J. Wise, T. R. Tabler, C. McAllister, T. Barr, M. Hart-Kothari, K. Tarvin, C. Saller, G. Sandusky, C. Mitchell, M. V. Iacocca, J. Brown, B. Rabeno, C. Czerwinski, N. Petrelli, O. Dolzhansky, M. Abramov, O. Voronina, O. Potapova, J. R. Marks, W. M. Suchorska, D. Murawa, W. Kycler, M. Ibbs, K. Korski, A. Spychala, P. Murawa, J. J. Brzezinski, H. Perz, R. Lazniak, M. Teresiak, H. Tatka, E. Leporowska, M. Bogusz-Czerniewicz, J. Malicki, A. Mackiewicz, M. Wiznerowicz, X. V. Le, B. Kohl, N. V. Tien, R. Thorp, N. V. Bang, H. Sussman, B. D. Phu, R. Hajek, N. P. Hung, V. T. P. Tran, H. Q. Thang, K. Z. Khan, R. Penny, D. Mallery, E. Curley, C. Shelton, P. Yena, J. N. Ingle, F. J. Couch, W. L. Lingle, T. A. King, A. M. Gonzalez-Angulo, G. B. Mills, M. D. Dyer, S. Y. Liu, X. L. Meng, M. Patangan, F. Waldman, H. Stoppler, W. K. Rathmell, L. Thorne, M. Huang, L. Boice, A. Hill, C. Morrison, C. Gaudioso, W. Bshara, K. Daily, S. C. Egea, M. D. Pegram, C. Gomez-Fernandez, R. Dhir, R. Bhargava, A. Brufsky, C. D. Shriver, J. A. Hooke, J. L. Campbell, R. J. Mural, H. Hu, S. Somiari, C. Larson, B. Deyarmin, L. Kvecher, A. J. Kovatich, M. J. Ellis, T. A. King, H. Hu, F. J. Couch, R. J. Mural, T. Stricker, K. White, O. Olopade, J. N. Ingle, C. Q. Luo, Y. Q. Chen, J. R. Marks, F. Waldman, M. Wiznerowicz, R. Bose, L. W. Chang, A. H. Beck, A. M. Gonzalez-Angulo, T. Pihl, M. Jensen, R. Sfeir, A. Kahn, A. Chu, P. Kothiyal, Z. N. Wang, E. Snyder, J. Pontius, B. Ayala, M. Backus, J. Walton, J. Baboud, D. Berton, M. Nicholls, D. Srinivasan, R. Raman, S. Girshik, P. Kigonya, S. Alonso, R. Sanbhadti, S. Barletta, D. Pot, M. Sheth, J. A. Demchok, K. R. M. Shaw, L. M. Yang, G. Eley, M. L. Ferguson, R. W. Tarnuzzer, J. S. Zhang, L. A. L. Dillon, K. Buetow, P. Fielding, B. A. Ozenberger, M. S. Guyer, H. J. Sofia, J.

D. Palchik, C. G. A. Network, Comprehensive molecular portraits of human breast tumours. *Nature.* **490**, 61-70 (2012).
97. N. R. Rose, M. A. McDonough, O. N. F. King, A. Kawamura, C. J. Schofield, Inhibition of 2-oxoglutarate dependent oxygenases. *Chemical Society Reviews.* **40**, 4364-4397 (2011).
98. P. Urquilla, A. Fong, S. Oksanen, S. Leigh, E. Turtle, L. Flippin, M. Brenner, E. Muthukrishnan, P. Fourney, A. Lin, D. Yeowell, C. Molineaux, Upregulation of endogenous erythropoietin (EPO) in healthy subjects by inhibition of hypoxia inducible factor (HIF) prolyl hydroxylase. *Blood.* **104**, 54A-54A (2004).
99. S. Richard, C. Campello, L. Taillandier, F. Parker, F. Resche, Haemangioblastoma of the central nervous system in von Hippel-Lindau disease. *J Intern Med.* **243**, 547-553 (1998).
100. G. L. Semenza, Targeting HIF-1 for cancer therapy. *Nat Rev Cancer.* **3**, 721-732 (2003).
101. L. Linde, B. Kerem, Introducing sense into nonsense in treatments of human genetic diseases. *Trends in Genetics.* **24**, 552-563 (2008).
102. R. S. Finkel, Read-Through Strategies for Suppression of Nonsense Mutations in Duchenne/Becker Muscular Dystrophy: Aminoglycosides and Ataluren (PTC124). *J Child Neurol.* **25**, 1158-1164 (2010).

2 Identification and biochemical characterisation of a prokaryotic PHD homologue

2.1 The presence of a putative PHD homologue in *Pseudomonas spp.*

The hypoxia inducible factor (HIF) hypoxia sensing and response system is conserved in all animals but likely not in other life forms (*1*). However, the structure solution of human PHD2 led to structurally-guided sequence alignments that predicted the existence of PHD homologues in organisms which did not contain HIF and associated oxygen sensing machinery, such as the gram-negative *Pseudomonas* genus (including *P. putida* and the opportunistic pathogen *P. aeruginosa*) (*2*).

P. putida is non-pathogenic soil bacterium and was the first organism to be patented for its use in the bioremediation of human disasters such as oil spills due to its ability to degrade organic solvents such as toluene and styrene into biodegradable plastics (*3, 4*). In contrast, *P. aeruginosa* is a clinically relevant opportunistic human pathogen. Lung infection by *P. aeruginosa* represents the primary disease phenotype for patients suffering from cystic fibrosis (CF)(*5*). *P. aeruginosa* colonises the hypoxic mucus zones in the airway lumen of CF patients (*6*) and adheres more strongly to CF epithelial cells (*7*). Indeed, *P. aeruginosa* infections have been shown to induce a HIF-mediated hypoxic response via production and excretion of small molecules such as cyanide (*8*). Further, the hypoxic conditions of the CF sputum have been shown to bolster *P. aeruginosa* inherent broad-spectrum antibiotic resistance through multidrug efflux pumps, making *P. aeruginosa* infection very difficult to eradicate (*9-11*). Interestingly,

recent studies have shown that treatment of *P. aeruginosa* with dimethyloxalylglycine (DMOG), a pan 2OG-oxygenases inhibitor, reduces *P. aeruginosa* adhesion to host cells and host cell mortality (*12*), raising the question of a role for 2OG oxygenases in bacterial virulence. Therefore, investigation into the substrate of the *Pseudomonas* PHD homologue (PPHD; 29% identity to PHD2) was pursued with the dual goal of performing the first characterisation of a PHD homologue prokaryotes and determining its functional role in *Pseudomonas spp*.

2.2 Characterisation of a *PPHD* insertional mutant strain of *P. aeruginosa*

2.2.1 PPHD insertional mutant strain shows upregulated production of pyocyanin

Investigations into the role of PPHD in *P. aeruginosa* began by analysing a *PPHD* mutant strain [*P. aeruginosa* PA01 containing a Tn5 transposon insertion in the *PA0310* (*PPHD*) gene was created by the University of Washington Department of Genome Sciences (*13*) and obtained from Dr. Gail Preston (Plant Sciences, Oxford University)]. Knockout of *PPHD* in *P. aeruginosa* results in a striking colour phenotype in which the *PPHD* insertional mutant strain appears blue, attributed to the increased production of pyocyanin, a redox active virulence factor (Figure 2.1 and Figure 2.3)(*14*).

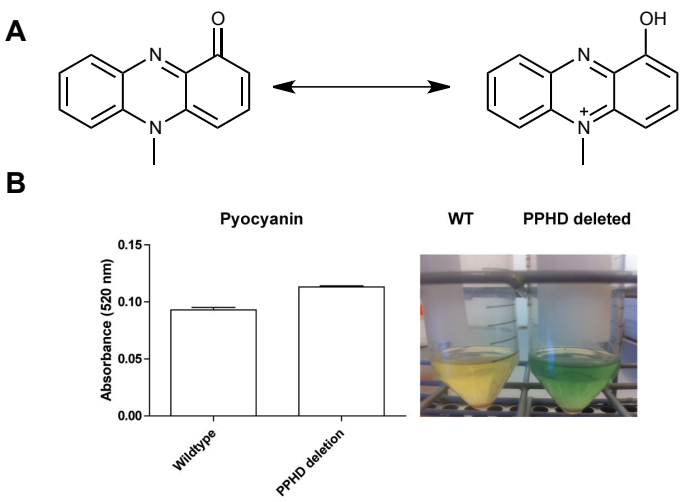

Figure 2.1. *P. aeruginosa PPHD* insertional mutant strain displays increased levels of pyocyanin. (**A**) Pyocyanin (5-methylphenazin-1-one) is a redox-active phenazine secreted by *P. aeruginosa*. (**B**) *P. aeruginosa PPHD* insertional mutant strain produces more pyocyanin. Figure and figure legend are adapted with permission from J.S. Scotti *et al*, Human oxygen sensing may have origins in prokaryotic elongation factor Tu prolyl-hydroxylation. *Proc Nat Acad Sci USA*. In press (2014).

Despite research that suggests pyocyanin induces host cell death through the generation of intracellular reactive oxygen species (ROS) such as H_2O_2 (*15, 16*), the precise mechanisms underlying the effect of pyocyanin have not been determined. Pyocyanin has been shown to upregulate HIF-α in human cells, likely via iron chelation mediated PHD inhibition (*15*). Studies have shown that pyocyanin mediates inactivation of vacuolar ATPase in humans (*17*), induces neutrophil apoptosis in mice (*18*), and is lethal to the model organism *C. elegans* (*19*). Importantly, concentrations of pyocyanin recovered from the sputum of CF patients have shown to inhibit the beating of human cilia *in vitro* (*20*), suggesting a direct link between pyocyanin and *P. aeruginosa* virulence in humans.

2.2.2 Evidence against a PPHD-dependent effect on P. aeruginosa virulence

Experiments in section 2.2.2 performed in collaboration with Dr. Lesley Bowman.

To test the effect of *PPHD* knockout on *P. aeruginosa* virulence, the association was measured between *P. aeruginosa* wildtype and *PPHD* insertional

mutant strains to human lung alveolar basal epithelial cells (A549 cells), which are susceptible to *P. aeruginosa* invasion in an immune-compromised cystic fibrosis patient (Figure 2.2)(*5*). No difference was observed between the wildtype and *PPHD* mutant strains.

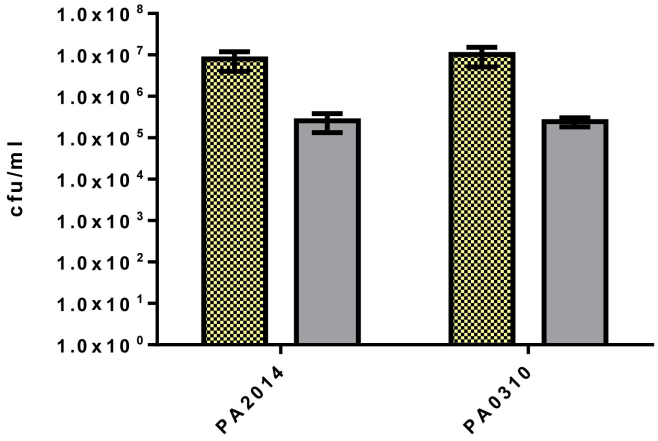

Figure 2.2. Association of *P. aeruginosa* wildtype (*PA2014*) and *PPHD* (*PA0310*) insertional mutant strain with A549 cells. Yellow bars represent the density of input bacteria and grey bars represent numbers of cell associated bacteria. Bacteria were cultured to mid-log phase, washed and added at a MOI of 30:1 to a confluent layer of A549 cells seeded at a density of 5 x 10^5 cells/ml. After 2 h incubation, non-adherent bacteria were removed by repeated washing. Cells were treated with 1 % saponin and cell lysates were plated for cell enumeration. Data is the mean of 3 biological replicates ± S.D.

2.2.3 PPHD insertional mutant strain shows impaired growth in the presence of iron chelators

Experiments in section 2.2.3 were performed by Dr. Steinar Paulsen.

Phenotypic analyses identified that the *P. aeruginosa PPHD* insertional mutant strain was more sensitive to growth in the presence of 2,2-bipyridine, an iron chelator (Figure 2.3), indicating that PPHD may play a role in iron metabolism. The link between iron metabolism and the requirement for the ferrous ion for PHD catalysis also provided the first hint of similarity between PPHD and the human PHDs, in that inhibition of the PHDs via iron chelators causes HIF-α upregulation in human cells (*21*).

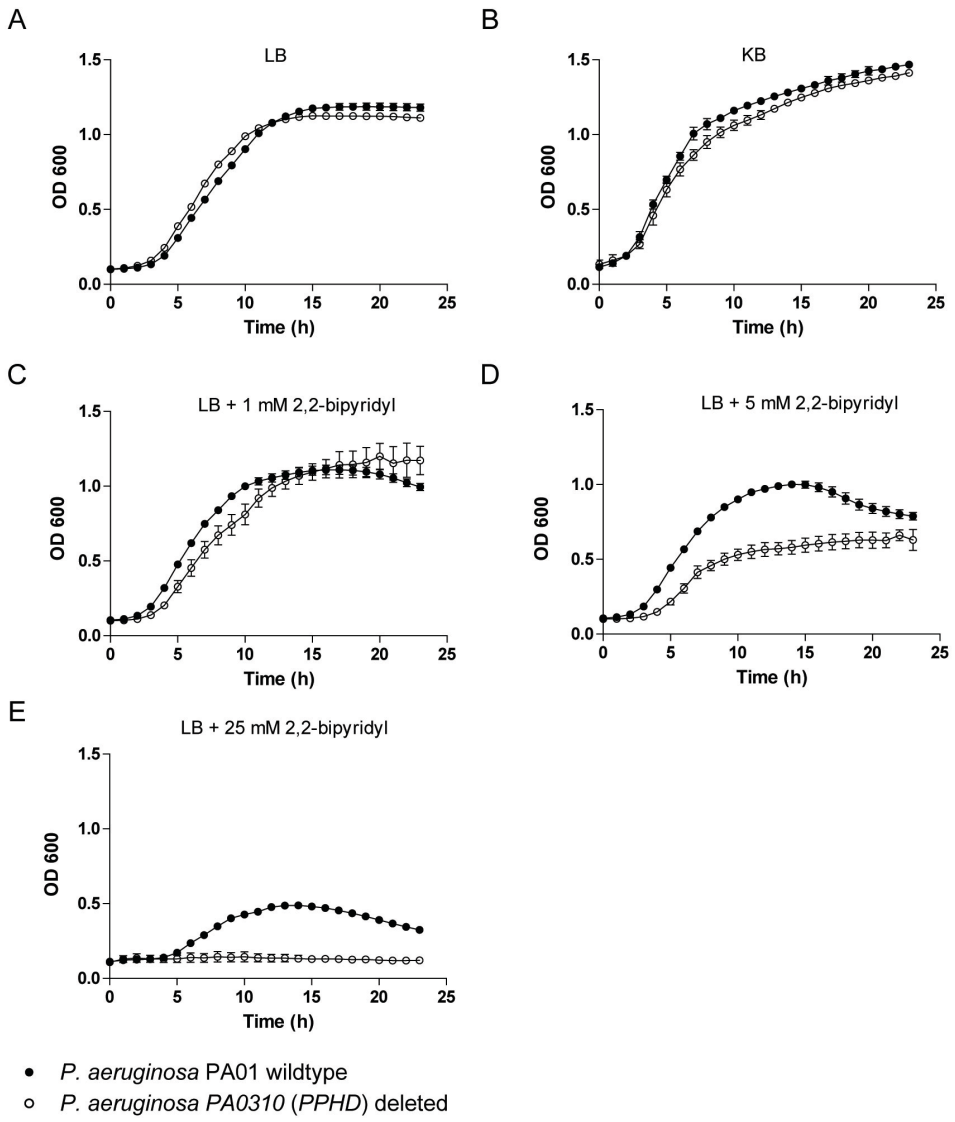

Figure 2.3. A *P. aeruginosa PPHD* insertional mutant strain shows impaired growth in the presence of iron-chelators. (**A**-**E**) Growth curves of *P. aeruginosa* wildtype and knockout in the presence of 2,2-bipyridine revealing inhibited growth in the *PPHD* insertional mutant strain. Figure and figure legend are adapted with permission from J.S. Scotti *et al*, Human oxygen sensing may have origins in prokaryotic elongation factor Tu prolyl-hydroxylation. *Proc Nat Acad Sci USA*. In press (2014).

PPHD transcription was then investigated in multiple different contexts, including in the presence of iron chelators, by quantitative real-time polymerase chain reaction (qRT-PCR) (Figure 2.4). qRT-PCR is a method used for relative quantification of mRNA of multiple target genes of interest in different cellular

contexts in which total RNA is extracted from lysed cells, reverse transcribed to cDNA, and PCR amplification of 100-200 bp fragments of the genes of interest is monitored by a fluorescent probe (*22*). Accurate analysis of qRT-PCR data relies on comparison to a housekeeping gene of which expression has been shown to be invariable across numerous conditions (typically *rpoD* in *Pseudomonas spp.*)(*23*).

P. aeruginosa PA01 qRT-PCR of PA0310 (*PPHD*) gene

Growth	Ct	ΔCT	ΔΔCT	Fold increase relative to LB
LB (OD600 = 0.4)	23	3	0	1
KB	23	2.8	-0.2	1.1
LB_KNO_3	26.5	3.5	0.5	0.7
OD600=1.6	24.5	2.2	-0.8	1.7
OD600=0.8	25	3.3	0.3	0.4
5 mM 2,2-dipyridyl	24.5	3.9	-0.9	1.8
Anaerobic	25.5	3	0	1.0

Figure 2.4. qRT-PCR of *P. aeruginosa PPHD* in different conditions. Transcription of *PPHD* monitored from *P. aeruginosa* grown in LB (Luria Broth), KB (King's Broth), LB + KNO_3, LB at late log-phase (OD_{600}=0.8) LB in stationary phase (OD_{600}=1.6), LB + 5 mM 2,2-bipyridine, and LB in anaerobic conditions. Ct is defined as the cycle at which the fluorescence is determined to be statistically significant above background; values were calculated using ABI Prism 7300 SDS software and correspond to the mean of three experiments, each performed in triplicate.

The qRT-PCR results reveal that the transcription of *PPHD* in *P. aeruginosa* is upregulated in the presence of iron chelators and in stationary phase relative to log phase, suggesting a link between PPHD and iron regulation in *P. aeruginosa*. There is no change in *PPHD* transcription in anoxia.

2.3 Investigation into a PPHD substrate

2.3.1 Expression and purification of recombinant PPHD

Initial characterisation of a *P. aeruginosa PPHD* insertional mutant strain prompted the investigation into possible PPHD substrates. The non-pathogenic

strain *P. putida* was chosen for recombinant expression and purification of PPHD (all subsequent mentions of PPHD refer to $PPHD_{putida}$ unless otherwise noted). The *PPHD* gene was amplified by PCR from *P. putida* genomic DNA and cloned into pET28a vector with an *N*-terminal hexahistidine tag. pET28a_PPHD was transformed into *E. coli* BL21 (DE3) and PPHD overexpression was induced through addition of isopropyl β-D-1-thiogalactopyranoside (IPTG). After cell harvesting and lysis, large quantities (>70 mg) of >95% pure (by SDS-PAGE), recombinant PPHD was obtained from a two-step purification procedure consisting of initial Ni-affinity chromatography and subsequent size exclusion chromatography (Figure 2.5; for details see Experimental Procedures).

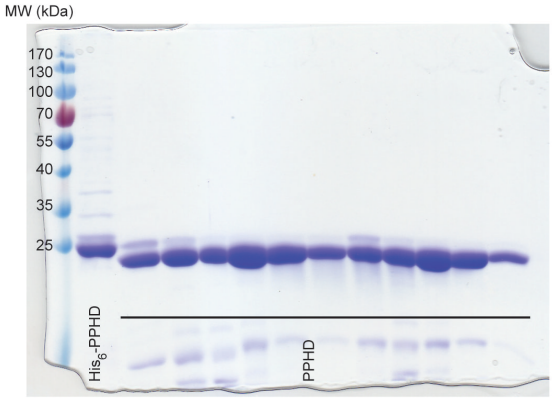

Figure 2.5. Purification of recombinant PPHD. Representative SDS-PAGE gel of recombinant PPHD. His_6-PPHD was purified by Ni-affinity chromatography after which the *N*-terminal hexahistidine tag was cleaved overnight with thrombin and pure PPHD was isolated by size exclusion chromatography.

2.3.2 Analysis of endogenous PPHD binding partners

To analyse possible PPHD substrates, it was first necessary to identify intracellular PPHD binding partners. Purified recombinant PPHD with an *N*-terminal hexahistidine tag was incubated with Ni-affinity resin and *P. putida* cell lysate, after which low imidazole wash pulled out proteins bound to PPHD,

revealing elongation factor Tu (EF-Tu) as a predominant PPHD binding partner (Table 2.6)(for a detailed description of the role of EF-Tu in cells, see section 2.4).

Table 2.6. Interaction studies of hexahistidine-tagged PPHD$_{putida}$ in *P. putida* reveal possible association between PPHD$_{putida}$ and EF-Tu. The higher protein score suggests increased abundance and confidence in the correct peptide identification. Peptide number, peptide score and sequence refer to number of peptides identified per protein and relative number of *b/y* ions matched per representative peptide. Q88CM1 refers to PPHD$_{putida}$. See Experimental Procedures for details. Figure and figure legend are adapted with permission from J.S. Scotti *et al*, Human oxygen sensing may have origins in prokaryotic elongation factor Tu prolyl-hydroxylation. *Proc Nat Acad Sci USA*. In press (2014).

Uniprot Accession	Protein name	Gene Name	Protein Score	Peptide Number	Peptide Score	Peptide Sequence
Q88QN7	Elongation factor Tu-B	*tufB*	854	104	36.09	LLDEGR
Q88QP8	Elongation factor Tu-A	*tufA*	685	104	36.09	LLDEGR
Q88CM1	Putative uncharacterized protein	*PP_5159*	836	135	28.45	ALAAECR
Q88BZ2	Putative uncharacterized protein	*PP_5391*	340	2088	1.91	MAAAKTPEAR
Q88JK1	Universal stress protein family	*PP_2648*	176	89	0.73	TIELAK
Q88QN6	30S ribosomal protein S10	*rpsJ*	146	7212	79.74	LIDQSTQEIVETAKR
Q88PS2	Peptidyl-prolyl cis-trans isomerase	*slyD*	117	166	8.38	MLIAANK
Q88DZ0	Ketol-acid reductoisomerase	*ilvC*	78	2486	0.68	NEIEPNIKK
Q88QM9	30S ribosomal protein S3	*rpsC*	78	225	8.29	AVQNAMR
Q88EH2	Pterin-4-alpha-carbinolamine dehydratase	*phhB*	73	1235	2.72	VAETAEGRK
Q88MI0	30S ribosomal protein S2	*rpsB*	54	1290	9.32	IHIVNLEK
Q88QM2	30S ribosomal protein S14	*rpsN*	38	4485	16.48	LTGRPHGVYRK
Q88KB0	Putative uncharacterized protein	*PP_2380*	37	3208	1.57	EVKAIELPAGK
Q88MP1	2,3,4,5-tetrahydropyridine-2,6-dicarboxylate N-succinyltransferase	*dapD*	36	1981	2.05	NSLNGAVECK
Q88BZ1	Putative uncharacterized protein	*PP_5392*	35	882	15.77	IFDLEQR

2.3.3 PPHD hydroxylates elongation factor Tu (EF-Tu) Pro54 containing peptide

The strong association between PPHD and EF-Tu was of interest in the light of previous results in *Shewanella oneidensis*, which contains a putative hydroxylase closely related to PPHD (38% identity). Global proteomic studies on *S. oneidensis* showed that Pro54 of EF-Tu$_{oneidensis}$ was modified by a +16 Da shift, consistent with the incorporation of a single oxygen atom (*24*). Therefore, a series of tiled synthetic peptide arrays encompassing all 19 prolines in the entire EF-Tu$_{putida}$ sequence were tested as recombinant PPHD substrates by matrix-assisted laser desorption/ionisation (MALDI) mass spectrometry (MS)(Table 2.7).

Table 2.7. Peptides based on *P. putida* EF-Tu (Uniprot: Q88QP8) that were screened for PPHD$_{putida}$ dependent hydroxylation. The 14 distinct peptides encompass all 19 prolines in the EF-Tu sequence. Methionines were mutated to other amino acid residues in order to avoid potential false positives due to methionine oxidation in the mass spectrometer. All peptides were synthesised to produce a *C*-terminal amide residue. Peptide screening was performed by Dr. Wei Ge. Figure and figure legend are adapted with permission from J.S. Scotti *et al*, Human oxygen sensing may have origins in prokaryotic elongation factor Tu prolyl-hydroxylation. *Proc Nat Acad Sci USA*. In press (2014).

Peptide Sequence	Residue Range	Mutations from native EF-Tu	Hydroxylation Observed
AKEKFDRSL**P**HVNVGTIGH	2-20	-	NO
IVEFKIDSA**P**EEKARGITI	44-63	-	**YES**
HYAHVDC**P**GHADYVKNLITG	76-95	M92L	NO
ILVCSAADG**P**A**P**QTREHILL	103-122	M113A	NO
LLSRQVGV**P**YIVVFLNKADL	121-140	-	NO
DLLSTYDF**P**GDDT**P**IIIGSA	156-175	-	NO
VETLDAYI**P**E**P**VRAIDQ**P**FL	196-215	S201A	NO
PVRAIDQ**P**FLL**P**IEDVFSIS	206-225	M216L	NO
ERGIVRVQD**P**LEIVGLRDTT	236-255	-	NO
ERGQVLVK**P**GSVK**P**HTKFTA	291-310	-	NO
SKEEGGRHT**P**FFKGYR**P**QFY	316-335	-	NO
GRHT**P**FFKGYR**P**QFYFRTTD	321-340	-	NO
VTGNCEL**P**EGVELVL**P**GDNI	341-360	M353L, M355L	NO
EL**P**EGVEAVA**P**GDNIQLTVT	346-365	M353A, M355A, M362L	NO

MALDI-MS relies laser-induced ionisation of sample by a matrix, typically a small organic molecule such as α-cyano-4-hydroxycinnamic acid (CHCA) and is

an effective method for screening 20mer (~2000-2500 Da) oligopeptide substrates (*25*). In agreement with the *S. oneidensis* results, a +16 Da shift was observed on a peptide that is identical to residues 44-63 of EF-Tu and contains Pro54 as the central and only proline residue (sequence: H_2N-IVEFDKIDSAPEEKARGITI-$CONH_2$, mol. wt. 2231.5 Da)(Figure 2.8*A*). Subsequent MS/MS analyses of the modified peptide (EF-Tu_{44-63}) revealed selective Pro54 hydroxylation (Hyp54)(Figure 2.8*B*).

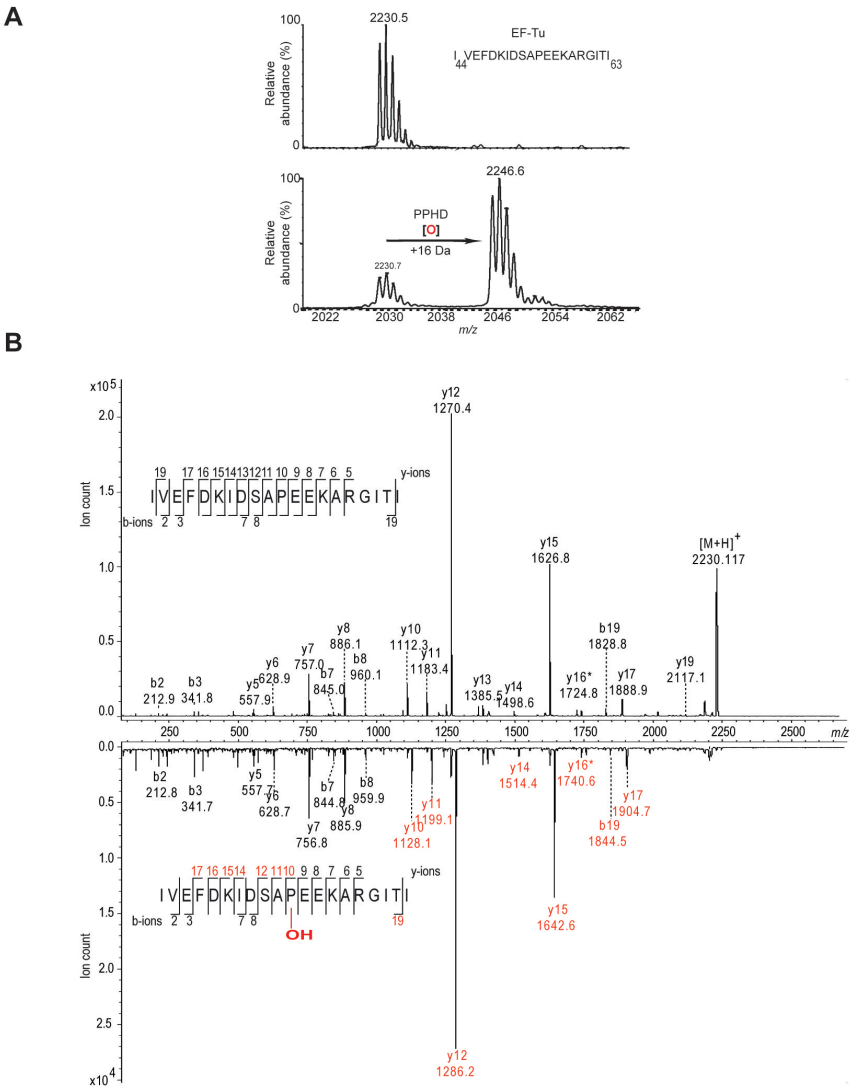

Figure 2.8. Identification of a PPHD substrate. (**A**) EF-Tu is a PPHD substrate; MALDI spectrum showing a +16 Da peak revealing PPHD-dependent prolyl-hydroxylation of EF-Tu$_{44\text{-}63}$ at Pro54. (**B**) MS/MS analysis of modified and unmodified EF-Tu$_{44\text{-}63}$ confirms hydroxylation at Pro54 (Hyp54). Figure and figure legend are adapted with permission from J.S. Scotti *et al*, Human oxygen sensing may have origins in prokaryotic elongation factor Tu prolyl-hydroxylation. *Proc Nat Acad Sci USA*. In press (2014).

2.3.4 PPHD catalyses trans-4 prolyl-hydroxylation

Experiments performed in collaboration with Dr. Nikita Loik.

It was of interest to next establish the stereochemistry of PPHD-catalysed prolyl-hydroxylation. 1 mg of EF-Tu$_{44\text{-}63}$ peptide fully hydroxylated at Pro54 was

hydrolysed in boiling 5.7 M HCl, derivatised with 6-aminoquinolyl-*N*-hydroxysuccinimidyl carbamate, and subjected to LC-MS/MS amino-acid analysis (*26*), in which the stereochemistry of hydroxyproline was determined by comparison of elution times with the two hydroxyproline standards (for details, see Experimental Procedures). It was shown that, similar to PHD2 and the CP4Hs (*27*), PPHD hydroxylates proline in the *trans*-4 position (Figure 2.9).

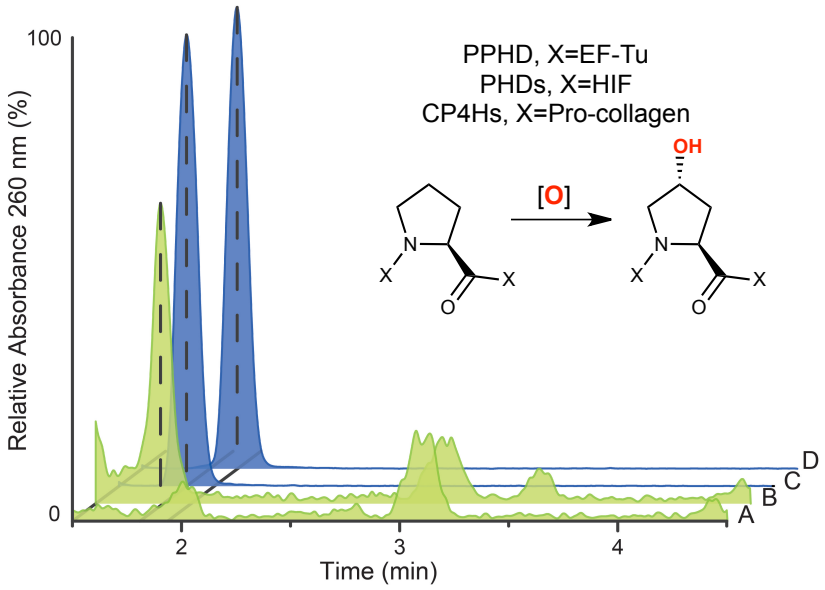

Figure 2.9. PPHD catalyses *trans* 4-hydroxylation of prolyl residues, identical to the PHDs and CP4Hs. Amino-acid analysis demonstrates that PPHD hydroxylates EF-Tu$_{44-63}$ oligopeptide substrate at Pro54 in the 4-*trans* (2*S*,4*R*) stereochemistry. (**A**) EF-Tu$_{44-63}$ control; (**B**) EF-Tu$_{44-63}$ modified Hyp54; (**C**) *trans*-4-hydroxyproline standard; (**D**) *trans*-3-hydroxyproline standard. PPHD, the PHDs and CPHs all catalyse 4-*trans* prolyl-hydroxylation. Figure and figure legend are adapted with permission from J.S. Scotti *et al*, Human oxygen sensing may have origins in prokaryotic elongation factor Tu prolyl-hydroxylation. *Proc Nat Acad Sci USA*. In press (2014).

2.3.5 Expression and purification of recombinant EF-Tu

Notably, productive *in vitro* hydroxylation of peptides does not necessarily imply hydroxylation of full-length protein *in vitro* or *in vivo*, as demonstrated for other 2OG oxygenases (e.g. JMJD6) (*28*). Therefore, the *tufA* gene encoding for EF-Tu in *P. putida* was cloned into a pET28a expression vector

with a *N*-terminal hexahistidine tag, overexpressed in *E. coli*, and purified using Ni-affinity and size exclusion chromatography as per PPHD (Figure 2.10). Given that *E. coli* does not contain a PPHD homologue, recombinant EF-Tu expressed in *E. coli* was subjected to trypsin digestion and LC-MS/MS to confirm that EF-Tu was indeed not hydroxylated in *E. coli* (Figure 2.11).

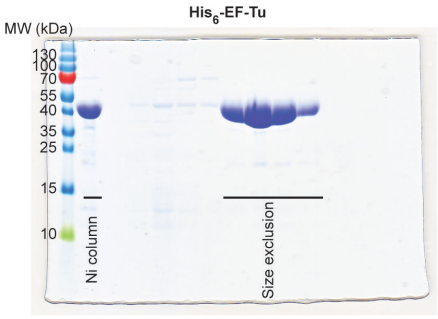

Figure 2.10. Purification of recombinant EF-Tu. Representative SDS-PAGE gel of recombinant EF-Tu. His_6-EF-Tu was purified by Ni-affinity and subsequent size exclusion chromatography.

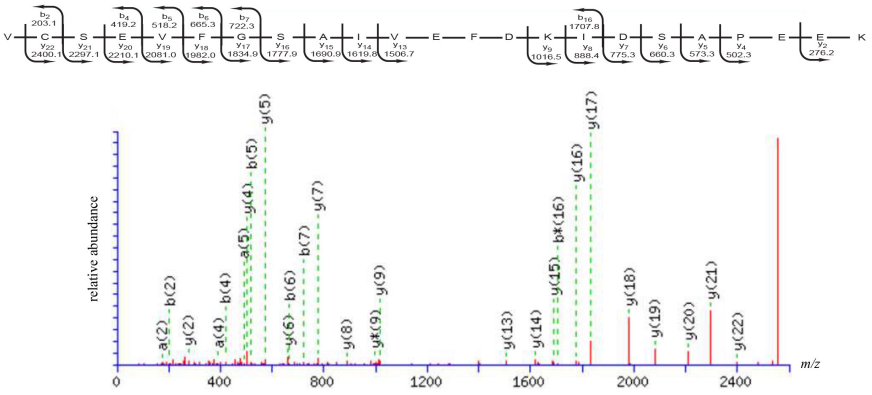

#	a	a*	b	b*	Seq.	y	y*	#
1	72.0808		100.0757		V			23
2	**175.0900**		**203.0849**		C	**2400.1275**	2383.1010	22
3	262.1220		290.1169		S	**2297.1183**	2280.0918	21
4	**391.1646**		**419.1595**		E	**2210.0863**	2193.0598	20
5	**490.2330**		**518.2279**		V	**2081.0437**	2064.0172	19
6	637.3014		**665.2963**		F	**1981.9753**	1964.9488	18
7	694.3229		**722.3178**		G	**1834.9069**	1817.8804	17
8	781.3549		809.3498		S	**1777.8854**	1760.8589	16
9	852.3920		880.3869		A	**1690.8534**	1673.8269	15
10	965.4761		993.4710		I	**1619.8163**	1602.7897	14
11	1064.5445		1092.5394		V	**1506.7322**	1489.7057	13
12	1193.5871		1221.5820		E	1407.6638	1390.6373	12
13	1340.6555		1368.6504		F	1278.6212	1261.5947	11
14	1455.6824		1483.6774		D	1131.5528	1114.5263	10
15	1583.7774	1566.7509	1611.7723	1594.7458	K	**1016.5259**	**999.4993**	9
16	1696.8615	1679.8349	1724.8564	**1707.8298**	I	**888.4309**	871.4044	8
17	1811.8884	1794.8619	1839.8833	1822.8568	D	**775.3468**	758.3203	7
18	1898.9204	1881.8939	1926.9154	1909.8888	S	**660.3199**	643.2933	6
19	1969.9576	1952.9310	1997.9525	1980.9259	A	**573.2879**	556.2613	5
20	2067.0103	2049.9838	2095.0052	2077.9787	P	**502.2508**	485.2242	4
21	2196.0529	2179.0264	2224.0478	2207.0213	E	405.1980	388.1714	3
22	2325.0955	2308.0690	2353.0904	2336.0639	E	**276.1554**	259.1288	2
23					K	147.1128	130.0863	1

Figure 2.11. Recombinant *P. putida* EF-Tu expressed in *E. coli* is not hydroxylated. MASCOT MS/MS spectrum of EF-Tu peptide fragment containing Pro54 (residues 35-57; *m/z* 2498.2 Da) reveals that recombinant *P. putida* EF-Tu is not hydroxylated.

2.3.6 PPHD hydroxylates full-length EF-Tu protein at Pro54

It was then of interest to investigate whether PPHD hydroxylates full-length EF-Tu at Pro54 *in vitro*. Therefore, full-length, purified PPHD and EF-Tu were incubated together in the presence of Fe(II), 2OG, and ascorbate in an analogous manner to peptide assays. Reactions were quenched subjected to trypsin digestion; tryptic peptides encompassing EF-Tu residues 35-57 (*m/z* 2555.2 and *m/z* 2571.2 correspond to EF-Tu$_{35\text{-}57}$ Pro54 and Hyp54, respectively)

were analysed by LC-MS/MS to quantify hydroxylation at Pro54. MS/MS confirmed that PPHD catalyses hydroxylation of Pro54 of full-length EF-Tu in a manner dependent on Fe(II), 2OG, and ascorbate (Figure 2.12).

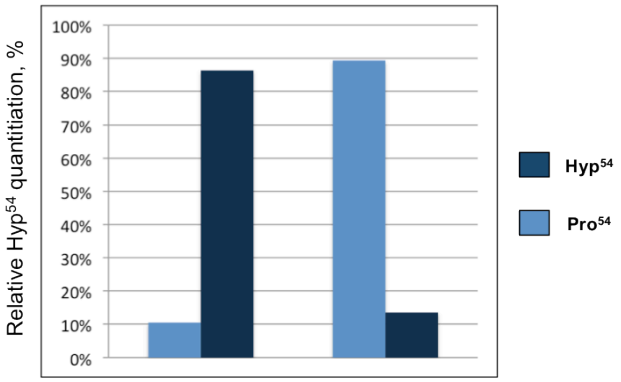

	Reaction	Control
EFTu	✓	✓
PPHD	✓	✓
Fe	✓	
2OG	✓	
Asc	✓	

Figure 2.12. PPHD hydroxylates EF-Tu full-length protein in a Fe(II), 2OG, and ascorbate dependent manner. Quantification was performed in the MASCOT suite by analysing the total ion score corresponding to digested peptides containing Pro54/Hyp54 – Pro54: *m/z* 852.74, $[M+3H]^{3+}$; Hyp54: *m/z* 858.07 $[M+3H]^{3+}$.

2.3.7 Monitoring endogenous EF-Tu hydroxylation: creation of a PPHD knockout strain of P. putida

Having confirmed that PPHD catalyses hydroxylation of both EF-Tu peptide fragment and full-length protein *in vitro*, it was of interest to establish the endogenous hydroxylation status of EF-Tu in *Pseudomonas*. For this series of experiments, it was necessary to generate a *PPHD* knockout strain of *P. putida*. Therefore, a full-knockout strain was generated by two-step allelic replacement (for a scheme detailing the creation of a *PPHD* knockout strain in *P. putida*, see Figure 2.13)(*29, 30*).

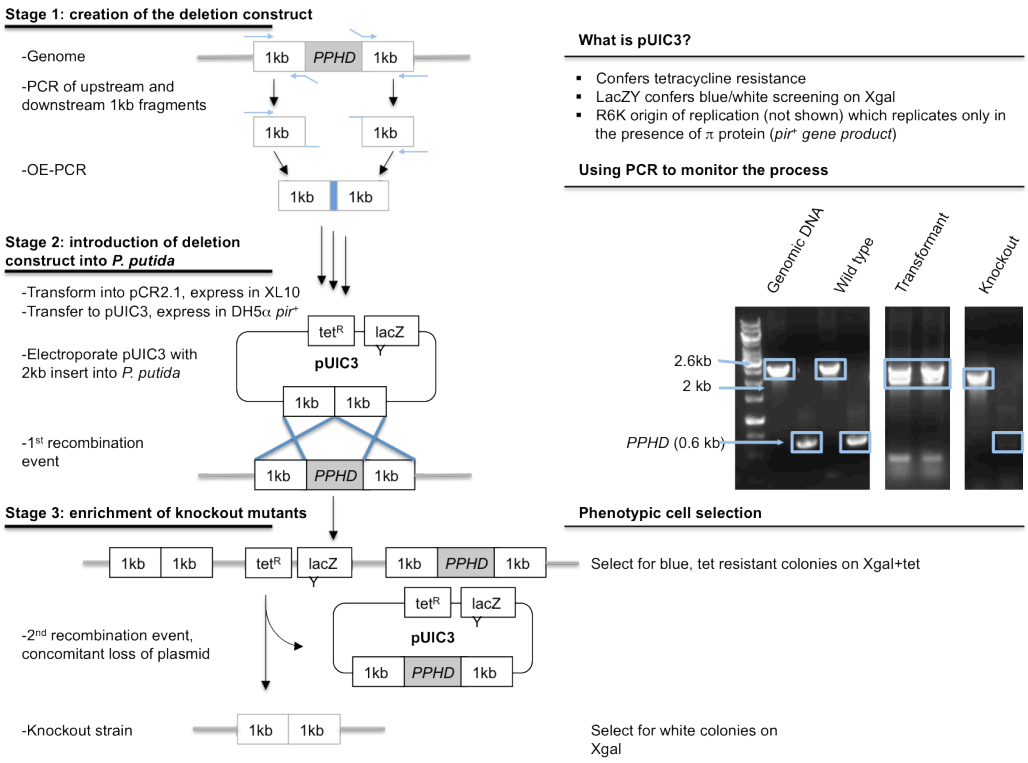

Figure 2.13. Creation of a *PPHD* knockout strain of *P. putida*. (**A**) Step-by-step schematic illustrating the mechanism of full-gene knockout in *P. putida* by a two-step double homologous recombination strategy. (**B**) Characteristics of suicide vector pUIC3. (**C**) PCR and agarose gel electrophoresis can be used to monitor the process and confirm successful creation of knockout strain (for detail, see Experimental Procedures).

The knockout strain was then transformed with the constitutively active *Pseudomonas* expression vectors pBBR5_MCS2_PPHD and pBBR5_MCS2_PPHD(D126A) encoding for PPHD and a catalytically inactive PPHD mutant with an alanine point mutation in its metal-binding aspartate residue (both plasmids obtained from Dr. Gail Preston, University of Oxford). *P. putida* UWC1 (KT2440) wildtype, the *PPHD* knockout strain, the *PPHD* knockout strain expressing recombinant PPHD, and the *PPHD* knockout strain expressing catalytically inactive PPHD were grown to stationary phase, lysed, and the soluble fraction was analysed by SDS-PAGE. The EF-Tu containing band was excised from the gel and subjected to trypsin digested and LC-MS/MS.

Unfortunately, despite high (>50%) peptide coverage of the EF-Tu protein, the peptide containing Pro54 was not observed. The expected tryptic-peptide sequence of *P. putida* EF-Tu (EF-Tu_{50-57}: H_2N-IDSAPEEK-CO_2H) in the region surrounding Pro54 was thought to present potential issues for ionisation in the mass spectrometer due to its strong overall negative charge. Trypsin is known to miss cleavage sites if they are adjacent to a negatively charged residue, such as aspartate (*31*), suggesting that different proteases, and thus different lengths of proteolytic peptides, may promote the detection of a peptide containing Pro54 by varying its length, polarity, and charge state. However, after digestions with trypsin, ArgC, and trypsin combined with acetylation of lysine residues (such that trypsin only cleaves *C*-terminal to arginine residues)(*32*), the peptide containing Pro54 was still not observed.

2.3.8 Endogenous EF-Tu is hydroxylated at Pro54 in P. aeruginosa

It was of interest then to demonstrate endogenous EF-Tu hydroxylation in *P. aeruginosa*. A strain of *P. aeruginosa* PAO1 containing a transposon insertion in the *PA0310* (*PPHD*) gene (*13*) was obtained (Dr. Gail Preston, University of Oxford). Slight differences exist between the peptide sequences of the switch I loop regions of EF-$Tu_{aeruginosa}$ and EF-Tu_{putida}. EF-Tu residues 47-63 are identical except for two mutations, $Lys49_{putida}$/$Gln49_{aeruginosa}$ and $Ser52_{putida}$/$Asn52_{aeruginosa}$, both of which were thought to affect the ionisation of the peptide of interest by LC-MS/MS.

P. aeruginosa PAO1 wildtype and a *PA0310* (*PPHD*) insertional mutant strain were grown to stationary phase in aerobic (21% O_2) and anaerobic conditions (<0.01% O_2), lysed, analysed by SDS-PAGE, and the EF-Tu containing

band was excised in the same way as for *P. putida*. In contrast to experiments performed in *P. putida*, ions corresponding to the expected tryptic-peptide sequence of *P. aeruginosa* EF-Tu (EF-Tu_{46-59}: H_2N-AFDQIDNAPEEKAR-CO_2H) in the region surrounding Pro54 were observed, perhaps due to its longer comparative length (14 residues for *P. aeruginosa* vs 8 residues for *P. putida*). The results confirmed that EF-$Tu_{aeruginosa}$ hydroxylation was observed at Pro54 in the wildtype, but not in the $PPHD_{aeruginosa}$ insertional mutant strain when grown in aerobic conditions. Further, EF-Tu hydroxylation was not observed in either the wildtype or $PPHD_{aeruginosa}$ insertional mutant strain when grown in anaerobic conditions, confirming that EF-Tu is a PPHD substrate in cells and PPHD-dependent hydroxylation of EF-Tu is oxygen dependent (Figure 2.14) [mass spectometric analyses were performed by Dr. Holger Kramer].

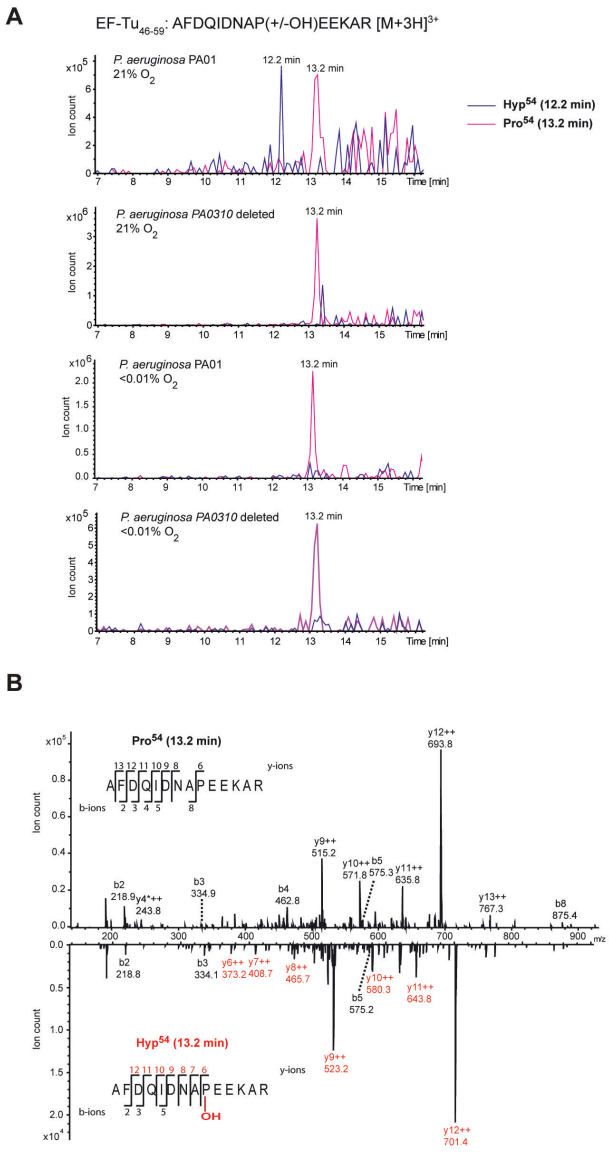

Figure 2.14. Hydroxylation of EF-Tu at Pro54 is catalysed by PPHD in *P. aeruginosa*. (**A**) Extracted ion chromatograms (EICs) and (**B**) associated MS/MS analyses of *P. aeruginosa* PA01 wildtype and *PA0310* (*PPHD*) insertional mutant strains grown in aerobic (21% O_2) and anaerobic (<0.01% O_2) conditions demonstrates EF-Tu Pro54 is hydroxylated in cells in the wildtype and not mutant strain in an oxygen dependent manner (*m/z* 535.25 and *m/z* 540.59 correspond to Pro54 and Hyp54, respectively). Figure and figure legend are adapted with permission from J.S. Scotti *et al*, Human oxygen sensing may have origins in prokaryotic elongation factor Tu prolyl-hydroxylation. *Proc Nat Acad Sci USA*. In press (2014).

Overall, the results in this section demonstrate that PPHD catalyses the *trans* 4-hydroxylation of EF-Tu residue Pro54 in 3 different contexts: i) a 20mer

EF-Tu$_{44-63}$ oligopeptide fragment, ii) full-length EF-Tu protein, and iii) endogenously in cells.

2.4 The role of EF-Tu in prokaryotes

2.4.1 EF-Tu is critical for bacterial translation

Protein synthesis on the ribosome requires a family of crucial and highly conserved GTP-hydrolysing proteins known as GTPases (*33*). The GTPase protein superfamily encompasses notable subfamilies implicated in a plethora of intracellular signalling pathways, including the **Ra**t **s**arcoma (Ras) GTPases, which comprise the human oncogenes *HRAS*, *KRAS*, and *NRAS*, and G proteins, which are activated by G protein-coupled receptors (GPCRs)(*34, 35*). The translational GTPases are characterised by a GTP-binding domain, which is conserved from prokaryotes through to eukaryotes, and GTP-hydrolysis mediated conformational changes in two conserved loop regions, known as switch I and switch II (*36*). EF-Tu is a GTPase and in rapid growth conditions is the most abundant protein in most bacterial cells, containing on average ~10-fold higher concentration than ribosomes (*37, 38*). Yet, like ribosomes, EF-Tu concentrations vary significantly with growth rate (*38, 39*). The intracellular concentration of EF-Tu can be said to mirror its critical role in bacterial translation – to deliver aminoacyl-tRNAs (aa-tRNAs) to the ribosome A-site via a ternary complex of aa-tRNA:EF-Tu:GTP (Figure 2.15 and Table 2.16)(*40-42*).

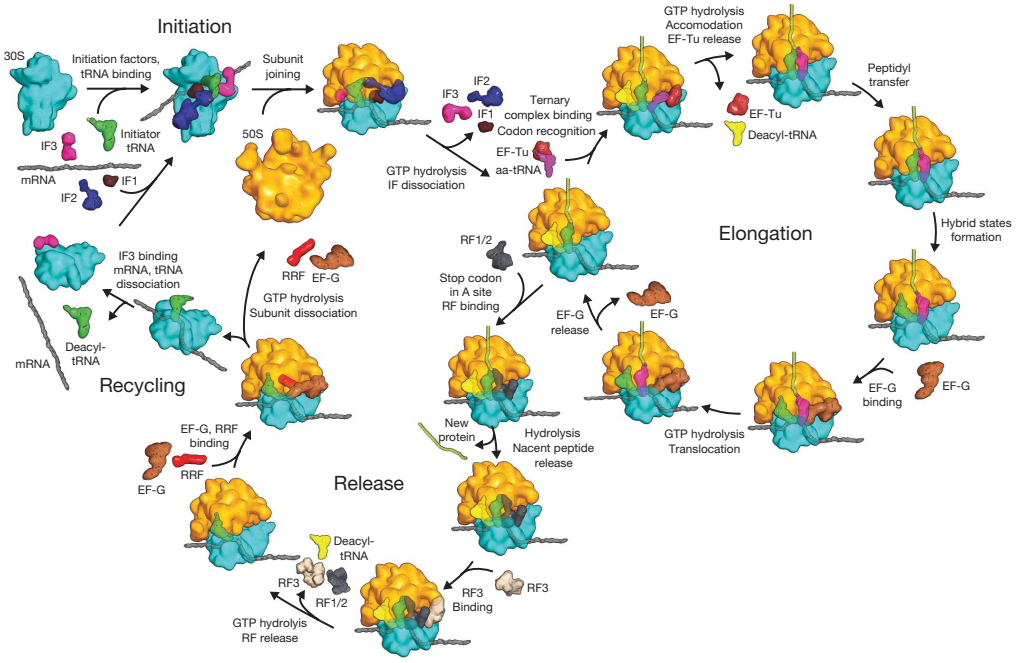

Figure 2.15. Overview of bacterial translation. EF-Tu is critical to the elongation phase where it brings aa-tRNA to the ribosome in a ternary complex of EF-Tu:GTP:aa-tRNA; successful codon-anticodon recognition triggers EF-Tu GTP hydrolysis and release from the ribosome. Reprinted by permission from Macmillan Publishers Ltd: [*Nature*] (T. M. Schmeing, V. Ramakrishnan, What recent ribosome structures have revealed about the mechanism of translation. *Nature.* **461**, 1234-1242 (2009)), copyright (2009) Reprinted with permission from the Nature Publishing Group. www.nature.com

Table 2.16. **Summary of proteins involved in bacterial translation.** Overview of bacterial ribosomal associated proteins involved in translation and their proposed function(s) during the three phases of translation: initiation, elongation, and termination (*42*).

Initiation	
IF1	Binds to 30S in the A-site, preventing tRNA from entering and increases affinity for IF2.
IF2	A GTPase. Binds along with IF1, fMet-tRNA(fMet), and mRNA to 30S-IF3 complex to produce the 30S initiation complex (30S-IC). Promotes 30S-IC and 70S subunit joining, followed by IF3 release. Subsequent IF2 GTP hydrolysis and phosphate release promotes IF2 and IF1 release and movement of the fMet-tRNA(fMet) into the peptidyl transferase centre.
IF3	Binds to free 30S subunit post termination - first step in bacterial translation, stimulates association of other IFs to form 30S-IC. Prevents the reassociation of ribosomal subunits in the absence of an initiation complex.
Elongation	
EF-Tu	Delivers aminoacyl-tRNAs (aa-tRNAs) to the A site on the ribosome via an EFTu:GTP:aa-tRNA ternary complex.
EF-Ts	Catalyses nucleotide exchange of GDP to GTP in EF-Tu via ternary complex.
EF-G	Mediates GTP-driven translocation, moving the mRNA and tRNAs with respect to the ribosome. Also involved in ribosomal recycling.
Termination	
RF1	Binds UAA and UAG stop codons, triggering peptide release.
RF2	Binds UAA and UGA stop codons, triggering peptide release.
RF3	A GTPase. Binds to ribosome-RF1/2 complex in GDP form, causing RF3 to exchange GDP for GTP, resulting in RF1/2 release from the ribosome, subsequent GTP hydrolysis causes RF3 to dissociate leaving an mRNA and a deacylated tRNA in the P site.
RRF	Ribosome recycling factor: works with EF-G to dissociate the ribosomal subunits. GTP hydrolysis by EF-G seems to be involved.

2.4.2 Mechanism of EF-Tu GTP hydrolysis on the ribosome

While the GTPase activity of isolated EF-Tu is low (*43*), successful binding of an aa-tRNA to its cognate mRNA codon on the ribosome dramatically increases that rate of EF-Tu GTPase activity, despite the 80 Å distance separating the codon-anticodon recognition and EF-Tu nucleotide binding sites (*41, 44, 45*). Mutation studies have shown that EF-Tu His84 is critical for successful GTP hydrolysis on the ribosome; His84Ala reduces the rate of EF-Tu GTP hydrolysis by 10^6-fold (*46*). Initial structural analyses on isolated EF-Tu trapped in its active GTP-bound conformation revealed the presence of a 'hydrophobic gate' consisting of residues Val20 of the P loop (*E. coli* residues 18-23) and Ile60 of the switch I loop (*E. coli* residues 40-62). The gate was predicted to 'open' upon ribosome-binding, allowing His84 to act as a general base and abstract a proton from a buried water molecule coordinating it for nucleophilic attack on the γ-phosphate of GTP (Figure 2.17)(*47-49*).

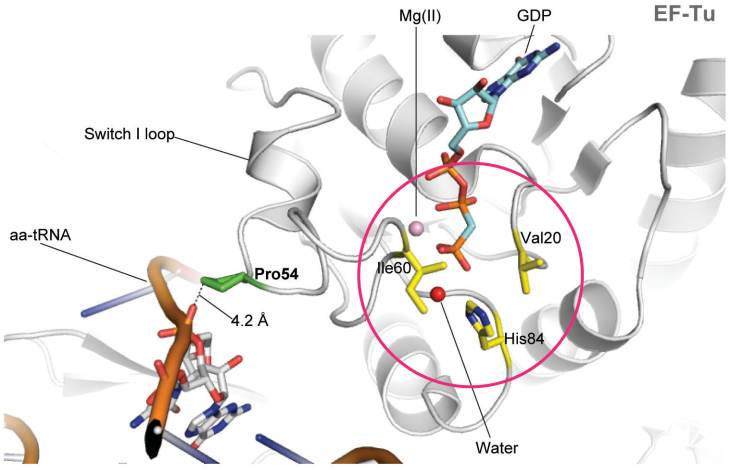

Figure 2.17. View from a crystal structure of *T. thermophilus* EF-Tu stalled on the ribosome in a translationally active state showing the location of Pro54 (PDB ID: 2XQD)(*50*). The C-4 of Pro54 is positioned 4.2 Å from a phosphate of aa-tRNA; EF-Tu (grey), aa-tRNA (orange/grey), GDP (cyan), hydrophobic gate residues (yellow sticks), Mg(II) (pink sphere), nucleophilic water (red sphere), Pro54 (green sticks). The EF-Tu GTP hydrolysis site is circled (magenta).

However, recent crystallographic studies on the 70*S* ribosome bound to EF-Tu and aa-tRNA revealed that the His84 is positioned in its catalytically active conformation not by the opening of the hydrophobic gate, but by a hydrogen bond to the backbone phosphate of 23*S* rRNA residue A2662 (*50*). The toxin α-sarcin, which is active against both prokaryotic and eukaryotic ribosomes, cleaves 23*S* rRNA between G2661 and A2662, the same phosphate group that positions His84 of EF-Tu, suggesting that His84 coordination by A2662 is a universal mechanism involved in triggering GTP hydrolysis on the ribosome (*50-52*). Following GTP hydrolysis, EF-Tu dissociates from the ribosome, whereupon GDP is exchanged for GTP through the action of exchange factor EF-Ts. The cycle repeats and iteratively increases the length of the nascent polypeptide chain (*40, 53-56*).

2.4.3 Potential implications of a PTM at EF-Tu Pro54

PPHD hydroxylates EF-Tu residue Pro54(53), which is located on the switch I loop, 7 residues *N*-terminal to Ile60. Crystallographic and cryo-EM studies have shown that the switch I loop is a conformationally flexible region of EF-Tu that plays a key role in coupling GTP hydrolysis to substantial conformational changes from a translationally active GTP-bound state to an inactive GDP-bound state (*50, 57*). Previous analyses of post-translational modifications on the switch I loop have identified that Lys56 methylation in *E. coli* EF-Tu affects the rate of EF-Tu GTP hydrolysis (*58, 59*). In the crystal structure of EF-Tu in its translationally active state bound to the 70S ribosome, the C-4 of Pro54 is positioned 4.2 Å from a backbone phosphate in aa-tRNA (Figure 2.17)(*50*). Given that both translational machinery in general and the aforementioned proline is conserved in the model organisms *T. thermophilus*, *E. coli.*, and *Pseudomonas spp.*, it is reasonable to assume that Pro54 (Pro53 in *E. coli*) would be found in a similar region in 3-dimensional space. Thus, a PTM at Pro54 is tremendously interesting due to its proximity to multiple critical elements in translation – from codon-anticodon recognition to GTPase hydrolysis – and might alter EF-Tu:aa-tRNA interactions and/or the rate of GTP hydrolysis.

2.4.4 EF-Tu plays various roles in the cell

Other than its key role in translation, EF-Tu has been shown to be involved in the immune response in plants, whereby the recognition of extracellular EF-Tu of pathogenic origin (i.e. *Pseudomonas aeruginosa*) activates a signalling cascade that confers resistance to a broad range of bacteria (*60*). In *P.*

aeruginosa, EF-Tu forms a complex with nucleoside-diphosphate kinase that tunes its ability to synthesise GTP, providing a significant source of GTP for translational biosynthesis (*61*). In *Bacillus subtilis*, EF-Tu affects cell morphology through an interaction with cytoskeletal protein MreB (membrane protein B)(*39*). Therefore, PPHD-catalysed hydroxylation of EF-Tu residue Pro54 in *Pseudomonas spp.* is of particular interest and could affect immune function, cytoskeletal integrity, and/or bacterial translation.

2.5 Kinetic studies on PPHD

The kinetic properties of PHD2 *in vitro* are thought to reflect its role as an oxygen sensor. The PHD2 K_m for O_2 (260 μM) is higher than the concentration of dissolved oxygen in air, about 200 μM)(*62, 63*) and the reaction of a PHD2:Fe(II):2OG:HIF-1α(CODD) complex with oxygen proceeds at a slower rate (~100-fold) compared to other 2OG oxygenases, such as taurine 2OG dioxygenase (TauD)(*64, 65*). Therefore, it was of interest to characterise the biochemical properties of PPHD and determine whether PPHD behaves like PHD2 *in vitro*.

The Michaelis-Menten kinetic parameters of PPHD were investigated using the 20-residue EF-Tu peptide fragment, EF-Tu_{44-63}, and MALDI-TOF mass spectrometry. PPHD catalysis was found to be dependent on Fe(II), 2OG, O_2, and, similar to the PHDs and CPHs, sodium L-ascorbate (Figure 2.18)(*66-68*). The precise role of ascorbate in 2OG oxygenase catalysis is unknown as it is not required by all 2OG oxygenases for *in vitro* catalysis and can be substituted for other reducing agents (e.g. dithiothreitol) with varying success (*68*); therefore, it may be that ascorbate plays the role of more than just a reducing agent.

Compared to PHD2, PPHD was observed to have a similar K_m for oligopeptide substrate fragment [47.2 ± 8.5 μM for EF-Tu$_{44-63}$ vs 36.7 ± 9.0 μM for 19mer HIF-1α CODD (residues 556-574)](*69*), suggesting that PPHD and PHD2 may interact similarly with their respective substrate fragments. In contrast, PPHD was observed to have a lower K_m for O_2 (47.5 ± 9.2 μM for PPHD; 229 ± 60 μM for PHD2)(*62*), yet a higher K_m value for 2OG (184 ± 22 μM for PPHD; 55 ± 11 μM for PHD2)(*62*), Fe(II) (6.3 ± 0.7 μM for PPHD; <1 μM for PHD2) and L-ascorbate (1,064 ± 95 μM for PPHD/EF-Tu$_{44-63}$; 54 ± 10 μM for PHD2/HIF-1α CODD) (*68, 70*). While these values may not represent cellular activities, the results reveal that PPHD likely does not function as an oxygen sensor in *Pseudomonas spp*.

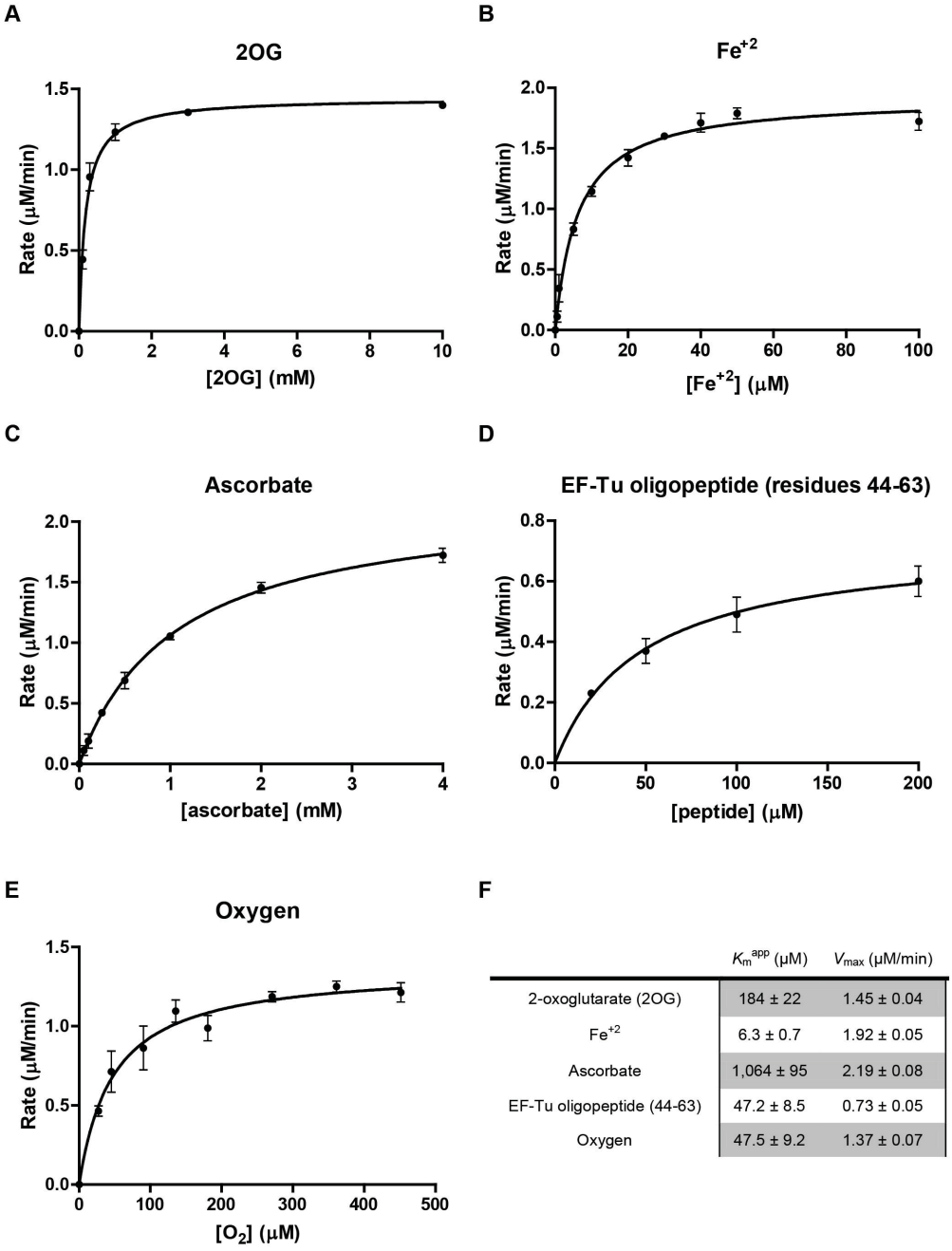

	K_m^{app} (μM)	V_{max} (μM/min)
2-oxoglutarate (2OG)	184 ± 22	1.45 ± 0.04
Fe^{+2}	6.3 ± 0.7	1.92 ± 0.05
Ascorbate	1,064 ± 95	2.19 ± 0.08
EF-Tu oligopeptide (44-63)	47.2 ± 8.5	0.73 ± 0.05
Oxygen	47.5 ± 9.2	1.37 ± 0.07

Figure 2.18. PPHD K_m^{app} determination. (**A**) 2OG (**B**) Fe(II) (**C**) sodium L-ascorbate (**D**) EF-Tu_{44-63} (**E**) oxygen and (**F**) table summarising kinetic parameters. Figure and figure legend are adapted with permission from J.S. Scotti *et al*, Human oxygen sensing may have origins in prokaryotic elongation factor Tu prolyl-hydroxylation. *Proc Nat Acad Sci USA*. In press (2014).

2.6 PPHD and EF-Tu binding monitored by ^{1}H NMR

Experiments in section 2.6 (except 2.6.1, 2.6.2, 2.6.7, and 2.6.8) were performed in collaboration with Dr. Ivanhoe Leung.

2.6.1 Purification of recombinant Hyp54 modified EF-Tu

In order to analyse the effect of hydroxylation of EF-Tu Pro54 on PPHD and EF-Tu binding, it was important to first prepare recombinant EF-Tu hydroxylated at Pro54 (Hyp54). To an *E. coli* BL21(DE3) cell lysate (from 20 g cells) containing overexpressed *N*-terminal hexahistidine tagged EF-Tu was added an excess of pure, untagged PPHD (20 mg), Fe(II) (8 mM), 2OG (20 mM), and sodium L-ascorbate (20 mM), and allowed to incubate at room temperature for one hour, after which purification of EF-Tu proceeded normally. EF-Tu was identified as pure and free from any detectable PPHD by SDS-PAGE and complete conversion to Hyp54 was confirmed by whole protein MS (+16 Da shift observed from relative to unmodified EF-Tu) and by trypsinolysis and subsequent MS/MS (selective hydroxylation of EF-Tu observed only on Pro54)(Figure 2.19).

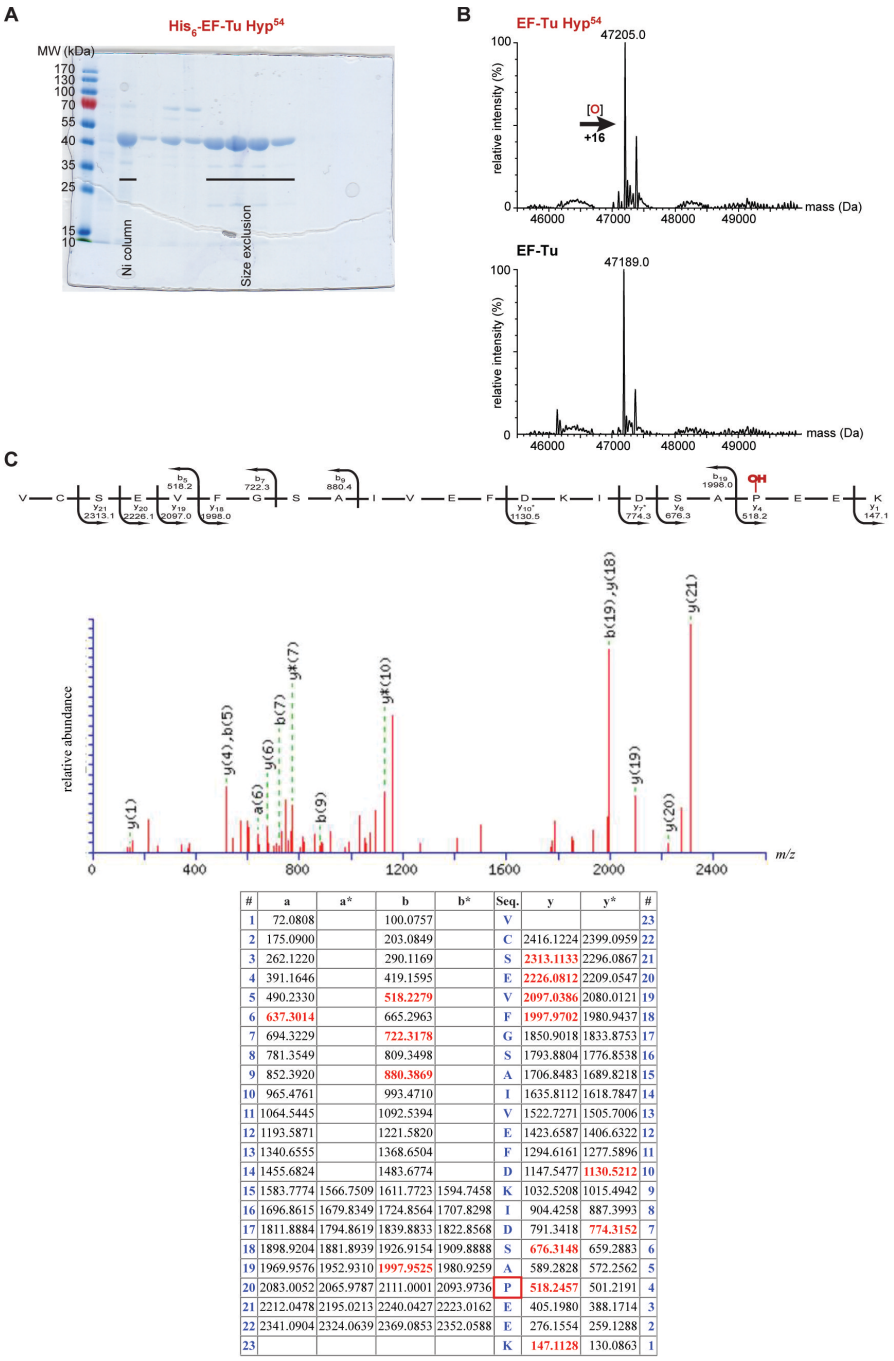

#	a	a*	b	b*	Seq.	y	y*	#
1	72.0808		100.0757		V			23
2	175.0900		203.0849		C	2416.1224	2399.0959	22
3	262.1220		290.1169		S	**2313.1133**	2296.0867	21
4	391.1646		419.1595		E	**2226.0812**	2209.0547	20
5	490.2330		**518.2279**		V	**2097.0386**	2080.0121	19
6	**637.3014**		665.2963		F	**1997.9702**	1980.9437	18
7	694.3229		**722.3178**		G	1850.9018	1833.8753	17
8	781.3549		809.3498		S	1793.8804	1776.8538	16
9	852.3920		**880.3869**		A	1706.8483	1689.8218	15
10	965.4761		993.4710		I	1635.8112	1618.7847	14
11	1064.5445		1092.5394		V	1522.7271	1505.7006	13
12	1193.5871		1221.5820		E	1423.6587	1406.6322	12
13	1340.6555		1368.6504		F	1294.6161	1277.5896	11
14	1455.6824		1483.6774		D	1147.5477	**1130.5212**	10
15	1583.7774	1566.7509	1611.7723	1594.7458	K	1032.5208	1015.4942	9
16	1696.8615	1679.8349	1724.8564	1707.8298	I	904.4258	887.3993	8
17	1811.8884	1794.8619	1839.8833	1822.8568	D	791.3418	**774.3152**	7
18	1898.9204	1881.8939	1926.9154	1909.8888	S	**676.3148**	659.2883	6
19	1969.9576	1952.9310	**1997.9525**	1980.9259	A	589.2828	572.2562	5
20	2083.0052	2065.9787	2111.0001	2093.9736	P	**518.2457**	501.2191	4
21	2212.0478	2195.0213	2240.0427	2223.0162	E	405.1980	388.1714	3
22	2341.0904	2324.0639	2369.0853	2352.0588	E	276.1554	259.1288	2
23					K	**147.1128**	130.0863	1

Figure 2.19. Purification and verification of EF-Tu 100% modified Hyp54. (**A**) SDS-PAGE gel of His_6-EF-Tu modified Hyp54; protein was collected after size exclusion chromatography. (**B**) Whole-protein MS on hydroxylated EF-Tu and unmodified EF-Tu reveals a +16 Da relative shift and therefore complete conservation of Pro54 to Hyp54. Calculated mass of His_6-EF-Tu: 47184.7 Da (*N*-terminal methionine cleaved). (**C**) MS/MS spectrum of EF-Tu peptide fragment (residues 35-57; *m/z* 2515.2 Da) confirms that the +16 Da shift observed in whole-protein MS corresponds to selective oxidation of Pro54 (Hyp54).

2.6.2 Challenges in assaying recombinant EF-Tu activity

The effect of a PTM (e.g. Lys56 methylation in *E. coli* EF-Tu)(*58*) on EF-Tu GTPase activity is commonly assayed by measuring EF-Tu dependent GTP hydrolysis (*58, 59*). In cells, EF-Tu GTP binding and hydrolysis is triggered by accurate codon-anticodon recognition on the ribosome (*40, 42*). Isolated EF-Tu has very minimal GTPase activity due to a 500-fold increased affinity for GDP over GTP (K_d for GDP = 1 nM; K_d for GTP = 500 nM)(*71, 72*), such that isolated EF-Tu overwhelming exists in its GDP-bound state. To overcome this issue, *in vitro* ribosome-free assays typically include kirromycin, an EF-Tu targeting antibiotic that induces translational arrest by binding to EF-Tu and precluding EF-Tu departure from the ribosome post GTP hydrolysis (*73-75*). Kirromycin effectively mimics the action of both EF-Ts and aa-tRNA by equalising the affinities of the EF-Tu for GTP and GDP (EF-Tu:kirromycin K_d for GDP or GTP = 1 nM)(*75*), thereby permitting uncoupled EF-Tu GTP hydrolysis in the absence of the ribosome or other cofactors.

2.6.3 EF-Tu GTP hydrolysis can be monitored by ^{1}H NMR

Current procedures to quantify the amount of hydrolysed GTP have not deviated from earlier methods, which typically rely on the use of radioactive [γ-^{32}P]-GTP (*71, 76*). Safety considerations prompted the search for an alternative method that could monitor GTP hydrolysis in real-time with minimal safety concerns. It was discovered that ^{1}H NMR could be effectively used to quantify kirromycin-dependent EF-Tu catalysed GTP hydrolysis through integration of the distinguishable GTP and GDP signals.

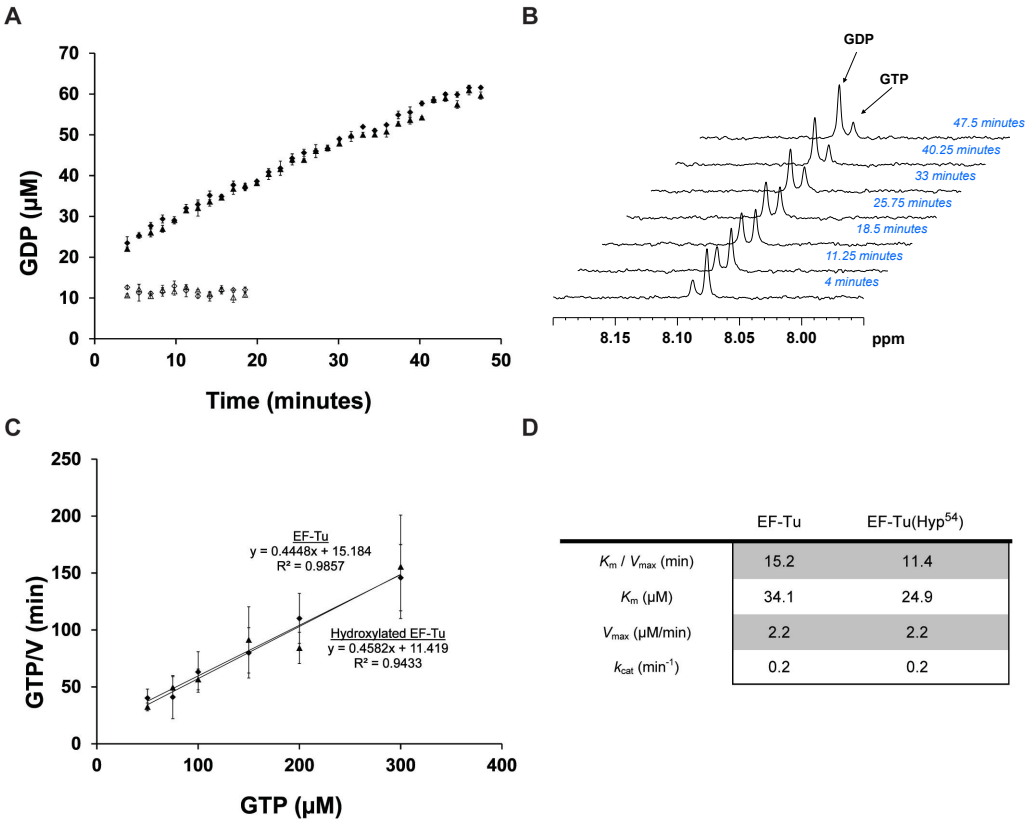

Figure 2.20. EF-Tu catalysed GTP to GDP turnover as monitored by ^{1}H NMR. (**A**) EF-Tu catalysed GTP to GDP turnover is kirromycin dependent and there is no difference between unhydroxylated EF-Tu and EF-Tu modified Hyp54: ◆ EF-Tu with kirromycin; ▲ EF-Tu(Hyp54) with kirromycin; ◇ EF-Tu without kirromycin; △ EF-Tu(Hyp54) without kirromycin. (**B**) Representative ^{1}H NMR overlaid spectra revealing EF-Tu GTP hydrolysis monitored in real-time. (**C**) Hanes plot for the determination of kinetics parameters for EF-Tu and EF-Tu(Hyp54). ◆ EF-Tu with kirromycin; ▲ EF-Tu(Hyp54) with kirromycin. (**D**) Table summarising kinetic parameters. Figure and figure legend are adapted with permission from J.S. Scotti *et al*, Human oxygen sensing may have origins in prokaryotic elongation factor Tu prolyl-hydroxylation. *Proc Nat Acad Sci USA*. In press (2014).

As a proof of concept, EF-Tu GTP hydrolysis was first shown to be kirromycin dependent. Subsequent analyses on the rate of GTP hydrolysis for EF-Tu modified Hyp54 and unmodified EF-Tu revealed no appreciable difference in their kinetic parameters. Experimental EF-Tu k_{cat} values (0.2 min^{-1}) were in accordance with those described in the literature (0.2 min^{-1})(Figure 2.20)(*77*).

2.6.4 Addition of aa-tRNA reveals no difference in the rate of EF-Tu and EF-Tu Hyp54 GTP hydrolysis

The addition of aa-tRNA has been shown to affect the rate of EF-Tu GTP hydrolysis (*78*). Given the proximity of the EF-Tu switch I loop to aa-tRNA in crystal structures of EF-Tu bound to the ribosome, it was of interest to determine whether the addition of aa-tRNA to the reaction would have a differential effect on EF-Tu Pro54/Hyp54 GTP hydrolysis. As in the absence of aa-tRNA, no difference between unhydroxylated EF-Tu and EF-Tu Hyp54 was observed (Figure 2.21).

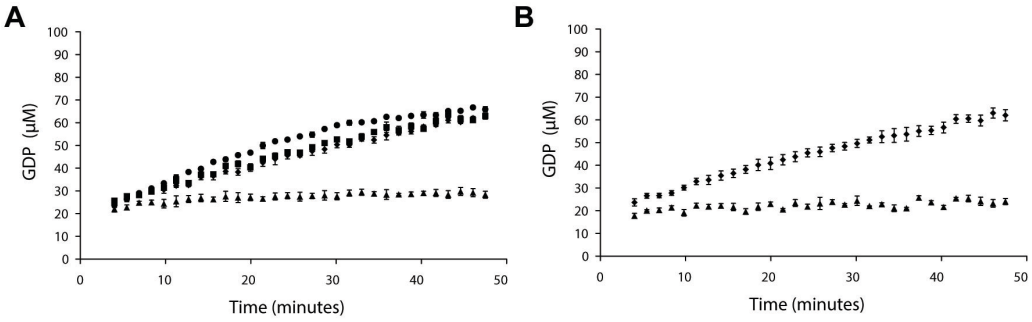

Figure 2.21. Hyp54/Pro54 status does not effect aa-tRNA assisted EF-Tu catalysed GTP hydrolysis. (**A**) EF-Tu Pro54 in the presence of ◆ kirromycin; ▲ kirromycin and *E. coli* aa-tRNA; ● kirromycin, *E. coli* tRNA, *E. coli* aa-tRNA synthetase (no ATP, so no aa-tRNA formation, thus negative control); ■ kirromycin and ATP (negative control) (**B**) EF-Tu Hyp54 in the presence of ◆ kirromycin; ▲ kirromycin and *E. coli* aa-tRNA. Figure and figure legend are adapted with permission from J.S. Scotti *et al*, Human oxygen sensing may have origins in prokaryotic elongation factor Tu prolyl-hydroxylation. *Proc Nat Acad Sci USA*. In press (2014).

2.6.5 PPHD decreases the rate of EF-Tu GTP hydrolysis in a metal(II), 2OG and Hyp54 dependent manner

In contrast, the addition of PPHD to the EF-Tu GTP hydrolysis reaction halved the rate of GTP hydrolysis in a manner dependent on Zn(II) [used as a surrogate for paramagnetic Fe(II)] and 2OG (Figure 2.22, *A* and *B*). Further, the addition of potent inhibitors of the human PHDs, IOX3 [*N*-(1-chloro-4-hydroxyisoquinolin-3-yl)carbonylglycine] and hydroxythiazole A [(*E*)-2-(3-

hydroxy-2-((2-((naphthalen-2-ylmethyl)sulfonyl)acetyl)imino)-2,3-dihydrothiazol-4-yl)acetic acid](*79*) (chemical structures shown in Figure 2.22, *C* and *D*), rescued the effect and re-established normal rates of EF-Tu GTP hydrolysis (Figure 2.22, *C* and *D*), suggesting that bulky 2OG-mimetic inhibitors bind to the PPHD active site and occlude the EF-Tu switch I loop. Importantly, and in contrast to isolated EF-Tu/EF-Tu(Hyp54), the rate of GTP hydrolysis in the presence of PPHD was dependent on Pro54/Hyp54 status (Figure 2.22*A*); PPHD decreased the rate of unhydroxylated EF-Tu GTP hydrolysis but did not affect that of EF-Tu Hyp54. Therefore, PPHD has a stronger affinity to substrate (unhydroxylated EF-Tu) than to product (hydroxylated EF-Tu), supporting Michaelis-Menten enzymology characterised by initial substrate binding, catalysis, and product release.

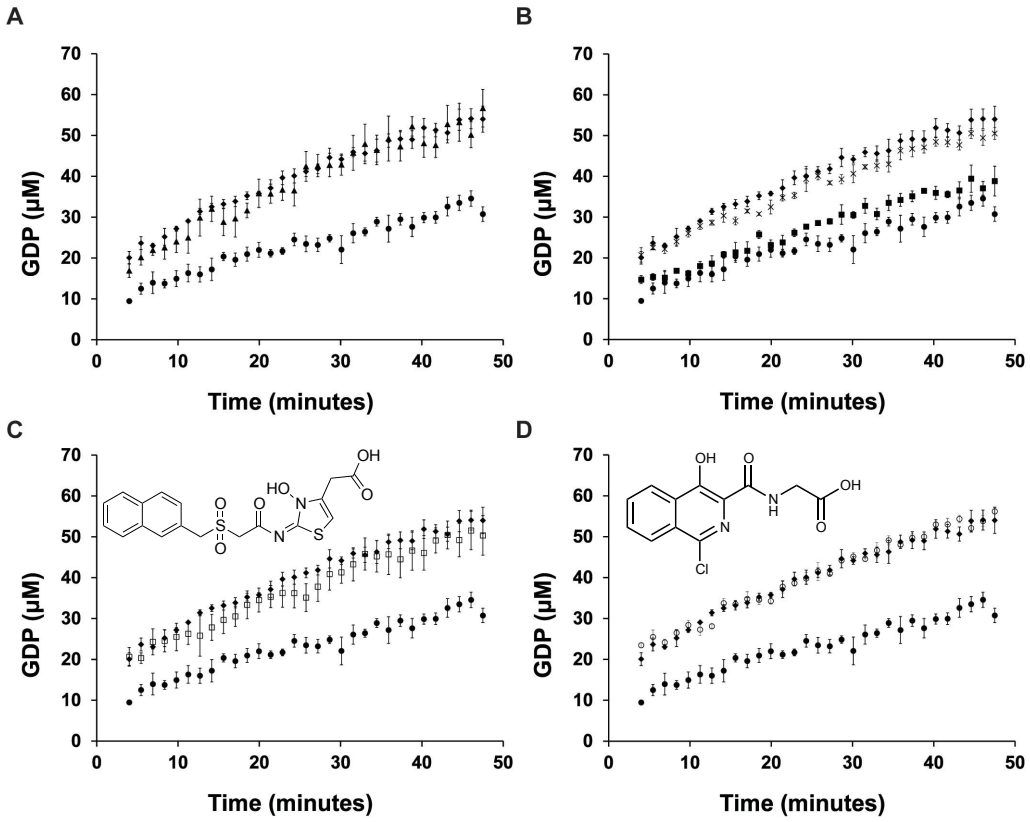

Figure 2.22. Addition of PPHD affects EF-Tu GTP hydrolysis. (**A**) The rate of GTP hydrolysis is halved in the presence of PPHD-Zn(II)-2OG: ◆ EF-Tu only; ● EF-Tu in the presence of PPHD-Zn(II)-2OG; ▲ EF-Tu(Hyp54) in the presence of PPHD-Zn(II)-2OG. (**B**) The rate of GTP hydrolysis is dependent on the presence of Zn(II) and 2OG in the PPHD active site: ◆ EF-Tu only; ● EF-Tu in the presence of PPHD-Zn(II)-2OG; ■ EF-Tu in the presence of PPHD-Zn(II); × EF-Tu in the presence of *apo* PPHD. (**C**) ◆ EF-Tu only; ● EF-Tu in the presence of PPHD-Zn(II)-2OG; □ EF-Tu in the presence of PPHD-Zn(II)-hydroxythiazole A. Hydroxythiazole A chemical structure overlayed on graph. (**D**) ◆ EF-Tu only; ● EF-Tu in the presence of PPHD-Zn(II)-2OG; ○ EF-Tu in the presence of PPHD-Zn(II)-IOX3. IOX3 chemical structure overlayed on graph. Figure and figure legend are adapted with permission from J.S. Scotti *et al*, Human oxygen sensing may have origins in prokaryotic elongation factor Tu prolyl-hydroxylation. *Proc Nat Acad Sci USA*. In press (2014).

2.6.6 Human PHD2 decreases EF-Tu GTP hydrolysis

EF-Tu GTP hydrolysis was then monitored in the presence of other prolyl-hydroxylases to ensure a PPHD-dependent effect (Figure 2.23). The addition of the choanoflagellate *Monosiga brevicollis* P4H-Zn(II)-NOG (mbP4H; obtained in pure form from the CJS group) did not lower the rate of EF-Tu GTP hydrolysis as did PPHD. However, the addition of PHD2-Zn(II)-2OG decreased the rate of GTP

hydrolysis to the same extent as that of PPHD-Zn(II)-2OG. Further, the effect of PHD2 was unresponsive to bulky PHD inhibitors (hydroxythiazole A) and Hyp54 status, both of which had been shown to rescue the rate of EF-Tu GTP hydrolysis in the presence of PPHD. These results imply that PHD2 interacts with EF-Tu either outside the vicinity of its active site or in such a way as to leave its active site unobstructed. Further, these results were of interest from an evolutionary perspective, especially given no demonstrated cross-reactivity between PPHD and PHD2 substrates and the inability of the choanoflagellate mbP4H to produce the same effect, suggesting that PPHD and PHD2 may have coevolved with their substrates.

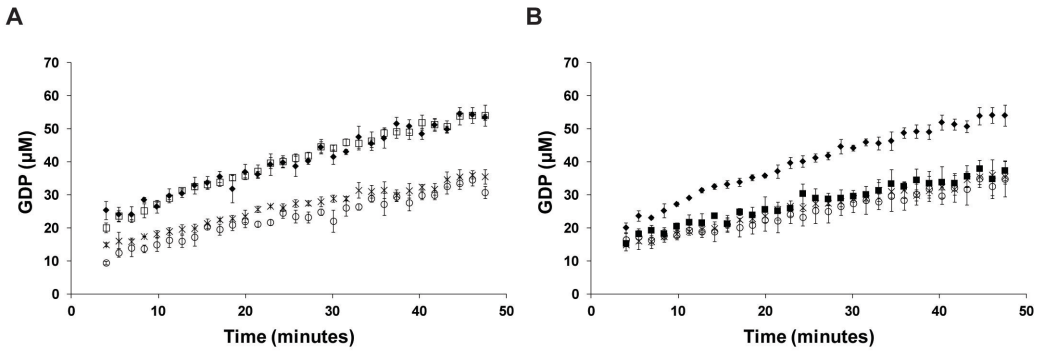

Figure 2.23. Addition of PHD2 affects EF-Tu GTP hydrolysis differently from PPHD. (**A**) The rate of GTP hydrolysis is halved in the presence of PPHD-Zn(II)-2OG: □ EF-Tu only; ◆ EF-Tu in the presence of *Monosiga brevicollis* P4H-Zn(II)-2OG; ○ EF-Tu in the presence of PPHD-Zn(II)-2OG; × EF-Tu in the presence of PHD2-Zn(II)-2OG. (**B**) The effect of PHD2 on the rate of GTP hydrolysis is not rescued by bulky PHD inhibitors or EF-Tu modified Hyp54: ◆ EF-Tu only; × EF-Tu in the presence of PHD2-Zn(II)-2OG; ■ EF-Tu(Hyp54) in the presence of PHD2-Zn(II); ○ EF-Tu in the presence of PHD2-Zn(II)-hydroxythiazole A.

2.6.7 PPHD knockout reveals no affect on global translation rate in P. aeruginosa

Experiments in this section were performed in collaboration with Joongoo Lee.

The observation that PPHD binds to EF-Tu and decreases the rate of GTP hydrolysis raised the question as to whether a stoichiometric binding effect might affect translation in cells. Although unlikely given the high intracellular EF-

Tu levels, the *in vivo* translation rates of *P. aeruginosa* PAO1 wildtype and *PA0310* insertional mutant strains were measured using a standard ^{35}S-methionine incorporation technique (*26*). In *P. aeruginosa*, no difference was observed in the preliminary studies on the global translation rate between the *PPHD* insertional mutant strain and the wildtype strain under standard growth conditions (Figure 2.24).

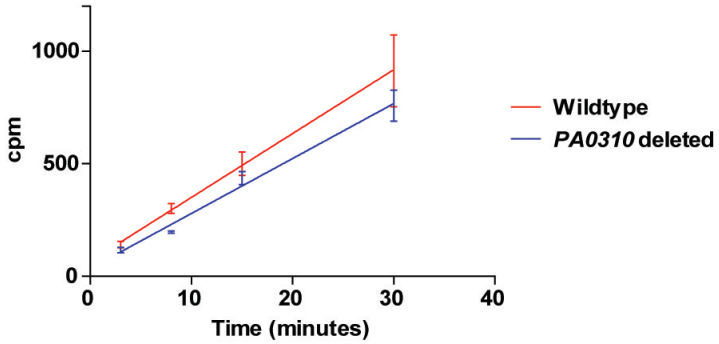

Figure 2.24. Growth of *P. aeruginosa* PAO1 wildtype and *PA0310* (*PPHD*) insertional mutant strains reveals no apparent difference on relative global translation rate. Cells were grown to log phase (OD_{600} = 0.5) and relative translation rate was measured by ^{35}S-methionine incorporation. Figure and figure legend are adapted with permission from J.S. Scotti *et al*, Human oxygen sensing may have origins in prokaryotic elongation factor Tu prolyl-hydroxylation. *Proc Nat Acad Sci USA*. In press (2014).

2.6.8 PPHD knockout likely does not affect translational accuracy in P. putida

Experiments in this section were performed in collaboration with Dr. Armin Thalhammer.

Given that no difference was observed between *P. aeruginosa* PAO1 wildtype and *PPHD* insertional mutant strains with respect to global translation rate, it was of interest to determine whether Pro54 hydroxylation affects translational accuracy. For this series of experiments, a dual luciferase reporter cassette was designed [D.Phil. thesis, Dr. Armin Thalhammer, Chemistry; for more details see reference (*80*)], which could be used to monitor translational accuracy by measuring the ratio in intensities between the first, *Renilla reniformis* (*Renilla*), and the second, *Photinus pyralis* (Firefly), luciferase in the

presence of different codons in a linker region flanked by the two luciferases (*80*). The well-established site and orientation specific single-copy chromosomal mini-Tn7 transposon integration system was chosen as an effective expression system (*81*). Single-copy reduces possible fluctuation in luciferase signal intensity cause by plasmid copy number variation. IPTG-inducible expression from a lacI-repressed Plac promoter enables superior luciferase intensities. Two stop codons (TGA and TAA) and matched sense codons (CGA and CAA) were tested in the presence of the ribosomal-targeting antibiotics streptomycin and paromomycin (Figure 2.25).

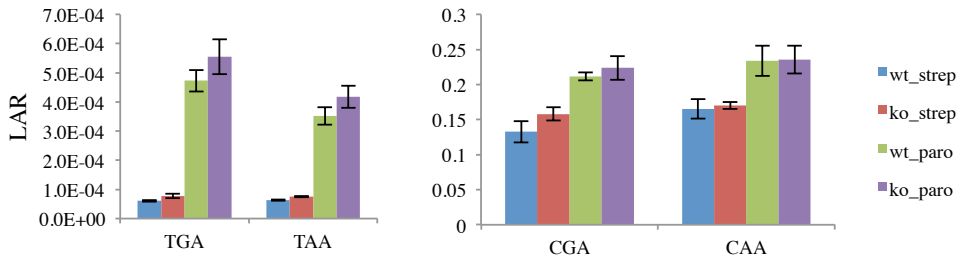

Figure 2.25. Monitoring translation accuracy in *P. putida*. Paromomycin strongly increases dual-luciferase ratio at stop codons and slightly at sense codons relative to streptomycin. PPHD knockout shows ~20% higher luciferase ratio at stop codons in the presence of paromomycin (5 μg/mL) or streptomycin [(2 μg/mL), $P<0.05$ for streptomycin], indicating the possible presence of a PPHD-mediated effect on stop-codon readthrough. Values are mean ± sd of three biological replicates. Luciferase activity ratio (LAR) = Fluc/Rluc (Firefly luciferase / *Renilla* luciferase).

Streptomycin binds to the phosphate backbone of 16S RNA near protein S12 and stabilises the high-tRNA affinity *ram* state of the ribosome, whereas paromomycin binds to the decoding site of ribosomal 16S RNA and directly affects decoding (*82*). Thus, a greater difference in stop-codon readthrough is expected in the presence of paromomycin (Figure 2.25). Yet we also observe a ~20% higher luciferase ratio for both TGA and TAA stop codons for the PPHD knockout relative to wildtype, suggesting that hydroxylation at Pro54 may play a

role in translation accuracy in *P. putida*. However, repeated experiments revealed a mixture of statistically significant and insignificant results, suggesting that the modest ~20% difference observed may be due to other factors. Further work is required to determine if *PPHD* knockout affects translational accuracy in the presence of streptomycin.

2.6.9 Presence of EF-Tu increases the affinity of PPHD for 2OG

To measure binding constants of metal(II) and 2OG to PPHD, a paramagnetic relaxation enhancement based NMR technique was employed in which displacement of ordered water bound to metal(II) within the PPHD active site is monitored as a function of ligand concentration (for details, see Experimental Procedures)(*83*). The addition of EF-$Tu_{protein}$ was found to significantly stabilise PPHD:2OG binding, decreasing the PPHD 2OG K_d by ~50-fold (8 ± 4 μM) compared to the absence of any substrate (2OG K_d >400 μM) and in the presence of EF-Tu_{44-63} (2OG K_d >400 μM)(Figure 2.26*A*), and results were comparable to PHD2 (2OG K_d <2 μM) as shown using soft ionisation ESI-MS (*70*). In contrast, monitoring reaction of PPHD with EF-Tu_{44-63} peptide substrate by ^{1}H NMR revealed a roughly 33% excess of succinate over product formation (ratio of succinate to hydroxylated product is ~4:3)(Figure 2.26, *B* and *C*). These differences are of interest as they suggest that interactions between PPHD and fully-folded EF-Tu protein contribute to PPHD folding and order the active site; and that the 20mer peptide is more flexible in nature and unable to effectively stabilise a PPHD:2OG complex.

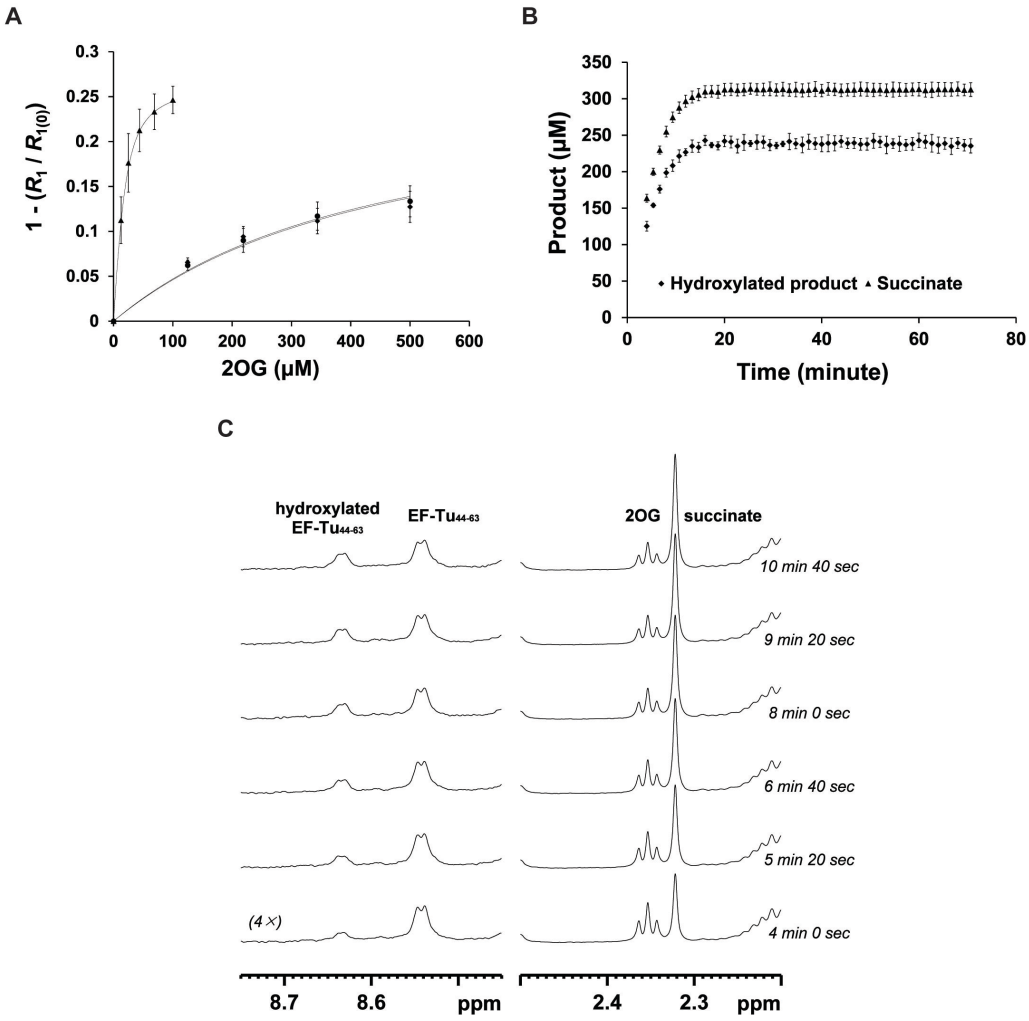

Figure 2.26. Using ^{1}H NMR to monitor PPHD catalysis reveals differences between full-length protein and peptide fragment substrates. (**A**) PPHD 2OG K_d in the presence of EF-Tu protein (8 ± 4 μM)(▲) compared to the absence of any substrate (>400 μM)(◆) and in the presence of EF-Tu$_{44-63}$ (>400 μM)(●). (**B**) The ratio of succinate to hydroxylated product is ~4:3 (**C**) PPHD activity monitored by ^{1}H NMR: 2OG oxidation into succinate and the hydroxylation of EF-Tu$_{44-63}$. Figure and figure legend are adapted with permission from J.S. Scotti *et al*, Human oxygen sensing may have origins in prokaryotic elongation factor Tu prolyl-hydroxylation. *Proc Nat Acad Sci USA*. In press (2014).

2.6.10 Presence of EF-Tu affects PPHD affinity for metal(II)

Similar to the effect observed with PPHD:2OG binding, the addition of unhydroxylated EF-Tu$_{protein}$ decreased the PPHD metal(II) K_d [paramagnetic Mn(II) used as a surrogate for Fe(II)] by ~4 fold (8 ± 3 μM in the presence of EF-Tu$_{protein}$, 2 ± 0.5 μM with no substrate present)(Figure 2.27, *A* and *B*). Analogous

to the absence of a PPHD-dependent effect on EF-Tu modified Hyp54 GTP hydrolysis, the addition of hydroxylated EF-$Tu_{protein}$ did not affect PPHD metal(II) K_d (2 ± 1 μM in the presence of hydroxylated EF-$Tu_{protein}$)(Figure 2.27*C*). In particular the higher K_d for Fe(II) in the presence of substrate is of interest given the phenotypic results in *P. aeruginosa*, supporting a role for PPHD in iron metabolism.

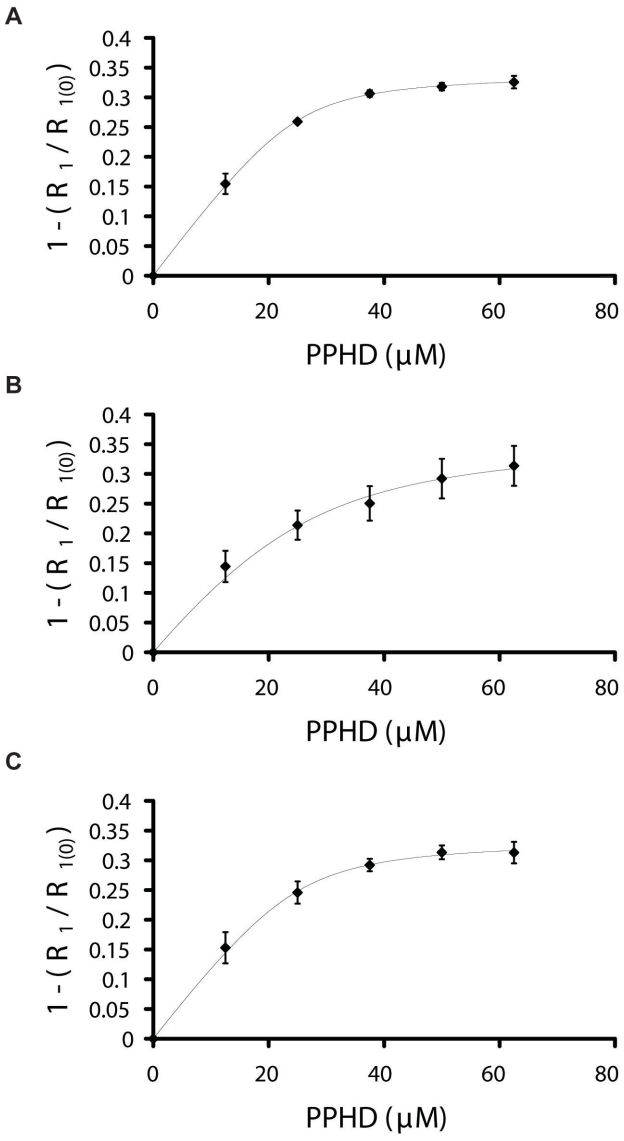

Figure 2.27. Using ^{1}H NMR to monitor the K_d of Mn(II) to PPHD$_{putida}$. K_d of Mn(II) to PPHD (**A**) in the absence of any substrate (2 ± 0.5 μM), (**B**) in the presence of unhydroxylated EF-Tu protein (8 ± 3 μM), and (**C**) in the presence of EF-Tu(Hyp54) (2 ± 1 μM) shows that EF-Tu modulation of PPHD metal(II) binding is dependent on Pro54/Hyp54 status. Figure and figure legend are adapted with permission from J.S. Scotti *et al*, Human oxygen sensing may have origins in prokaryotic elongation factor Tu prolyl-hydroxylation. *Proc Nat Acad Sci USA*. In press (2014).

2.6.11 NMR studies imply interactions between PPHD and EF-Tu

Overall, the solution studies demonstrated that Pro54 hydroxylation likely does not play a role in translation rate/accuracy by substantially

modulating the rate of EF-Tu GTP hydrolysis. The observations that i) addition of PPHD slows the rate of EF-Tu GTP hydrolysis in a metal(II)- and 2OG-dependent manner; ii) binding of metal(II) and 2OG to PPHD is strikingly affected by the presence/absence of EF-Tu; and iii) the location of Pro54 on the conformationally flexible EF-Tu switch I loop combine to suggest that PPHD binding to EF-Tu involves sequestration of the switch I loop, preventing EF-Tu from alternating between GTP- and GDP-bound conformations. In order to verify these conclusions, crystallographic studies were initiated in order to obtain a structure of the PPHD:EF-Tu complex (Chapter 3).

2.7 Hydroxylation of EF-Tu Pro54 does not affect EF-Tu:EF-Ts binding

2.7.1 Insights into a potential role of Pro54 hydroxylation in EF-Tu:EF-Tu binding

After successful GTP hydrolysis on the ribosome, EF-Tu retains bound GDP. Given that the K_d of GDP to EF-Tu is 500-fold lower than that of GTP (*71*), GTP will not spontaneously displace GDP in solution. EF-Ts binds to EF-Tu:GDP and displaces the nucleotide, after which GTP and aa-tRNA displace EF-Ts to regenerate a translationally active EF-Tu:GTP:aa-tRNA ternary complex (*42, 54, 84*). A crystal structure of an *E. coli* EF-Tu:EF-Ts complex (PDB ID: 1EFU) reveals that EF-Ts inserts its *C*-terminal α-helix into the EF-Tu nucleotide binding site (Figure 2.28)(*85*). Although the EF-Tu switch I loop is disordered in the complex, the proximity of the switch I loop to the EF-Tu nucleotide binding site raised the question as to whether a PTM on the EF-Tu switch I loop could affect EF-Tu:EF-Ts binding by ordering the switch I loop.

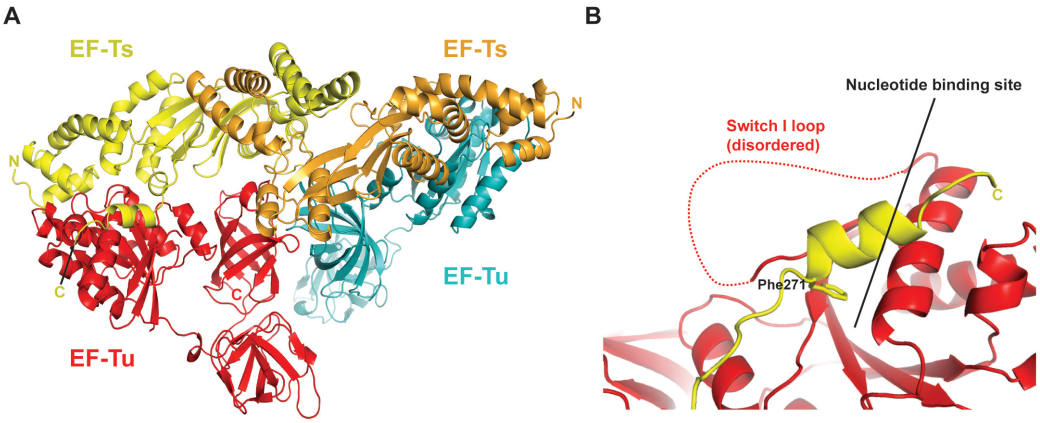

Figure 2.28. Views from a crystal structure of an EF-Tu:EF-Ts complex. (**A**) Overall structure of the EF-Tu:EF-Ts heterodimer complex from *E. coli* (PDB ID: 1EFU). (**B**) The EF-Ts *C*-terminal α-helix is positioned to insert Phe^{271} into the EF-Tu nucleotide binding site [no nucleotide or Mg(II) bound]. Notably, the switch I loop is disordered.

2.7.2 EF-Tu:EF-Ts binding is unaffected by Pro54 hydroxylation status

Experiments in section 2.7.2 were performed in collaboration with Dr. Ivanhoe Leung.

To test the hypothesis that Pro54 hydroxylation may affect EF-Tu:EF-Ts binding, NMR was used to monitor the binding of unhydroxylated EF-Tu and EF-Tu modified Hyp54 to EF-Ts by taking advantage of the appearance/disappearance of labelled protein signals in the presence of an interaction partner (in this case EF-Tu) in solution. The gene encoding for *P. putida* EF-Ts was cloned into a pET28a expression vector and recombinant ^{15}N-labeled EF-Ts was expressed and purified in the same way as for PPHD and EF-Tu proteins, the only difference being that *E. coli* was grown in ^{15}N labelled media (Figure 2.29*A*).

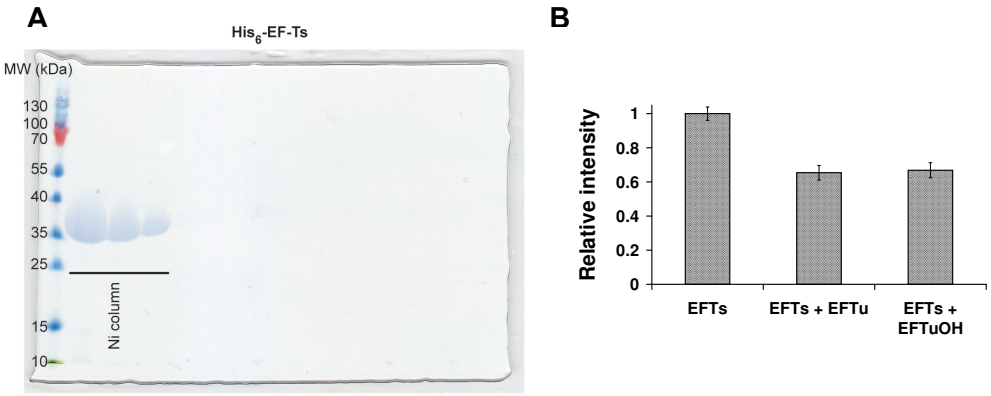

Figure 2.29. Hydroxylation of EF-Tu at Pro54 does not affect EF-Ts binding. (**A**) Representative SDS-PAGE gel revealing pure recombinant EF-Ts after Ni-affinity chromatography. (**B**) Hydroxylation of EF-Tu does not affect EF-Ts binding; relative intensity of collective ^{15}N NMR signals monitored in the presence/absence of EF-Tu (Hyp54).

Hydroxylation at Pro54 did not appreciably affect EF-Tu:EF-Ts binding (Figure 2.29*B*), suggesting that the disorder of the switch I loop in the EF-Tu:EF-Ts complex structure may reflect the lack of a defined role for the switch I loop in EF-Tu:EF-Ts complex formation.

2.8 Hydroxylation of EF-Tu Pro54 affects its stability in solution

Given the link between EF-Tu abundance and overall cell stability and its known ability to act as a protein-folding chaperone during cellular stress (*86, 87*), it was of interest to investigate whether Pro54 hydroxylation may alter the overall stability of EF-Tu. The stability of unhydroxylated EF-Tu and EF-Tu Hyp54 was assayed directly by circular dichroism (CD) spectroscopy, in which measurements of protein folding/unfolding are directly observed by monitoring the intensity of circularly polarised light at 222 nm, indicative of protein secondary structure (*88*). EF-Tu is highly unstable in the absence of Mg(II) (K_d: 1 nM)(*89*), so the ion (5 mM) was added to all buffers. Interestingly, CD revealed a

slight, yet consistent, 1.5 °C increase in EF-Tu stability (T_m) upon Pro54 hydroxylation (50.5 ± 0.1 °C for unhydroxylated EF-Tu vs 52.0 ± 0.1 °C for EF-Tu Hyp54)(Figure 2.30).

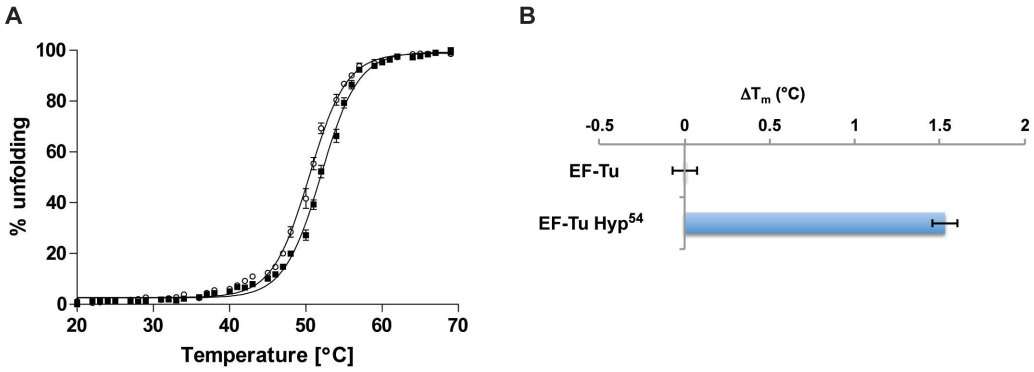

Figure 2.30. Pro54 hydroxylation increases EF-Tu stability in solution. (**A**) Normalised CD spectra of ○ EF-Tu:GDP and ■ EF-Tu:GDP Hyp54 monitored at 222 nm; data points shown as mean ± std. error of triplicates and fitted to a Boltzmann sigmoidal curve using GraphPad Prism software. (**B**) Graph summarising T_m values derived from the Boltzmann fit; EF-Tu was used as a reference.

Such a deviation is of interest in light of the intracellular abundance of EF-Tu and its reported connection to heat shock tolerance in prokaryotes, suggesting that hydroxylation of EF-Tu may play a role in overall cell stability.

2.9 Studies on the effects of pyocyanin, PPHD and EF-Tu in human cells

Experiments in section 2.9 were performed in collaboration with Dr. Tzu-Lan Ye, who provided the figures.

2.9.1 Pyocyanin upregulates HIF-1α in human cells

Previous studies have shown that the redox active pyocyanin is capable of upregulating HIF-1α in human cells (*15*). To confirm these results and determine whether the effect extends to human A549 cells (i.e. basal lung epithelial cells susceptible to *P. aeruginosa* infection), three different human cell lines were subjected to various concentrations of pyocyanin. Interestingly, pyocyanin was

found to upregulate HIF-1α at a comparable level to that observed as a result of DMOG treatment (Figure 2.31). Given that pyocyanin is an iron chelator and PHD regulation by iron availability is well-established (*90*), it is likely that pyocyanin induced HIF-1α upregulation in human cells is due, at least in part, to iron sequestration.

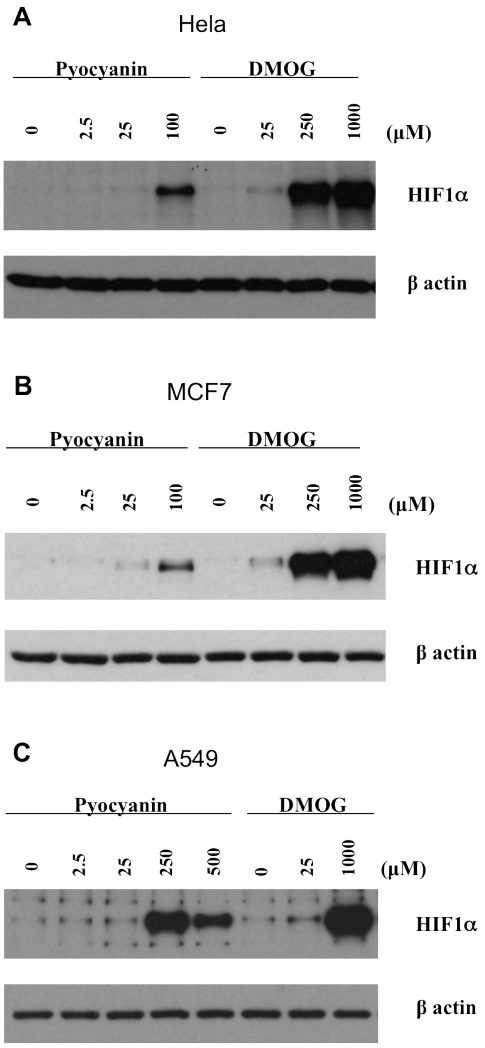

Figure 2.31. Pyocyanin up-regulates HIF-1α in human cells. (**A**) Hela, (**B**) MCF7 and (**C**) A549 cell lines. Cells were 90-95 % confluent when treated with compounds for 6 hours at 37 °C.

2.9.2 Expression of PPHD/EF-Tu in human cells may regulate HIF-1α levels

The in-solution studies revealed that PHD2 was able to decrease the rate of EF-Tu GTP hydrolysis to a similar extent as PPHD (see section 2.6.6), suggesting that the presence of PPHD or EF-Tu in human cells may upregulate HIF-1α by competition with the PHDs. To test this hypothesis, human expression vectors encoding for PPHD$_{putida}$ and EF-Tu$_{putida}$ were transfected into HEK293T cells and changes in HIF-1α levels were monitored by immunoblotting (Figure 2.32). Although transfection efficiencies were low (and thus the experiment will require repeating), the results suggest a possible effect of PPHD$_{putida}$ / EF-Tu$_{putida}$ on HIF-1α levels.

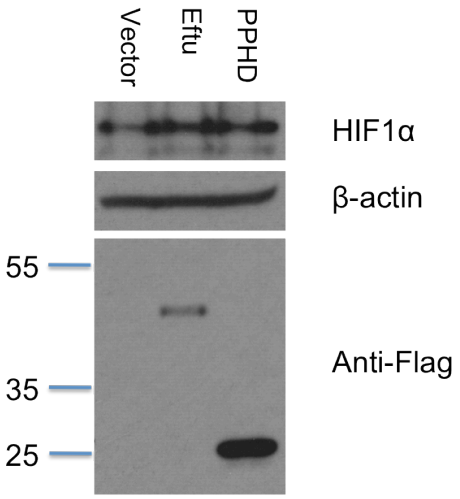

Figure 2.32. Transfection of PPHD and EF-Tu possibly upregulates HIF-1α in human cells. HEK293T cells were transfected with either pcDNA_LIC_PPHD or pcDNA_LIC_EF-Tu. Experiment performed and figure provided by Dr. Tzu-Lan Ye.

Taken together, the observations that i) PPHD knockout increases pyocyanin production, ii) pyocyanin upregulates HIF-1α in human cells likely via PHD inhibition by iron sequestration, and iii) PPHD and EF-Tu proteins upregulate HIF-1α in human cells suggest that during some infections prolyl-hydroxylases on 'both sides of the fence' (i.e. in human and bacterial cells) may

be involved in 'cross-talk' and are regulated by bacterial virulence factors, iron availability, and possibly 2OG. Finally, the results suggest that the roles of the PHDs and the PPHDs may encompass more than hypoxic sensing in an isolated organism.

2.10 Conclusions

This Chapter describes work on the identification and biochemical/biophysical characterisation of a PHD2 homologue in *Pseudomonas spp.* A *P. aeruginosa PPHD* insertional mutant strain was found to possess an interesting phenotype, resulting from the upregulation of pyocyanin, an important virulence factor.

Importantly, PPHD was found to catalyse the *trans*-4 prolyl-hydroxylation of EF-Tu at Pro54 *in vitro* and in cells. In-solution NMR studies revealed that PPHD regulates the rate of EF-Tu GTP hydrolysis in a metal(II), 2OG and Pro54/Hyp54 dependent manner. The results implied that PPHD and EF-Tu share a substantial interaction interface and an induced fit binding mode. No evidence was observed for a PPHD dependent effect on global translation rate in *P. aeruginosa*, nor on EF-Tu:EF-Ts binding *in vitro*. However, Pro54 hydroxylation was shown to alter EF-Tu stability in solution. Finally, pyocyanin and PPHD/EF-Tu protein were observed to upregulate HIF-1α in human cells, suggesting that prolyl-hydroxylases in both bacteria and animals may be play roles in addition to hypoxic sensing in their respective organisms. For a more detailed discussion of the evolutionary relationship of PPHD and human PHD2, see Chapter 6.

2.11 Experimental Procedures

2.11.1 Protein purification

E. coli BL21(DE3) cells were transformed with the pET28a_PPHD, pET28a_EF-Tu, or pET28a_EF-Ts plasmid (encoding for proteins with an *N*-terminal hexahistidine tag) and were grown (37 °C; 180 rpm) to an OD_{600} of 0.6; recombinant protein production was induced with 0.5 mM β-D-1-thiogalactopyranoside (IPTG). The cells were allowed to continue to grow at 18°C overnight, harvested by centrifugation (10,000x*g*; 7 min), and stored at -80 °C.

Cell pellets were resuspended in 50 mM HEPES pH 7.5, 500 mM NaCl, 20 mM imidazole, 1 mM tris(2-carboxyethyl)phosphine (TCEP), one EDTA-free protease inhibitor tablet (Roche), and approximately 1 mg DNAseI (bovine pancreas, grade II, Roche) at room temperature with gentle stirring. Cells were lysed on ice by sonication (Sonics VibraCell VCX-500, 13 mM probe at 60% intensity consisting of a 3 s pulse followed by 4 s rest, for a total time of 8 min), and the lysate was then cleared by centrifugation (50,000x*g*; 20 min). The supernatant was then loaded onto a 5 mL HisTrap FF column preequilibrated with the resuspension buffer at a rate of 2 mL/min – a rate maintained for all wash and elution steps – and purified using an AKTA FPLC system (GE Healthcare). The column was washed with 10 column volumes of 50 mM HEPES pH 7.5, 500 mM NaCl, 50 mM imidazole, 1 mM TCEP and protein was eluted with 50 mM HEPES pH 7.5, 500 mM NaCl, 250 mM imidazole, 1 mM TCEP. In the case of EF-Tu, all purification steps were performed in the presence of 10 mM $MgCl_2$ and trace (1 μM) GDP to enhance EF-Tu stability by increasing occupancy of GDP

in the nucleotide binding site; the Mg(II) ion is essential for the continued integrity of EF-Tu as it is necessary for binding of GDP ($K_D \sim 1$ nM) (*89*).

The purified sample was then exchanged to 50 mM HEPES pH 7.5, 200 mM NaCl using a PD-10 column (Millipore). If cleavage of the *N*-terminal hexahistidine tag was desired, the appropriate volume of 10x thrombin cleavage buffer and 1 unit thrombin (Novagen) per 1 mg of protein were added, and the mixture was left at 4 °C overnight. PPHD or EF-Tu was further purified using a Superdex 75 size exclusion column (GE Healthcare) preequilibrated in 50 mM HEPES pH 7.5, 200 mM NaCl (PPHD), 50 mM HEPES pH 7.5, 200 mM NaCl, 10 mM $MgCl_2$, 1 μM GDP (EF-Tu). Proteins were eluted using the same buffer. PPHD- or EF-Tu-containing fractions were pooled, concentrated to 35 mg/mL (PPHD) or 20 mg/mL (EF-Tu), by diafiltration, aliquoted (20 μL), flash frozen in liquid N_2, and stored at -80 °C.

2.11.2 Generation of a *PPHD* (*PA0310*) insertional mutant strain of *P. aeruginosa*

A *Pseudomonas aeruginosa* PA01 strain containing a transposon insert in the *PA0310* gene was obtained from the PA01 mutant library generated and verified by the University of Washington Genome Sciences as described (*33*).

2.11.3 *P. aeruginosa* growth determination

Immediately upon dilution, cultures in triplicate, in 96-well plates, were placed in a plate reader (Infinite M200; TECAN) at 28 °C and grown within the plate reader. The optical density at 600 nm (OD_{600}) was automatically read during growth every 60 min, and data were collected by Magellan software

(TECAN). All assays were performed in triplicate and plotted as mean ± standard deviation.

2.11.4 *P. aeruginosa* pyocyanin quantification

5 mL cultures of *P. aeruginosa* wildtype and *PA0310* insertional mutant strains grown to stationary phase were extracted with 3 mL of $CHCl_3$ and back extracted with 1 mL of 0.2 HCl, yielding a deep red solution, of which the aqueous phase was decanted and the absorbance was measured at 520 nm as reported previously (*34*). All assays were performed in triplicate and plotted as mean ± standard deviation.

2.11.5 *P. aeruginosa* global translation rate assay

Cultures (1 mL) of *P. aeruginosa* wildtype and *PA0310* insertional mutant strains were grown in LB medium at 37 °C with shaking to log phase (OD_{600} = 0.5), whereupon ^{35}S-methionine was added to a final concentration of 10 µCi/mL and growth was continued at 37 °C with shaking. At the specified time points, 100 µl was removed from biological triplicates and placed on ice before the addition of 10 µl BSA (4 mg/mL) and 20 µl 50% (w/v) trichloroacetic acid (Sigma). The protein pellet was isolated by centrifugation (25,000xg; 2 min), washed twice with 300 µl of cold ethanol, and solubilised in 50 µl 8 M urea. 10 µl was then added to 5 mL of Optiphase scintillant and ^{35}S-methionine incorporation was measured by scintillation counting.

2.11.6 PPHD pull-down in *P. putida*

Pseudomonas putida substrain KT2440 was grown (37 °C; 180 rpm) overnight in LB media, harvested by centrifugation (10,000x*g*; 7 min), resuspended in binding buffer (50 mM Tris-HCl pH 7.5, 125 mM NaCl, 5 mM imidazole) lysed on ice by sonication and the lysate was cleared by centrifugation (50,000x*g*; 20 min). 1 mL of cleared lysate was added to loose Ni-Sepharose beads (GE Healthcare), preincubated for 1 hour with 1 mg of pure hexahistidine-tagged PPHD in binding buffer, and washed three times with the same buffer. Proteins were eluted from the beads in elution buffer (50 mM Tris-HCl pH 7.5, 500 mM NaCl, 250 mM imidazole), precipitated in MeOH/$CHCl_3$, and subjected to trypsinolysis and MS/MS quantitation and analysis using MASCOT as described.

2.11.7 Generation of a *PPHD* (*PP_5159*) knockout strain of *P. putida*

A *PP_5159* (*PPHD*) knockout mutant of *P. putida* was constructed using overlap extension-(OE) polymerase chain reaction (PCR) coupled to a two-step allelic exchange utilising the suicide vector pUIC3 as previously described (*35, 36*), with the following 5′ flanking primers (PP5159_uF: 5′-TTGCCGTACAGGCCGAGAACTCGCCATACGCCTT-3′; PP5159_uR: 5′-GCACTGATCAATCGGATGACCCGTTCTGATAGGC-3′) and 3′ flanking primers (PP5159_dF: 5′-CCGATTGATCAGTGCGGCGCGCATCATATCCATT-3′; PP5159_dR: 5′-GTGCTCAAGGCCAAGTTT GCCGAGCCACAGATCC-3′)(primers PP5159_uR and PP5159_dF are complementary).

Summary. The method relies upon cloning ~1 kb regions of the genome upstream and downstream of the gene of interest. Then, these regions are ligated

together using overlap-extension PCR (OE-PCR) and transformed into an *E. coli* helper strain, DH5α *pir*$^{+}$, which expresses the π protein required for pUIC3 replication. pUIC3 containing the overlapping 2 kb region containing the 1 kb upstream and 1 kb downstream genomic regions is then electroporated into *P. putida*. Upon electroporation, the first homologous recombination event occurs and the entire pUIC3 plasmid is integrated into the genome of *P. putida* in the region near the wild type sequence containing PPHD. Finally, these transformants are grown in the presence of tetracycline to induce the second recombination event, resulting in the exchange of the 2 kb insert with the endogenous sequence containing the PPHD gene and concomitant loss of the pUIC3 plasmid. Since the second recombination event results in the loss of the *tet*^{R} gene, successful knockouts do not grow in the presence of tetracycline, enrichment of successful double recombinants can be achieved by adding cycloserine, an antibiotic which kills actively growing cells.

Stage 1. The first step was to design primers that amplify 1 kb regions upstream and downstream of PPHD (Table 2.33). When designing the primers, it was important to engineer a ~15 bp overlap between the 3′-5′ upstream reverse primer and the 5′-3′ downstream forward primer. Since the downstream cloning strategy involved the use of a TA-cloning vector, it was unnecessary to engineer restriction sites.

Table 2.33. Primers for knockout of PPHD by homologous recombination.

Primer	Sequence 5′-3′
PP5159_Upstream_F	TTGCCGTACAGGCCGAGAACTCGCCATACGCCTT
PP5159_Upstream_R	GCACTGATCAATCGGATGACCCGTTCTGATAGGC
PP5159_Downstream_F	CCGATTGATCAGTGCGGCGCGCATCATATCCATT
PP5159_Downstream_R	GTGCTCAAGGCCAAGTTTGCCGAGCCACAGATCC

With the appropriate primers, PCR was performed to amplify the 1 kb upstream and downstream regions. PCR conditions were identical to those already described. Amplified DNA fragments were analysed by 1% agarose gel electrophoresis and subsequently purified using a PCR Purification Kit (Fermentas). The two amplified upstream and downstream fragments were joined to make a single 2 kb fragment by Overlap-Extension PCR (OE-PCR), utilising the 15 bp overlap between the Upstream_R and Downstream_F primers. For this step, *Taq* polymerase was used to ensure the addition of TA overhangs. OE-PCR was performed using 15 amplification cycles without primers, followed by addition of 1 µL of each primer (Upstream_F, Downstream_R) and 0.5 µL more *Taq* polymerase and amplification was continued for 20 additional cycles (Table 2.34).

Table 2.34. OE-PCR thermocycler conditions for amplification of homologous recombination insert.

Segment	Cycles	Temperature (°C)	Time
Initial denaturation	1	95	2 min
Denaturation		95	40 s
Annealing	15	55	1 min
Extension		68	1 min 45 s
Pause	-	-	-
Denaturation		95	40 s
Annealing	20	55	1 min
Extension		68	1 min 45 s
Final extension	1	68	7 min
Final hold		4	~

PCR products were analysed by 1% agarose gel electrophoresis and the appropriate 2 kb band was excised and purified using a GeneJET Gel Extraction Kit (Fermentas).

Stage 2. The purified 2 kb fragment with TA overhangs was immediately ligated into the TA-cloning vector pCR2.1 (Invitrogen) according to the manufacturer's instructions. The ligation mixture was then transformed into

Ultracompetent *E. coli.* XL10 cells (Agilent) and plated on LB medium supplemented with kanamycin (30 μg/mL), ampicillin (100 μg/mL), IPTG (0.5 mM), and X-gal (80 μg/mL). White colonies were analysed for the presence of insert using colony PCR. DNA was isolated by MiniPrep and verified by Sanger sequencing using the M13 promoter and terminator primers. pUIC3 and pCR2.1 containing the 2 kb insert were simultaneously digested with *Xba*I and *Spe*I (NEB) for 4 h at 37 °C and the reactions were monitored for completion by 1% agarose gel electrophoresis. The pUIC3 restriction enzyme digest was then incubated at 80 °C for 20 min to heat inactivate *Xba*I/*Spe*I, allowed to cool on ice, after which 1 μL Alkaline Phosphatase (NEB) was added to prevent self-ligation and the reaction was incubated at 37 °C for 1 h. The digests were purified using a PCR Purification Kit (Fermentas). The purified digests were mixed in an approximate 3:1 molar ratio, ligated, transformed into $CaCl_2$ competent *E. coli.* DH5α *pir*$^+$, and plated on LB medium supplemented with tetracycline (10 μg/mL). Purification of the 2 kb insert by gel extraction was run in parallel but did not yield any colonies.

Stage 3. Successful transformants were analysed for the presence of insert by colony PCR using Upstream_F and Downstream_R primers. Colonies with pUIC3 plasmids containing the 2 kb insert were grown overnight at 37 °C in 5 mL 2TY medium supplemented with tetracycline (10 μg/mL) and DNA was isolated by MiniPrep. pUIC3 was electroporated into *P. putida* and blue colonies were selected on LB medium supplemented with tetracycline (10 μg/mL), IPTG (0.5 mM), and X-gal (80 μg/mL). Upon electroporation, the first homologous recombination ever occurs spontaneously and successful transconjugants are blue on X-gal due to the integration of pUIC3, which contains LacZY, into the *P.*

putida genome. To enrich double crossover mutants, purified transconjugants were inoculated in 10 mL LB broth with tetracycline (10 μg/mL) and grown overnight. 100 μl of the overnight culture was diluted in 10 mL LB broth *without* tetracycline and incubated with shaking (180 rpm) at 28 °C for 30 min. Tetracycline was then added to a final concentration of 10 μg/mL and cultures were allowed to incubate for an additional 2 h, after which cycloserine was added to a final concentration of 800 μg/mL. Incubation was continued for 3 h. Cells were then plated onto LB medium supplemented with X-gal (80 μg/mL) and streaked for single colonies. White colonies were analysed by colony PCR for the presence of the PPHD gene.

PCR analysis. Conveniently, this whole process was monitored effectively by PCR using the primers already described because one expects different length PCR products depending on the stage of the process. For the wild type, one expects to see a 2.6 kb PCR product when using primers Upstream_F and Downstream_R, due to the presence of the endogenous PPHD sequence in between those 1 kb flanking regions. In initial transformants having undergone the first recombination event, one expects two bands, one of 2.6 kb and one of 2 kb, corresponding to the endogenous 2.6 kb (w/ PPHD) and insert 2 kb (w/o PPHD), respectively, due to the genomic integration of pUIC3 into *P. putida*. Finally, a successful knockout should only show the insert 2kb fragment and the lack of the endogenous 2.6 kb fragment, as well as sensitivity to tetracycline. All of these conditions were observed (see main text). Furthermore, multiple additional rounds of colony-PCR using 3 different primers which bind to various regions of the PPHD gene were tested against both wild type *P. putida* and the

PPHD knockout and in all of these experiments the knockout was confirmed to lack the PPHD gene (data not shown).

2.11.8 PPHD kinetic assays

Standard hydroxylation assays for $PPHD_{putida}$ were carried out by preparing a reaction mix of 10 μM PPHD, 100 μM EF-Tu_{44-63} (H_2N-IVEFDKIDSAPEEKARGITI-$CONH_2$), 50 μM Fe(II)(prepared from $(NH_4)_2Fe(SO_4)_2$), 2 mM 2OG, 4 mM sodium L-ascorbate in 50 mM HEPES pH 7.5, 500 mM NaCl, 5% (v/v) glycerol. For determinations of apparent K_m of Fe(II), 2OG, ascorbate, and O_2, each cofactor concentration was varied and reactions were incubated at 37 °C for 30 minutes. For determination of apparent K_m of EF-Tu_{44-63} oligopeptide time courses at various concentrations of EF-Tu_{44-63} were carried out and steady-state reaction rate was determined. All reactions were quenched with an equal volume of 20% (v/v) formic acid. The extent of substrate hydroxylation was analysed by MALDI-TOF-MS (matrix-assisted laser-desorption ionisation–time-of-flight mass spectrometry). Recrystallised CHCA (α-cyano-4-hydroxycinnamic acid) MALDI matrix (1 μL) and quenched assay solution (1 μL) were spotted onto a 96-well MALDI sample plate and analysed using a Waters Micromass™ MALDI micro MX™ mass spectrometer in the positive ion reflectron mode with the following settings as described (*16*): laser energy 100-150, pulse 1950, detector 2350, suppression 700. Raw data was further analysed with MassLynx™ version 4.1. Data were fitted to the Michaelis-Menten equation using GraphPad Prism and kinetic parameters were determined from the fit. All assays were performed in triplicate and plotted as mean ± standard deviation.

2.11.9 MS/MS analysis of EF-Tu$_{44-63}$ modified Hyp54

MALDI-TOF mass spectrometry was carried out using a Bruker Ultraflex TOF/TOF mass spectrometer (*37*). The instrument was calibrated in MS mode directly before data acquisition with Peptide Calibration Standard II (Bruker Daltonics, Coventry, UK) using monoisotopic peptide masses. Peptides were spotted onto a MALDI sample as in PPHD$_{putida}$ kinetic assays. Sample ionisation was achieved with a nitrogen laser (337 nm) at 35-45% laser energy and MS/MS spectra were acquired by Laser-induced fragmentation (LIFT)(*38*).

2.11.10 Amino Acid analysis of EF-Tu$_{44-63}$ Hyp54

Amino acid hydrolysate was prepared by exposure of milligram quantities of Hyp54 modified EF-Tu$_{44-63}$ to constant boiling HCl (5.7 M) for 24 h at 110 °C under nitrogen atmosphere and dried by rotary evaporation. Standards were derivatised with 6-aminoquinolyl-*N*-hydroxysuccinimidyl carbamate by mixing amino acid hydrolysate diluted in 0.1 M HCl and derivatising solution (add 1 mL of 2B AccQTag reagent diluents (acetonitrile) to 2A (AccQTag reagent), vortexed and heated at 55 °C for 10 min. Derivatised amino acids, specifically hydroxyproline, were analysed against 4 standards (*cis*-3-, *trans*-3-, *cis*-4-, *trans*-4-hydroxyproline) on an AccQTag Ultra reversed phase C18 column, 2.1 x 100 mm, particles 1.7 µm (Waters). 1 µL of the sample was injected and separated by linear gradient elution of A [5% (v/v) AccQTag Eluent A)] to B [98.7% acetonitrile, 1.3% (v/v) formic acid], 0-25% over 25 min at a flow rate of 0.7 mL/min at 55 °C. UV detection was performed at a wavelength of 260 nm as described (*26*). The flow was split at 1:1 ratio before the mass spectrometer. The

relative stereochemistry of hydroxyproline was determined by comparison of elution times with the *trans*-3 and *trans*-4 hydroxyproline standards.

2.11.11 *In vitro* PPHD and EF-Tu protein-protein hydroxylation assay

An adaptation of the standard MALDI hydroxylation assay was performed in the presence of both full-length proteins to confirm that PPHD hydroxylates EF-Tu at Pro54 *in vitro* (Table 2.35).

Table 2.35. Composition of full-length PPHD and EF-Tu hydroxylation assay.

Reagent	Stock concentration (μM)	Volume added (μL)	Final concentration (μM)
PPHD	580	17	100 μM
EF-Tu	170	30	50 μM
Na ascorbate	4,000	10	400 μM
Na 2-oxoglutarate	4,000	10	400 μM
$(NH_4)_2Fe(SO_4)_2$	4,000	5	200 μM
Buffer D		28	

All stock reagents were dissolved in buffer D (50 mM HEPES pH 7.5, 500 mM NaCl, 1 mM TCEP, 5% glycerol) with the exception of $(NH_4)_2Fe(SO_4)_2$, which was dissolved in 20 mM HCl in order to prevent *in situ* rapid oxidation to Fe^{3+}. An excess of PPHD was used in an effort to hydroxylate EF-Tu and more easily differentiate non-hydroxylated and hydroxylated EF-Tu by LC-MS/MS. The reaction was incubated for 4 h at 30 °C and immediately subjected to in-solution trypsin digestion and LC-MS/MS analysis as described previously. In order to accurately determine the relative percent of hydroxylation in both reaction mixtures, the hydroxylated and non-hydroylated peptides containing Pro54 were quantified by manual inspection of the total ion count of each peptide in the raw data file.

2.11.12 MS/MS analysis of Pro54/Hyp54 in *P. putida* cells

P. putida substrain UWC1, *P. putida* UWC1 *PPHD* knockout strain, *P. putida* UWC1 *PPHD* knockout strain transformed with pBBR5_MCS2_PPHD(Kan^R), and *P. putida* UWC1 *PPHD* knockout strain transformed with pBBR5_MCS2_PPHD(D126A)(Kan^R) were grown overnight in LB medium supplemented with kanamycin (30 µg/mL) for plasmid-containing strains. Cells were harvested by centrifugation (10,000x*g*; 7 min), resuspended in 1 mL 50 mM HEPES pH 7.5, 200 mM NaCl, 10 mM $MgCl_2$, lysed on ice by sonication and the lysate was cleared by centrifugation (18,000x*g*; 10 min). The supernatant was analysed by SDS-PAGE and the gel band containing EF-Tu was excised and washed twice for 2 hours in 200 µL 50% (v/v) MeOH, 5% (v/v) acetic acid in H_2O, then 200 µL of acetonitrile was added and the gel pieces were dehydrated twice for 5 mins at room temperature and dried in a speedvac. 30 µL of 10 mM dithiothreitol (DTT) in 100 mM NH_4HCO_3 was added and the mixture was incubated for 10 min at room temperature, after which the supernatant was removed. 30 µL of 50 mM iodoacetamide in H_2O was added and the mixture was incubated for 10 min at room temperature, after which the supernatant was removed. 200 µL acetonitrile was added and the gel pieces were dehydrated for 5 mins, after which the supernatant was removed and dried in the speedvac. The gel pieces were rehydrated in 100 mM NH_4HCO_3 for 10 min, after which the solution was removed and 200 µL acetonitrile was added and the gel pieces were dried as before. 30 µL of trypsin (20 ng/µL) in 50 mM NH_4HCO_3 was added and the solution was incubated at 37 °C overnight.

2.11.13 MS/MS analysis of Pro54/Hyp54 in *P. aeruginosa* cells

P. aeruginosa PA01 wildtype and *P. aeruginosa PA0310* (*PPHD*) knockout strain were grown to stationary phase overnight in LB medium in aerobic (21% O_2) and anaerobic (<0.01% O_2) conditions (for anaerobic growth LB medium was supplemented with KNO_3). Cells were harvested by centrifugation (10,000x*g*; 7 min), resuspended in 1 mL 50 mM HEPES pH 7.5, 200 mM NaCl, lysed by homogenisation and the lysate was cleared by centrifugation (18,000x*g*; 10 min). The supernatant was analysed by SDS-PAGE and the gel band containing EF-Tu was excised and washed twice for 2 hours in 200 µL 50% (v/v) MeOH, 5% (v/v) acetic acid in H_2O, then 200 µL of acetonitrile was added and the gel pieces were dehydrated twice for 5 mins at room temperature and dried in a speedvac. 30 µL of 10 mM dithiothreitol (DTT) in 100 mM NH_4HCO_3 was added and the mixture was incubated for 10 min at room temperature, after which the supernatant was removed. 30 µL of 50 mM iodoacetamide in H_2O was added and the mixture was incubated for 10 min at room temperature, after which the supernatant was removed. 200 µL acetonitrile was added and the gel pieces were dehydrated for 5 mins, after which the supernatant was removed and dried in the speedvac. The gel pieces were rehydrated in 100 mM NH_4HCO_3 for 10 min, after which the solution was removed and 200 µL acetonitrile was added and the gel pieces were dried as before. 30 µL of ArgC (2 ng/µL) in 50 mM NH_4HCO_3 was added and the solution was incubated at 37 °C overnight. The peptides were then dried in a speedvac.

Liquid chromatography-tandem mass spectrometry was performed using an Ultimate 3000 nano-HPLC system (Dionex, Sunnyvale, CA, USA) comprising a WPS-3000 micro auto sampler, a FLM-3000 flow manager and column

compartment, an LPG-3600 dual-gradient micro-pump, and an SRD-3600 solvent rack controlled by Hystar (Bruker Daltonics, Billerica, MA, USA) and DCMS link 2.0 software. Samples were concentrated on a trapping column Dionex (Sunnyvale, CA, USA), 300 µm i.d., 0.1 cm) at a flow rate of 20 µL/min. For the separation with a C18 Pepmap column (75 µm i.d., 15 cm, Dionex), a flow rate of 250 nL/min was used as generated by a cap-flow splitter cartridge (1/1000). Peptides were eluted by the application of a 30 min multi-step gradient using solvents A (98% H2O, 2% acetonitrile, 0.1% formic acid) and B (80% acetonitrile, 20% water, 0.1% formic acid): 2-10% B, 0-3 min; 10-25% B, 3-18 min; 25-50% B, 18-30 min, 50-90% B, 30-30.2 min. The liquid chromatography was interfaced directly with a 3D high capacity ion trap mass spectrometer (amaZon; Bruker Daltonics) utilising 10 µm i.d. distal coated SilicaTips (New Objective, Woburn, MA, USA) and nano-ESI mode. Smart parameter settings (SPS) on the ion trap were tuned for a target mass of 850 m/z, compound stability 100% and an ion charge control (ICC) target of 250,000. MS/MS analysis was initiated on a contact closure signal triggered by HyStar software (version 3.2). Up to five precursor ions were selected per cycle with active exclusion (0.5 min) in collision-induced dissociation (CID) mode. CID fragmentation was achieved using helium gas and a 30%–200% collision energy sweep with amplitude 1.0 (ions are ejected from the trap as soon as they fragment).

Raw LC-MS/MS data were processed and Mascot compatible files were created using DataAnalysis 4.0 software (Bruker Daltonics). Database searches were performed using the Mascot algorithm (version 2.4.1) and the UniProt_SwissProt database with bacterial taxonomy restriction (v2013.12.08, number of entries 541,762, after taxonomy filter: 328,677). The following

parameters were applied: 2+, 3+ and 4+ ions, peptide mass tolerance 0.3 Da, 13C = 2, fragment mass tolerance 0.6 Da, number of missed cleavages: two, instrument type: ESI-TRAP, fixed modifications: Carbamidomethylation (Cys), variable modifications: Oxidation (Met), Oxidation (Pro).

2.11.14 Production and purification of Hyp54 modified EF-Tu

An *E. coli* BL21(DE3) cell pellet transformed with the pET28a_EF-Tu plasmid (with an *N*-terminal hexahistidine tag) was prepared as described (see protein purification). 10 mg of purified, untagged $PPHD_{putida}$, Fe(II), 2OG, and sodium L-ascorbate were added to the cell lysate at a final concentration of 50 µM, 2 mM, and 4 mM, respectively. The cell lysate was allowed to incubate for 1 hour at room temperature and then purification of EF-Tu proceeded as previously described.

The hydroxylation status of Pro54 was then analysed by trypsinolysis and MSMS analysis. 1 mg of purified EF-Tu modified Hyp54 was precipitated in MeOH/$CHCl_3$ and dissolved in 100 µL 6 M urea in 100 mM Tris-HCl buffer, pH 7.8 and further diluted in 30 µL of the same buffer. 5 µL 200 mM dithiothreitol (DTT) in 100 mM Tris-HCl buffer, pH 7.8 was added and the mixture was vortexed and incubated for 10 min at room temperature. 30 µL 200 mM iodoacetamide in 100 mM Tris-HCl, pH 7.8 was added and the mixture was vortexed and incubated for 10 min at room temperature. 30 µL 200 mM dithiothreitol (DTT) in 100 mM Tris buffer, pH 7.8 was added and the mixture was vortexed and incubated for an additional 10 min at room temperature. The mixture was diluted with 775 µL MilliQ-H_2O and vortexed. 20 µL trypsin (2 µg/µL in 25 mM Tris-HCl buffer, pH 7.8; Promega, S. aureus V8, MS grade) was

added and incubated at 37 °C overnight. The digested peptides were purified and analysed as described (*40*).

2.11.15 PPHD$_{putida}$ 2OG turnover

Experiments were recorded using a Bruker AVIII 700 instrument equipped with a 5 mm inverse cryoprobe and 3 mm MATCH tubes were used throughout (total sample volume 160 µL). Unless otherwise stated, mixture contained 10 µM PPHD$_{putida}$, 50 µM Fe(II), 500 µM 2OG, 600 µM EF-Tu$_{44-63}$, 1.25 mM ascorbate and 100 mM NaCl. Buffer contained 50 mM Tris-D11 (pH 7.5) and 0.02% (w/v) NaN_3 dissolved in 90% H_2O and 10% D_2O. Standard ^1H experiments (16 transients) were used, and water suppression was achieved using the excitation sculpting method (2 ms Sinc1.1000 pulse).

2.11.16 NMR binding studies

Mixtures for binding studies contained 50 µM *apo* (no metal bound) PPHD$_{putida}$, 50 µM $MnCl_2$, 50 µM EF-Tu (full length or EF-Tu$_{44-63}$ oligopeptide where applicable), 10 mM $MgCl_2$ and 200 mM NaCl. Solutions were buffered using ~30 mM Tris-D11 and ~20 mM HEPES pH 7.5 dissolved in 36.25% H_2O and 63.75% D_2O. Experiments were recorded using a Bruker AVII 500 instrument equipped with a 5 mm inverse TXI probe and 3 mm MATCH tubes were used throughout (total sample volume 160 µL). Saturation recovery (90°_x–G_1–90°_y–G_2–90°_x–G_3–τ–acq) experiments were performed with 1 scan with a relaxation delay of at least 5 times T_1 between transients. The gradient pulses were achieved using 1 ms Sinebell gradient pulse (G_1 = 40%; G_2 = 27.1%; G_3 = 15%). The receiver gain was set to minimum value (rg = 1) to prevent receiver

overload. Typically, 10 delay points varied between 100 ms and 60 s were used. T_1 values were obtained using the *Bruker T1/T2 Relaxation* option and peak area was used for curve fitting. The titrant (typically ~0.2 µL) was added using a 1 µL plunger-in-needle syringe (SGE) and sample mixing was conducted using a 250 µL gas tight syringe (SGE). Binding constants were obtained by non-linear curve fitting using OriginPro 8.0 (OriginLab) with the equation as described (*43*).

EF-Tu GTP-GDP turnover experiments were recorded using a Bruker AVIII 700 instrument equipped with a 5 mm inverse cryoprobe and 3 mm MATCH tubes were used throughout (total sample volume 160 µL). Unless otherwise stated, solutions contained 10 µM unmodified or hydroxylated EF-Tu, 50 µM kirromycin, 100 µM GTP, 50 µM *apo*-$PPHD_{putida}$ (where applicable), 100 µM $ZnCl_2$ (where applicable), 100 µM 2OG (where applicable), 10 mM $MgCl_2$ and 200 mM NaCl. Solutions were buffered in 50 mM HEPES pH 7.5 dissolved in 90% H_2O and 10% D_2O. Standard ^1H experiments (16 transients) were used, and water suppression was achieved using the excitation sculpting method (2 ms Sinc1.1000 pulse). For K_m and k_{cat} measurements for WT and hydroxylated EF-Tu, GTP to GDP turnover (at different GTP concentrations) were monitored five minutes after mixing.

PPHD-Mn(II) binding experiments were performed in the same manner as 2OG-binding experiments, except that the mixture contained 25 µM $MnCl_2$, 62.5 µM EF-Tu (unhydroxylated or modified Hyp54 where applicable) and 200 mM NaCl. The titrant was *apo* $PPHD_{putida}$. Solutions were buffered using ~40 mM Tris-D11 and ~10 mM HEPES pH 7.5 dissolved in 18.75% H_2O and 81.25% D_2O.

2.11.17 Measurement of translational accuracy in *P. putida*

The reporter vectors described here encode for an in-frame fusion of *Renilla reniformis* luciferase (RLuc) and *Photinus pyralis* (Firefly) luciferase (FLuc), separated by a cloning site for insertion of codons of interest. As a donor plasmid, a custom vector (pGEM-T-Easy-2000)(D.Phil. thesis, Dr. Armin Thalhammer, Chemistry, University of Oxford)(*80*) was used, containing the above construct, flanked by *BamH*I and *Sal*I restriction sites. The luciferase insert was released by triple digest with *BamH*I/*Sal*I/*Bsa*I and isolated by extraction from a TAE-agarose gel. The fragment was then subcloned into the compatible *BamH*I and *Xho*I restriction sites of pUC18-mini-Tn7T-LAC (Genbank ID AY599234), a broad host-range directed genomic integration plasmid for protein production from a lacI-repressed Plac promoter (*81*).

Variants of this construct bearing stop codons or matched sense codons were generated by insertion of annealed oligonucleotides (Table 2.36) into the unique *Asc*I/*Sbf*I restriction sites of the reporter plasmid using enzymatic ligation assisted by nucleases (ELAN)(*91*).

Table 2.36. List of oligonucleotides for generation of dual-luciferase reporter vectors.

Oligonucleotide	Codon	Sequence 5′ – 3′
iDual_14F	TGA	cgcgCTACGTGCGATTGACCGTTCGGAGCtgca
iDual_14R		GCTCCGAACGGTCAATCGCACGTAG
iDual_15F	CGA	cgcgCTACGTGCGATCGACCGTTCGGAGCtgca
iDual_15R		GCTCCGAACGGTCGATCGCACGTAG
iDual_16F	TAA	cgcgCTACGTGCGATTAAACGTTCGGAGCtgca
iDual_16R		GCTCCGAACGTTTAATCGCACGTAG
iDual_17F	CAA	cgcgCTACGTGCGATCAAACGTTCGGAGCtgca
iDual_17R		GCTCCGAACGTTTGATCGCACGTAG
iDual_18F	TAG	cgcgCTACGTGCGATTAGACGTTCGGAGCtgca
iDual_18R		GCTCCGAACGTCTAATCGCACGTAG
iDual_19F	CAG	cgcgCTACGTGCGATCAGACGTTCGGAGCtgca
iDual_19R		GCTCCGAACGTCTAGTCGCACGTAG

Solutions of oligonucleotides (25 μM each, desalted, obtained from Sigma-Aldrich) in 1x T4 DNA ligase buffer (New England Biolabs) were heated to 95 °C followed by slow cooling to room temperature to facilitate annealing of complementary strands and generation of compatible overhangs for ligation. Restriction-ligation reactions (20 μL total volume) contained 30 ng circular parental reporter vector, 5 μM oligonucleotide duplex, 5 U *Asc*I (New England Biolabs), 10 U *Sbf*I-HF (New England Biolabs) and 200 U T4 DNA ligase (New England Biolabs) in 1× T4 DNA ligase buffer (New England Biolabs). Reactions were incubated at 37 °C for 1 h and at room temperature for 3–6 h. 2 μL of the reaction mixture was then transformed into 50 μL XL10-Gold cells (Agilent) as described and plated on LB agar supplemented with ampicillin (100 μg/mL). Colonies were rapidly screened for their luciferase activity ratio, and selected colonies were grown in 2TY medium with ampicillin (100 μg/mL). DNA was isolated by MiniPrep and verified by Sanger sequencing using a custom primer (iDF, 5′-CGTTGTACAAATTGTTAGGA-3′), which binds to the RLuc open reading frame immediately upstream of the *Asc*I/*Sbf*I oligonucleotide insertion site.

To determine translation accuracy in *P. putida*, reporter constructs were transformed into wild-type and *PPHD* knockout strains of *P. putida* by co-electroporation (25 μF, 200 Ω, 2.5 kV)(*81*) with pUXBF13, which contains the genes for mini-Tn7 genome integration, and plated on LB agar supplemented with gentamicin (30 μg/mL). Single, well-isolated colonies were grown in 1 mL of growth medium (2TY or LB) without antibiotic in 5 mL plastic tubes at 28 °C with shaking (180 rpm). Where indicated, protein production from the lac promoter was induced by addition of 1 mM IPTG.

All samples and detection reagents were pre-equilibrated to ambient temperature before measurement. Aliquots of log-phase or stationary-phase cultures were lysed by addition of an equal volume of 2x passive lysis buffer (Promega) and incubated at ambient temperature for 15-20 s. Lysates prepared by this method displayed higher luciferase activities and showed less sample-to-sample variation than those prepared using lysis buffer supplemented with lysozyme, or using freeze-thaw lysis (*92*).

Luciferase activity was measured using the DLR Dual Luciferase Assay kit (Promega) and a GloMax 20/20 luminometer (Promega). Briefly, 20 µL LAR II reagent was placed in a 1.5 mL Eppendorf tube, 4 µL of lysate was added, mixed rapidly and firefly luciferase activity was measured immediately (integration time 10 s). Subsequently, 20 µL Stop&Glo reagent (Promega) was added and *Renilla* luciferase activity was determined (integration time 10 s).

Relative activities of *Renilla* and firefly luciferase were at least 1,000-fold and 5-fold higher than buffer-only background, respectively. Hence, luciferase activities were used without blank correction. To compare translational accuracy among experimental conditions, the ratios of the corrected *Renilla* and firefly luciferase activities were calculated for at least three independent biological samples grown to mid-log phase (OD_{600} = 0.6) and reported as mean ± standard deviation (*93*).

2.11.18 EF-Tu T_m determination by circular dichroism (CD) spectroscopy

The secondary structure of EF-Tu:GDP and EF-Tu:GDP Hyp54 (0.5 mg/mL; dissolved in 50 mM HEPES pH 7.5, 100 mM NaCl, 5 mM MgCl2) was monitored independently at 222 nm from 20-90 °C in a Chirascan CD

spectrometer. The curves were normalised to reflect % unfolding. CD spectra were performed in triplicate and fitted to the Boltzmann sigmoidal curve using GraphPad Prism software; data are plotted as the mean ± the standard deviation.

2.11.19 EF-Tu:EF-Ts binding studies

For EF-Tu:EF-Ts binding experiments, it was necessary to first prepare ^{15}N-labelled EF-Ts. M9 salt solution (Table 2.37) containing $^{15}NH_4Cl$ (Cambridge Isotope Laboratories) was prepared and sterilised by autoclaving. Upon cooling, 500 µL of 1M MgSO4·H2O, 50 mL of 20% (w/v) glucose, and 0.5% (w/v) vitamin B1 were sterilised using a syringe filter (0.22 µM; Millipore) and added to the M9 salt solution to create ^{15}N-labelled M9 media for protein production. Expression and purification of ^{15}N-labelled EF-Ts was performed in the same manner as described (see section 2.11.1).

Table 2.37. M9 minimal media salt solution.

Salt	Amount per litre
Na_2HPO_4	6.0 g
KH_2PO_4	3.0 g
$^{15}NH_4Cl$	1.0 g
NaCl	0.5 g
$CaCl_2$	0.3 mg

For binding experiments, the collective ^{15}N intensity of isolated ^{15}N-labelled EF-Ts (50 µM) was compared with ^{15}N-labelled EF-Tu in the presence of EF-Tu (50 µM) or Hyp54 modified EF-Tu (50 µM). Buffer contained 50 mM Tris-D11 (pH 7.5) and 0.02% (w/v) NaN_3 dissolved in 90% H_2O and 10% D_2O. Experiments were performed in triplicate and plotted as mean ± standard deviation.

2.11.20 Effect of pyocyanin on HIF-1α protein levels in human cells

Hela, MCF7, A549 and HEK293T cells were cultured in DMEM supplement with 10% fetal bovine serum, 4 mM L-glutamine, 100 U/mL penicillin, and 100 µg/mL streptomycin. Cells were seeded to reach 90-100% confluency prior to compound treatment. Cells were exposed to DMSO or inhibitors at final 1% DMSO for 6 hours. Cells were harvested in urea/SDS buffer with 1 mM dithiothreitol following PBS rinse. Cell lysate were analysed with SDS-PAGE, electroblotted to PVDF membrane (Millipore) and probed with corresponding primary antibody for 1 hour at room temperature or overnight at 4 °C. Secondary antibody specific to primary antibody species conjugated with HRP were applied at room temperature for 1 hour. Target proteins were then detected with SuperSignal Chemiluminescent Substrates (Pierce). Experimental provided by Dr. Tzu-Lan Ye, who also performed the experiment.

2.11.21 Expression of PPHD$_{putida}$ and EF-Tu$_{putida}$ in human cells

HEK293T cells were seeded in 6-well plate so that 40% confluency was reached prior to transfection. 1.3 µg of vectors comprising full length PPHD$_{putida}$ (pcDNA-LIC-PPHD) and EF-Tu$_{putida}$ (pcDNA-LIC-EF-Tu) were each mixed with 200 µl serum-free medium (Opti-MEM) and 5 µL polyethylenimine and incubated at room temperature for 30 mins. The solutions were then added to cell culture in each well. After 24 hours, half of the transfected cells were transfected again as described above to increase transfection efficiency. Cells were harvested on the third day for immunobloting. Experimental provided by Dr. Tzu-Lan Ye, who also performed the experiment.

2.12 References

1. C. Loenarz, M. L. Coleman, A. Boleininger, B. Schierwater, P. W. Holland, P. J. Ratcliffe, C. J. Schofield, The hypoxia-inducible transcription factor pathway regulates oxygen sensing in the simplest animal, Trichoplax adhaerens. *EMBO Rep.* **12**, 63-70 (2011).
2. M. A. McDonough, V. Li, E. Flashman, R. Chowdhury, C. Mohr, B. M. Lienard, J. Zondlo, N. J. Oldham, I. J. Clifton, J. Lewis, L. A. McNeill, R. J. Kurzeja, K. S. Hewitson, E. Yang, S. Jordan, R. S. Syed, C. J. Schofield, Cellular oxygen sensing: Crystal structure of hypoxia-inducible factor prolyl hydroxylase (PHD2). *Proc Natl Acad Sci U S A.* **103**, 9814-9819 (2006).
3. S. Marques, J. L. Ramos, Transcriptional control of the Pseudomonas putida TOL plasmid catabolic pathways. *Mol Microbiol.* **9**, 923-929 (1993).
4. P. G. Ward, M. Goff, M. Donner, W. Kaminsky, K. E. O'Connor, A two step chemo-biotechnological conversion of polystyrene to a biodegradable thermoplastic. *Environ Sci Technol.* **40**, 2433-2437 (2006).
5. P. B. Davis, M. Drumm, M. W. Konstan, Cystic fibrosis. *Am J Respir Crit Care Med.* **154**, 1229-1256 (1996).
6. D. Worlitzsch, R. Tarran, M. Ulrich, U. Schwab, A. Cekici, K. C. Meyer, P. Birrer, G. Bellon, J. Berger, T. Weiss, K. Botzenhart, J. R. Yankaskas, S. Randell, R. C. Boucher, G. Doring, Effects of reduced mucus oxygen concentration in airway Pseudomonas infections of cystic fibrosis patients. *J Clin Invest.* **109**, 317-325 (2002).
7. L. Saiman, A. Prince, Pseudomonas aeruginosa pili bind to asialoGM1 which is increased on the surface of cystic fibrosis epithelial cells. *J Clin Invest.* **92**, 1875-1880 (1993).
8. M. W. Budde, M. B. Roth, The Response of Caenorhabditis elegans to Hydrogen Sulfide and Hydrogen Cyanide. *Genetics.* **189**, 521-U584 (2011).
9. B. Schaible, K. Schaffer, C. T. Taylor, Hypoxia, innate immunity and infection in the lung. *Respir Physiol Neurobiol.* **174**, 235-243 (2010).
10. B. Schaible, C. T. Taylor, K. Schaffer, Hypoxia increases antibiotic resistance in Pseudomonas aeruginosa through altering the composition of multidrug efflux pumps. *Antimicrob Agents Chemother.* **56**, 2114-2118 (2012).
11. D. J. Wolter, P. D. Lister, Mechanisms of beta-lactam resistance among Pseudomonas aeruginosa. *Curr Pharm Des.* **19**, 209-222 (2013).
12. B. Schaible, S. McClean, A. Selfridge, A. Broquet, K. Asehnoune, C. T. Taylor, K. Schaffer, Hypoxia modulates infection of epithelial cells by Pseudomonas aeruginosa. *PLoS One.* **8**, e56491 (2013).
13. M. A. Jacobs, A. Alwood, I. Thaipisuttikul, D. Spencer, E. Haugen, S. Ernst, O. Will, R. Kaul, C. Raymond, R. Levy, L. Chun-Rong, D. Guenthner, D. Bovee, M. V. Olson, C. Manoil, Comprehensive transposon mutant library of Pseudomonas aeruginosa. *Proc Natl Acad Sci U S A.* **100**, 14339-14344 (2003).
14. G. W. Lau, D. J. Hassett, H. Ran, F. Kong, The role of pyocyanin in Pseudomonas aeruginosa infection. *Trends Mol Med.* **10**, 599-606 (2004).
15. I. M. Ahmad, B. E. Britigan, M. Y. Abdalla, Oxidation of thiols and modification of redox-sensitive signaling in human lung epithelial cells

exposed to Pseudomonas pyocyanin. *J Toxicol Environ Health A.* **74**, 43-51 (2011).
16. D. J. Hassett, L. Charniga, K. Bean, D. E. Ohman, M. S. Cohen, Response of Pseudomonas aeruginosa to pyocyanin: mechanisms of resistance, antioxidant defenses, and demonstration of a manganese-cofactored superoxide dismutase. *Infect Immun.* **60**, 328-336 (1992).
17. H. Ran, D. J. Hassett, G. W. Lau, Human targets of Pseudomonas aeruginosa pyocyanin. *Proc Natl Acad Sci U S A.* **100**, 14315-14320 (2003).
18. L. Allen, D. H. Dockrell, T. Pattery, D. G. Lee, P. Cornelis, P. G. Hellewell, M. K. Whyte, Pyocyanin production by Pseudomonas aeruginosa induces neutrophil apoptosis and impairs neutrophil-mediated host defenses in vivo. *J Immunol.* **174**, 3643-3649 (2005).
19. B. Cezairliyan, N. Vinayavekhin, D. Grenfell-Lee, G. J. Yuen, A. Saghatelian, F. M. Ausubel, Identification of Pseudomonas aeruginosa phenazines that kill Caenorhabditis elegans. *PLoS Pathog.* **9**, e1003101 (2013).
20. R. Wilson, T. Pitt, G. Taylor, D. Watson, J. MacDermot, D. Sykes, D. Roberts, P. Cole, Pyocyanin and 1-hydroxyphenazine produced by Pseudomonas aeruginosa inhibit the beating of human respiratory cilia in vitro. *J Clin Invest.* **79**, 221-229 (1987).
21. A. C. Epstein, J. M. Gleadle, L. A. McNeill, K. S. Hewitson, J. O'Rourke, D. R. Mole, M. Mukherji, E. Metzen, M. I. Wilson, A. Dhanda, Y. M. Tian, N. Masson, D. L. Hamilton, P. Jaakkola, R. Barstead, J. Hodgkin, P. H. Maxwell, C. W. Pugh, C. J. Schofield, P. J. Ratcliffe, C. elegans EGL-9 and mammalian homologs define a family of dioxygenases that regulate HIF by prolyl hydroxylation. *Cell.* **107**, 43-54 (2001).
22. T. Wang, M. J. Brown, mRNA quantification by real time TaqMan polymerase chain reaction: validation and comparison with RNase protection. *Anal Biochem.* **269**, 198-201 (1999).
23. H. Savli, A. Karadenizli, F. Kolayli, S. Gundes, U. Ozbek, H. Vahaboglu, Expression stability of six housekeeping genes: A proposal for resistance gene quantification studies of Pseudomonas aeruginosa by real-time quantitative RT-PCR. *J Med Microbiol.* **52**, 403-408 (2003).
24. N. Gupta, S. Tanner, N. Jaitly, J. N. Adkins, M. Lipton, R. Edwards, M. Romine, A. Osterman, V. Bafna, R. D. Smith, P. A. Pevzner, Whole proteome analysis of post-translational modifications: applications of mass-spectrometry for proteogenomic annotation. *Genome Res.* **17**, 1362-1377 (2007).
25. A. Tholey, E. Heinzle, Ionic (liquid) matrices for matrix-assisted laser desorption/ionization mass spectrometry-applications and perspectives. *Anal Bioanal Chem.* **386**, 24-37 (2006).
26. W. Ge, A. Wolf, T. Feng, C. H. Ho, R. Sekirnik, A. Zayer, N. Granatino, M. E. Cockman, C. Loenarz, N. D. Loik, A. P. Hardy, T. D. Claridge, R. B. Hamed, R. Chowdhury, L. Gong, C. V. Robinson, D. C. Trudgian, M. Jiang, M. M. Mackeen, J. S. McCullagh, Y. Gordiyenko, A. Thalhammer, A. Yamamoto, M. Yang, P. Liu-Yi, Z. Zhang, M. Schmidt-Zachmann, B. M. Kessler, P. J. Ratcliffe, G. M. Preston, M. L. Coleman, C. J. Schofield, Oxygenase-catalyzed ribosome hydroxylation occurs in prokaryotes and humans. *Nat Chem Biol.* **8**, 960-962 (2012).

27. W. G. Kaelin, Jr., P. J. Ratcliffe, Oxygen sensing by metazoans: the central role of the HIF hydroxylase pathway. *Mol Cell.* **30**, 393-402 (2008).
28. C. J. Webby, A. Wolf, N. Gromak, M. Dreger, H. Kramer, B. Kessler, M. L. Nielsen, C. Schmitz, D. S. Butler, J. R. Yates, 3rd, C. M. Delahunty, P. Hahn, A. Lengeling, M. Mann, N. J. Proudfoot, C. J. Schofield, A. Bottger, Jmjd6 catalyses lysyl-hydroxylation of U2AF65, a protein associated with RNA splicing. *Science.* **325**, 90-93 (2009).
29. J. Jones, D. J. Studholme, C. G. Knight, G. M. Preston, Integrated bioinformatic and phenotypic analysis of RpoN-dependent traits in the plant growth-promoting bacterium Pseudomonas fluorescens SBW25. *Environ Microbiol.* **9**, 3046-3064 (2007).
30. P. B. Rainey, Adaptation of Pseudomonas fluorescens to the plant rhizosphere. *Environ Microbiol.* **1**, 243-257 (1999).
31. S. Kojima, N. Takagi, T. Minagawa, N. Fushimi, K. I. Miura, Effects of amino acid replacements around the reactive site of chicken ovomucoid domain 3 on the inhibitory activity toward chymotrypsin and trypsin. *Protein Eng.* **12**, 857-862 (1999).
32. M. M. Mackeen, H. B. Kramer, K. H. Chang, M. L. Coleman, R. J. Hopkinson, C. J. Schofield, B. M. Kessler, Small-molecule-based inhibition of histone demethylation in cells assessed by quantitative mass spectrometry. *J Proteome Res.* **9**, 4082-4092 (2010).
33. T. Margus, M. Remm, T. Tenson, Phylogenetic distribution of translational GTPases in bacteria. *BMC Genomics.* **8**, 15 (2007).
34. J. Downward, Targeting ras signalling pathways in cancer therapy. *Nat Rev Cancer.* **3**, 11-22 (2003).
35. S. R. Neves, P. T. Ram, R. Iyengar, G protein pathways. *Science.* **296**, 1636-1639 (2002).
36. T. E. Dever, M. J. Glynias, W. C. Merrick, GTP-binding domain: three consensus sequence elements with distinct spacing. *Proc Natl Acad Sci U S A.* **84**, 1814-1818 (1987).
37. A. V. Furano, Content of elongation factor Tu in Escherichia coli. *Proc Natl Acad Sci U S A.* **72**, 4780-4784 (1975).
38. F. S. Young, A. V. Furano, Regulation of the synthesis of E. coli elongation factor Tu. *Cell.* **24**, 695-706 (1981).
39. H. J. Defeu Soufo, C. Reimold, U. Linne, T. Knust, J. Gescher, P. L. Graumann, Bacterial translation elongation factor EF-Tu interacts and colocalizes with actin-like MreB protein. *Proc Natl Acad Sci U S A.* **107**, 3163-3168 (2010).
40. X. Agirrezabala, J. Frank, Elongation in translation as a dynamic interaction among the ribosome, tRNA, and elongation factors EF-G and EF-Tu. *Q Rev Biophys.* **42**, 159-200 (2009).
41. T. M. Schmeing, R. M. Voorhees, A. C. Kelley, Y. G. Gao, F. V. t. Murphy, J. R. Weir, V. Ramakrishnan, The crystal structure of the ribosome bound to EF-Tu and aminoacyl-tRNA. *Science.* **326**, 688-694 (2009).
42. T. M. Schmeing, V. Ramakrishnan, What recent ribosome structures have revealed about the mechanism of translation. *Nature.* **461**, 1234-1242 (2009).

43. E. Jacquet, A. Parmeggiani, Structure-function relationships in the GTP binding domain of EF-Tu: mutation of Val20, the residue homologous to position 12 in p21. *EMBO J.* **7**, 2861-2867 (1988).
44. T. Pape, W. Wintermeyer, M. V. Rodnina, Complete kinetic mechanism of elongation factor Tu-dependent binding of aminoacyl-tRNA to the A site of the E. coli ribosome. *EMBO J.* **17**, 7490-7497 (1998).
45. J. R. Mesters, A. P. Potapov, J. M. de Graaf, B. Kraal, Synergism between the GTPase activities of EF-Tu.GTP and EF-G.GTP on empty ribosomes. Elongation factors as stimulators of the ribosomal oscillation between two conformations. *J Mol Biol.* **242**, 644-654 (1994).
46. T. Daviter, H. J. Wieden, M. V. Rodnina, Essential role of histidine 84 in elongation factor Tu for the chemical step of GTP hydrolysis on the ribosome. *J Mol Biol.* **332**, 689-699 (2003).
47. H. Berchtold, L. Reshetnikova, C. O. Reiser, N. K. Schirmer, M. Sprinzl, R. Hilgenfeld, Crystal structure of active elongation factor Tu reveals major domain rearrangements. *Nature.* **365**, 126-132 (1993).
48. J. F. Eccleston, M. R. Webb, Characterization of the GTPase reaction of elongation factor Tu. Determination of the stereochemical course in the presence of antibiotic X5108. *J Biol Chem.* **257**, 5046-5049 (1982).
49. M. Kjeldgaard, P. Nissen, S. Thirup, J. Nyborg, The crystal structure of elongation factor EF-Tu from Thermus aquaticus in the GTP conformation. *Structure.* **1**, 35-50 (1993).
50. R. M. Voorhees, T. M. Schmeing, A. C. Kelley, V. Ramakrishnan, The mechanism for activation of GTP hydrolysis on the ribosome. *Science.* **330**, 835-838 (2010).
51. T. P. Hausner, J. Atmadja, K. H. Nierhaus, Evidence That the G2661 Region of 23s Ribosomal-Rna Is Located at the Ribosomal-Binding Sites of Both Elongation-Factors. *Biochimie.* **69**, 911-923 (1987).
52. F. Rambelli, M. Brigotti, M. Zamboni, M. Denaro, L. Montanaro, S. Sperti, Effect of the antibiotic purpuromycin on cell-free protein-synthesizing systems. *Biochem J.* **259**, 307-310 (1989).
53. A. Wittinghofer, R. Leberman, Elongation factor T from Bacillus stearothermophilus and Escherichia coli. Purification and some properties of EF-Tu and EF-Ts from Bacillus stearothermophilus. *Eur J Biochem.* **62**, 373-382 (1976).
54. A. Wittinghofer, R. Guariguata, R. Leberman, Bacterial elongation factor Ts: isolation and reactivity with elongation factor Tu. *J Bacteriol.* **153**, 1266-1271 (1983).
55. H. J. Wieden, K. Gromadski, D. Rodnin, M. V. Rodnina, Mechanism of elongation factor (EF)-Ts-catalyzed nucleotide exchange in EF-Tu. Contribution of contacts at the guanine base. *J Biol Chem.* **277**, 6032-6036 (2002).
56. K. B. Gromadski, H. J. Wieden, M. V. Rodnina, Kinetic mechanism of elongation factor Ts-catalyzed nucleotide exchange in elongation factor Tu. *Biochemistry.* **41**, 162-169 (2002).
57. E. Villa, J. Sengupta, L. G. Trabuco, J. LeBarron, W. T. Baxter, T. R. Shaikh, R. A. Grassucci, P. Nissen, M. Ehrenberg, K. Schulten, J. Frank, Ribosome-induced changes in elongation factor Tu conformation control GTP hydrolysis. *Proc Natl Acad Sci U S A.* **106**, 1063-1068 (2009).

58. M. Klagsbrun, A. V. Furano, Methylated amino acids in the proteins of bacterial and mammalian cells. *Arch Biochem Biophys.* **169**, 529-539 (1975).
59. J. M. Van Noort, B. Kraal, K. M. Sinjorgo, N. L. Persoon, E. S. Johanns, L. Bosch, Methylation in vivo of elongation factor EF-Tu at lysine-56 decreases the rate of tRNA-dependent GTP hydrolysis. *Eur J Biochem.* **160**, 557-561 (1986).
60. A. Brutus, S. Y. He, Broad-spectrum defense against plant pathogens. *Nat Biotechnol.* **28**, 330-331 (2010).
61. S. Mukhopadhyay, S. Shankar, W. Walden, A. M. Chakrabarty, Complex formation of the elongation factor Tu from Pseudomonas aeruginosa with nucleoside diphosphate kinase modulates ribosomal GTP synthesis and peptide chain elongation. *J Biol Chem.* **272**, 17815-17820 (1997).
62. D. Ehrismann, E. Flashman, D. N. Genn, N. Mathioudakis, K. S. Hewitson, P. J. Ratcliffe, C. J. Schofield, Studies on the activity of the hypoxia-inducible-factor hydroxylases using an oxygen consumption assay. *Biochem J.* **401**, 227-234 (2007).
63. M. Hirsila, P. Koivunen, V. Gunzler, K. I. Kivirikko, J. Myllyharju, Characterization of the human prolyl 4-hydroxylases that modify the hypoxia-inducible factor. *Journal of Biological Chemistry.* **278**, 30772-30780 (2003).
64. E. Flashman, L. M. Hoffart, R. B. Hamed, J. M. Bollinger, C. Krebs, C. J. Schofield, Evidence for the slow reaction of hypoxia-inducible factor prolyl hydroxylase 2 with oxygen. *Febs J.* **277**, 4089-4099 (2010).
65. J. C. Price, E. W. Barr, B. Tirupati, J. M. Bollinger, C. Krebs, The first direct characterization of a high-valent iron intermediate in the reaction of an alpha-ketoglutarate-dependent dioxygenase: A high-spin Fe(IV) complex in taurine/alpha-ketoglutarate dioxygenase (TauD) from Escherichia coli. *Biochemistry.* **42**, 7497-7508 (2003).
66. J. J. Hutton, Jr., A. L. Trappel, S. Udenfriend, Requirements for alpha-ketoglutarate, ferrous ion and ascorbate by collagen proline hydroxylase. *Biochem Biophys Res Commun.* **24**, 179-184 (1966).
67. J. J. Hutton, A. L. Tappel, Udenfrie.S, Cofactor and Substrate Requirements of Collagen Proline Hydroxylase. *Archives of Biochemistry and Biophysics.* **118**, 231-& (1967).
68. E. Flashman, S. L. Davies, K. K. Yeoh, C. J. Schofield, Investigating the dependence of the hypoxia-inducible factor hydroxylases (factor inhibiting HIF and prolyl hydroxylase domain 2) on ascorbate and other reducing agents. *Biochem J.* **427**, 135-142 (2010).
69. E. Flashman, E. A. Bagg, R. Chowdhury, J. Mecinovic, C. Loenarz, M. A. McDonough, K. S. Hewitson, C. J. Schofield, Kinetic rationale for selectivity toward N- and C-terminal oxygen-dependent degradation domain substrates mediated by a loop region of hypoxia-inducible factor prolyl hydroxylases. *J Biol Chem.* **283**, 3808-3815 (2008).
70. L. A. McNeill, E. Flashman, M. R. Buck, K. S. Hewitson, I. J. Clifton, G. Jeschke, T. D. Claridge, D. Ehrismann, N. J. Oldham, C. J. Schofield, Hypoxia-inducible factor prolyl hydroxylase 2 has a high affinity for ferrous iron and 2-oxoglutarate. *Mol Biosyst.* **1**, 321-324 (2005).

71. A. Parmeggiani, G. Sander, Properties and regulation of the GTPase activities of elongation factors Tu and G, and of initiation factor 2. *Mol Cell Biochem.* **35**, 129-158 (1981).
72. F. Mansilla, C. R. Knudsen, M. Laurberg, B. F. Clark, Mutational analysis of Escherichia coli elongation factor Tu in search of a role for the N-terminal region. *Protein Eng.* **10**, 927-934 (1997).
73. H. Wolf, G. Chinali, A. Parmeggiani, Kirromycin, an inhibitor of protein biosynthesis that acts on elongation factor Tu. *Proc Natl Acad Sci U S A.* **71**, 4910-4914 (1974).
74. H. Wolf, G. Chinali, A. Parmeggiani, Mechanism of the inhibition of protein synthesis by kirromycin. Role of elongation factor Tu and ribosomes. *Eur J Biochem.* **75**, 67-75 (1977).
75. J. P. Abrahams, M. J. van Raaij, G. Ott, B. Kraal, L. Bosch, Kirromycin drastically reduces the affinity of Escherichia coli elongation factor Tu for aminoacyl-tRNA. *Biochemistry.* **30**, 6705-6710 (1991).
76. P. Bhuta, G. Kumar, S. Chladek, Elongation-Factor Tu.Ribosome Dependent Guanosine 5'-Triphosphate Hydrolysis - Elucidation of the Role of the Aminoacyl Transfer Ribonucleic-Acid 3' Terminus and Site(S) Involved in the Inducing of the Guanosinetriphosphatase Reaction. *Biochemistry.* **21**, 899-905 (1982).
77. H. Rutthard, A. Banerjee, M. W. Makinen, Mg2+ is not catalytically required in the intrinsic and kirromycin-stimulated GTPase action of Thermus thermophilus EF-Tu. *J Biol Chem.* **276**, 18728-18733 (2001).
78. O. Fasano, W. Bruns, J. B. Crechet, G. Sander, A. Parmeggiani, Modification of elongation-factor-Tu . guanine-nucleotide interaction by kirromycin. A comparison with the effect of aminoacyl-tRNA and elongation factor Ts. *Eur J Biochem.* **89**, 557-565 (1978).
79. C. M. Tegley, V. N. Viswanadhan, K. Biswas, M. J. Frohn, T. A. N. Peterkin, C. Chang, R. W. Burli, J. H. Dao, H. Veith, N. Rogers, S. C. Yoder, G. Biddlecome, P. Tagari, J. R. Allen, R. W. Hungate, Discovery of novel hydroxy-thiazoles as HIF-alpha prolyl hydroxylase inhibitors: SAR, synthesis, and modeling evaluation. *Bioorg Med Chem Lett.* **18**, 3925-3928 (2008).
80. C. Loenarz, R. Sekirnik, A. Thalhammer, W. Ge, E. Spivakovsky, M. M. Mackeen, M. A. McDonough, M. E. Cockman, B. M. Kessler, P. J. Ratcliffe, A. Wolf, C. J. Schofield, Hydroxylation of the eukaryotic ribosomal decoding center affects translational accuracy. *Proc Natl Acad Sci U S A.* **111**, 4019-4024 (2014).
81. K. H. Choi, H. P. Schweizer, mini-Tn7 insertion in bacteria with single attTn7 sites: example Pseudomonas aeruginosa. *Nat Protoc.* **1**, 153-161 (2006).
82. A. P. Carter, W. M. Clemons, D. E. Brodersen, R. J. Morgan-Warren, B. T. Wimberly, V. Ramakrishnan, Functional insights from the structure of the 30S ribosomal subunit and its interactions with antibiotics. *Nature.* **407**, 340-348 (2000).
83. I. K. Leung, E. Flashman, K. K. Yeoh, C. J. Schofield, T. D. Claridge, Using NMR solvent water relaxation to investigate metalloenzyme-ligand binding interactions. *J Med Chem.* **53**, 867-875 (2010).

84. L. D. Dahl, H. J. Wieden, M. V. Rodnina, C. R. Knudsen, The importance of P-loop and domain movements in EF-Tu for guanine nucleotide exchange. *J Biol Chem.* **281**, 21139-21146 (2006).
85. T. Kawashima, C. Berthet-Colominas, M. Wulff, S. Cusack, R. Leberman, The structure of the Escherichia coli EF-Tu.EF-Ts complex at 2.5 A resolution. *Nature.* **379**, 511-518 (1996).
86. T. D. Caldas, A. El Yaagoubi, G. Richarme, Chaperone properties of bacterial elongation factor EF-Tu. *J Biol Chem.* **273**, 11478-11482 (1998).
87. A. Malki, T. Caldas, A. Parmeggiani, M. Kohiyama, G. Richarme, Specificity of elongation factor EF-TU for hydrophobic peptides. *Biochem Biophys Res Commun.* **296**, 749-754 (2002).
88. S. M. Kelly, N. C. Price, The application of circular dichroism to studies of protein folding and unfolding. *Bba-Protein Struct M.* **1338**, 161-185 (1997).
89. P. H. Anborgh, A. Parmeggiani, J. Jonak, Site-Directed Mutagenesis of Elongation-Factor Tu - the Functional and Structural Role of Residue Cys81. *European Journal of Biochemistry.* **208**, 251-257 (1992).
90. N. R. Rose, M. A. McDonough, O. N. King, A. Kawamura, C. J. Schofield, Inhibition of 2-oxoglutarate dependent oxygenases. *Chem Soc Rev.* **40**, 4364-4397 (2011).
91. G. J. Cost, Enzymatic ligation assisted by nucleases: simultaneous ligation and digestion promote the ordered assembly of DNA. *Nat Protoc.* **2**, 2198-2202 (2007).
92. J. R. de Wet, K. V. Wood, D. R. Helinski, M. DeLuca, Cloning of firefly luciferase cDNA and the expression of active luciferase in Escherichia coli. *Proc Natl Acad Sci U S A.* **82**, 7870-7873 (1985).
93. J. L. Jacobs, J. D. Dinman, Systematic analysis of bicistronic reporter assay data. *Nucleic Acids Res.* **32**, e160 (2004).

3 Crystal structures of PPHD, EF-Tu, and a PPHD:EF-Tu protein-protein complex

3.1 Crystal structure of PPHD

Although acting on, at least apparently, evolutionarily unrelated substrates, the observation that PPHD and PHD2 both catalyse *trans* prolyl-4-hydroxylation prompted investigations into their structural similarity, especially given their low sequence homology [(29% sequence identity over their catalytic domains (full-length PPHD and $PHD2_{181-426}$)](*1*). Therefore, structural studies on PPHD were pursued.

3.1.1 Differential scanning fluorimetry to probe optimal conditions for PPHD stability

Initial crystallisation experiments on PPHD were performed in a systematic manner, in which parameters were optimised sequentially. Differential scanning fluorimetry (DSF or T_m shift) can be used to probe the stability of purified proteins in the presence of small molecule ligands by monitoring the thermal unfolding of proteins in real-time (*2*). DSF has been of use in the identification of selective inhibitors of the Jumonji C (JmjC) histone demethylases (*2, 3*). DSF relies on the use of a fluorescent dye (*4, 5*), which is highly fluorescent in a non-polar environment; fluorescence increases exponentially as the hydrophobic core of the protein is revealed by thermal denaturation. The midpoint of the sigmoidal denaturation curve, at which the protein is 50% folded, corresponds to the T_m. The presence of (de)stabilising

ligands may alter the protein T_m by an arbitrary amount (ΔT_m), which reflects an (decrease) increase in overall protein stability. DSF can be performed in a medium-throughput manner and is of use in identifying optimal buffers/metals/ligands for protein crystallisation (*6*).

DSF was used to optimise the stability of PPHD in the presence of various buffers and metals. Most buffers, especially those outside the range of physiological pH (i.e. 6.5-7.5), were found to destabilise PPHD (Figure 3.1). An extreme example was 100 mM MES pH 6.0, which exhibited a ΔT_m of -10 °C. Notably, simple dilution of PPHD in water (trace HEPES pH 7.5 buffer) was found to be amongst the conditions causing the highest increase in stability (ΔT_m = 0)(Figure 3.1), suggesting that low buffer concentrations, which are ideal for crystallisation, may be optimal for PPHD stability. Although Tris-HCl pH 7.0 and PIPES pH 7.0 showed the best overall stabilisation (ΔT_m = 0)(Figure 3.1), HEPES pH 7.5 was chosen as the optimal PPHD buffer for crystallisation trials as its pK_a is the most stable ΔT_m over temperature changes (*7*), and its use would thus remove an additional variable during crystallisation at different temperatures. The results reveal that PPHD is most stable at neutral pH 7.

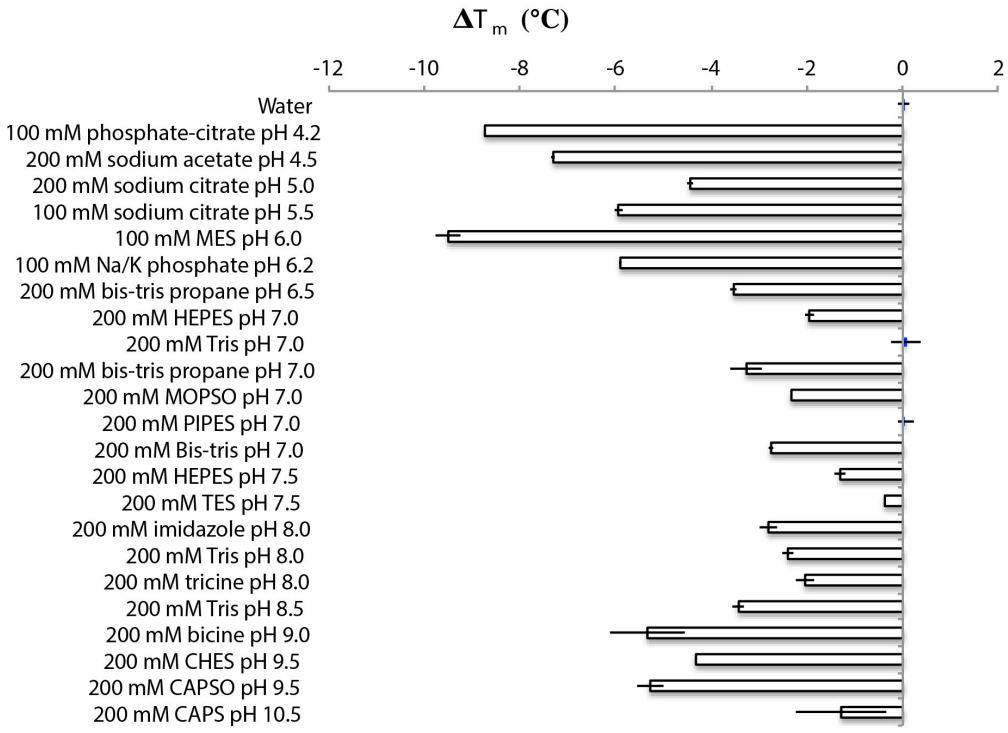

Figure 3.1. Differential scanning fluorimetry screen of various buffers for PPHD stabilisation. The results shown are the mean ± s.d. of duplicates with water as a reference.

Various metal ions were then screened for the stabilisation of PPHD. Mn(II) ions were found to stabilise *apo* PPHD (i.e. no metal bound)[prepared through overnight incubation of PPHD with ethylenediaminetetraacetic acid (EDTA)] to the same degree as Fe(II) ions (ΔT_m ~5 °C) (Figure 3.2). Both Co(II) and Ni(II) ions also manifested a similar degree of PPHD stabilisation (ΔT_m ~5 °C)(Figure 3.2). In contrast, Zn(II) and Cd(II) ions caused clear destabilisation of PPHD (ΔT_m >-10 °C)(Figure 3.2). Mg(II) ions were observed to have little effect on PPHD stability (ΔT_m ~ 0 °C)(Figure 3.2), likely suggesting that Mg(II) does not bind in the PPHD metal-binding site. Mn(II) ions (from $MnCl_2$) were chosen over Ni(II) ions as the preferred metal for crystallisation experiments on PPHD in order to avoid complications resulting from Ni(II) affinity to the *N*-terminal

hexahistidine tag of the recombinant PPHD and due to the resistance of Mn(II) ions to oxidation compared to those of Fe(II).

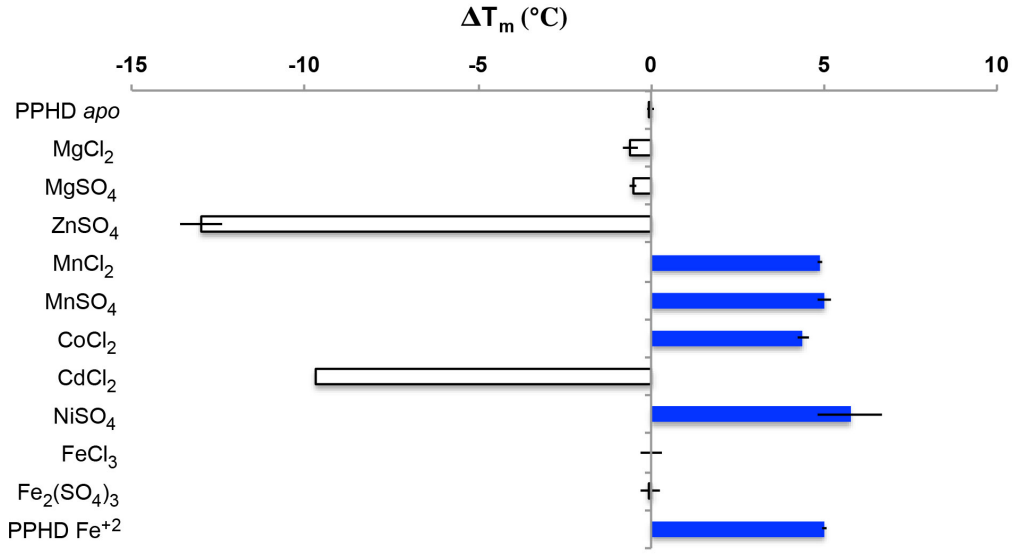

Figure 3.2. Differential scanning fluorimetry screen of various transition metals with PPHD. Results shown are the mean ± s.d. of duplicates with *apo* (no metal bound) PPHD as a reference.

3.1.2 Crystallisation trials, hit identification and optimisation

For crystallisation trials with PPHD, in addition to $MnCl_2$ [used as a surrogate for Fe(II) to promote a stable complex] was added a simple 2OG-mimetic inhibitor, *N*-oxalylglycine (NOG) (Fig 3.3).

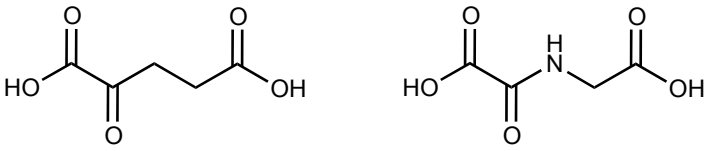

Figure 3.3. Structural comparison of 2OG (left) and NOG (right).

Crystallisation screening experiments on PPHD began with the testing of multiple commercial crystallisation screens at both 20 and 4 °C – i.e. the JCSG+, PACT Premier, SaltRx, Index, MIDAS, Structure, and PEGION screens (Molecular Dimensions and Hampton Research)(*8-13*). Initial crystal hits were observed in

JCSG+ well C3.2 at 20 °C in the presence of 0.2 M ammonium nitrate and 20% (w/v) PEG 3350 and were of a haystack morphology (Figure 3.4*A*). Numerous rounds of seeding and optimisation around ammonium nitrate and PEG 3350 concentration, as well as PPHD concentration, did not improve the haystack morphology and/or reproducibility of the crystals. To overcome this issue, both the Additive and Detergent Screens (Hampton Research)(*14-17*) were then attempted, from which small single crystals of hexagonal morphology were visible in the presence of 10% (w/v) benzyldimethyldodecylammonium bromide (BAM), a cationic detergent (Figure 3.4*B*). After further optimisation, 400 µm x 150 µm x 150 µm rhombohedral crystals were harvested and taken to the synchrotron X-ray source at Diamond Light Source for diffraction studies.

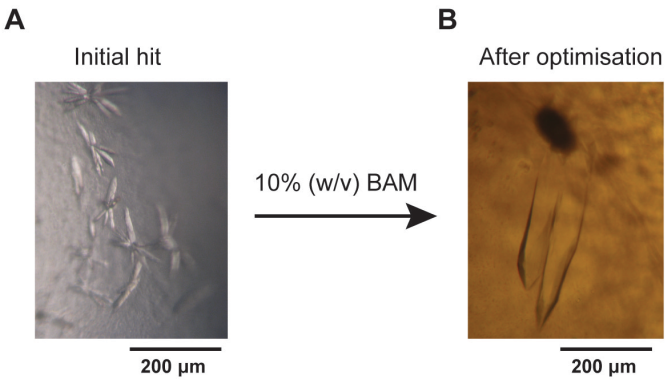

Figure 3.4. Optimisation of PPHD crystallisation. (**A**) Haystack morphology PPHD crystals from JCSG well C3. (**B**) Subsequent optimisation by addition of 10% (w/v) BAM produced diffraction quality crystals in the hexagonal space group *P* 6_5 2 2.

3.1.3 Crystallisation and data collection in the P 6_5 2 2 crystal form

A complete dataset to 2.4 Å resolution (of PPHD crystals derived from Figure 3.4*B*) was collected in the hexagonal space group *P* 6_5 2 2 with one PPHD molecule in the asymmetric unit. The structure was solved by molecular replacement (MR) using the MR-PHASER (*18*) subroutine of the PHENIX

crystallographic software package (*19*) using a structure of human PHD2 (PDB ID: 2G1M)(*1*) as a search model.

Cocrystallisation of PPHD and EF-Tu_{44-63} was pursued in tandem with the work on isolated PPHD. $MnCl_2$ and NOG were used as before. Initial hits were observed in PACT well B2 in the presence of 0.1 M MIB buffer (malonic acid, imidazole, boric acid) pH 5.0 and 25% (w/v) PEG 1500 (Figure 3.5). Despite the haystack morphology of the crystals, a single crystal of the putative PPHD:EF-Tu_{44-63} complex was successfully harvested, from which a complete dataset to 2.0 Å resolution was collected.

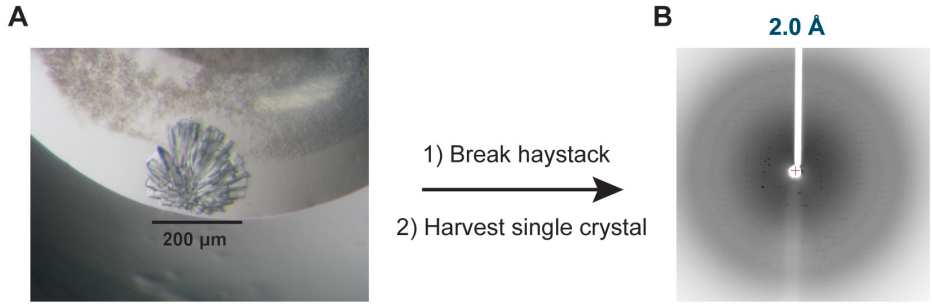

Figure 3.5. PPHD crystallisation in the *P* 1 crystal form. (**A**) Haystack morphology PPHD crystals from PACT well B2. (**B**) The haystack was broken and a single crystal was harvested that diffracted to 2.0 Å in the triclinic space group *P* 1.

The data for the putative PPHD:EF-Tu_{44-63} complex was indexed in the triclinic space group *P* 1. There are 8 PPHD molecules in the asymmetric unit, of which 4 are translationally pseudosimilar to the remaining 4 (Figure 3.6). Translational pseudosymmetry is defined by a strong origin peak in the asymmetric unit at a distance defined by a non-crystallographic symmetry (NCS) operator (x+*a*, y+*b*, z+*c*) other than identity, and can often complicate data processing by causing incorrect assignment of a higher symmetry space group (*20*). Further, pseudosymmetry in crystallographic data is quite common. As of

2006, roughly 8% of structures deposited in the PDB exhibited some form of pseudosymmetry (*20*). In this case, the pseudosymmetric NCS operator is (x, y+0.5, z) and the resulting incorrect space group of higher symmetry is the monoclinic space group *C* 2. The space group was correctly identified as triclinic *P* 1. Subsequent analyses revealed that electron density was observed for Mn(II) and NOG; yet, no electron density for EF-Tu$_{44\text{-}63}$ was observed in the PPHD active site (see section 3.4 for the successful determination of a PPHD:EF-Tu complex structure). However, due to the higher resolution of the *P* 1 over the original *P* 6_5 2 2 crystal form (2.0 Å vs 2.4 Å, respectively), model building and structure refinement were performed using the 2.0 Å resolution data via the iterative use of COOT (*21*) and PHENIX (*19*) until R_{work} and R_{free} converged. Mn(II), NOG, and water molecules (and not EF-Tu$_{44\text{-}63}$ peptide) were modelled in the final stages of refinement based on the $F_{obs} - F_{calc}$ electron density map.

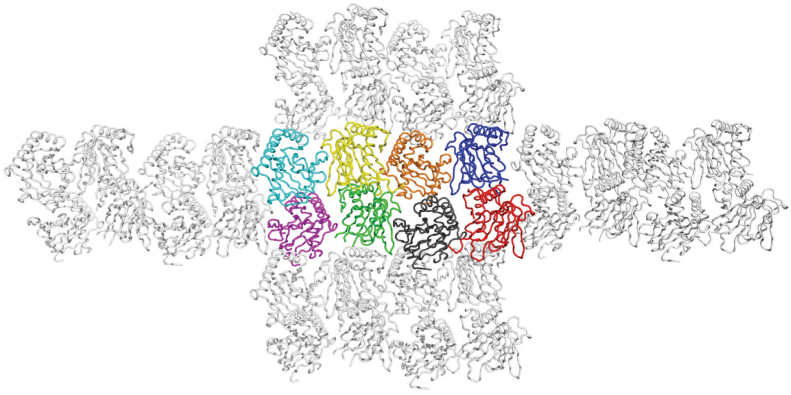

Figure 3.6. Crystal packing of isolated PPHD in the triclinic *P* 1 space group reveals translational pseudosymmetry within the asymmetric unit. View from a crystal structure showing packing of PPHD with 8 molecules in the asymmetric unit (space group: *P* 1; unit cell dimensions: 45.33 Å, 62.16 Å, 132.83 Å); chains A (red), B (green), C (blue), D (yellow), E (magenta), F (cyan), G (orange), H (black), and selected symmetry related molecules (grey). Chains A, C, G and H are translationally pseudosymmetrical to chains B, D, E and F.

3.1.4 Overall structure of PPHD and comparison with that of human PHD2

Consistent with all structurally characterised 2OG oxygenases (*22*), the PPHD structure contains a core DSBH (jelly-roll) fold, which is composed of 8 β-strands (I-VIII) that pack to form a major and minor β-sheet that surround the metal- and 2OG-binding sites (Figure 3.7*A*). Five antiparallel β-strands [β1-β2(I)-β4(III)-β7(VI)-β9(VIII)] form the major β-sheet and four antiparallel β-strands [β3(II)-β5(IV)-β6(V)-β8(VII)] form the minor β-sheet. A cluster of helices (α1-α3) packs against the major β-sheet. Two 3_{10}-helices, $3_{10}1$ and $3_{10}2$, are present in loops connecting the βIII-βIV and the βIV-βV strands, respectively.

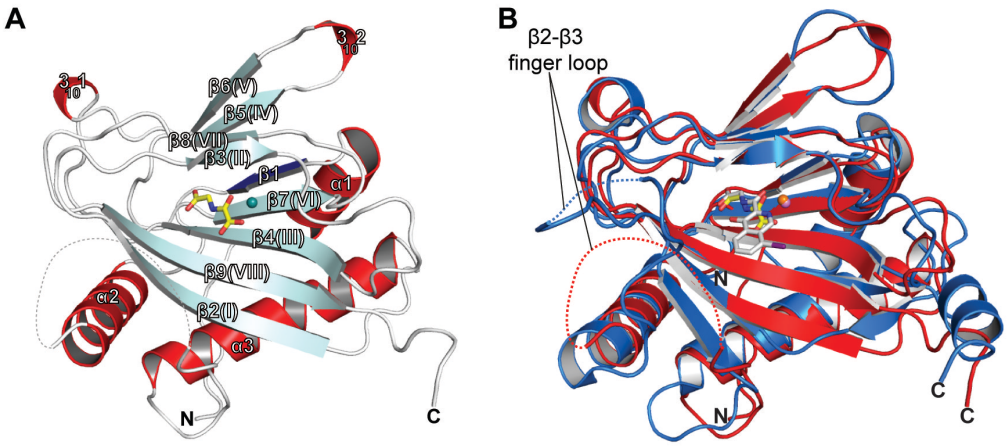

Figure 3.7. The overall structure of PPHD reveals structural homology to that of human PHD2. (**A**) Ribbons representation of an overall structure of PPHD; DSBH-associated β-strands (pale cyan), roman numerals indicate strands in core DSBH, DSBH-extension β-strands (dark blue), α-helices (red), loops (white), NOG (yellow), Mn(II) (teal sphere). (**B**) Superposition of PPHD(red):NOG(yellow) and human PHD2(blue):**1**(grey) [**1**: *N*-(4-hydroxy-8-iodoisoquinolin-3-yl)carbonylglycine] structures reveals that their overall folds are very similar (PDB ID: 2G1M). Mn(II) (pink sphere) is present in the metal-binding site of PPHD and Fe(II) (orange sphere) in that of PHD2. Figure and figure legend are adapted with permission from J.S. Scotti *et al*, Human oxygen sensing may have origins in prokaryotic elongation factor Tu prolyl-hydroxylation. *Proc Nat Acad Sci USA*. In press (2014).

Superimposition of PPHD and human PHD2 structures (PDB ID: 2G1M; r.m.s.d. value of 1.7 Å over 181 Ca atoms)(*1*) reveals that their overall folds and catalytic domains are very similar, with two exceptions: i) the *C*-terminus of

PPHD is present in a loop conformation, yet is α-helical in PHD2; and ii) PHD2 contains one additional β-strand (β2) in its major β-sheet which is not present in PPHD, likely due to disorder in that region (residues 47-71) of PPHD (Figure 3.7*B*). The disordered region (residues 47-71) corresponds to the β2-β3 finger loop of PHD2 (Figure 3.7*B*), which has been shown to be conformationally flexible and important in HIF-α substrate binding (*1, 23*). The β5(II)-β6(III) loop (residues 128-134) represents another noteworthy disordered region in the structure, positioned at the active site opening directly *C*-terminal to the HXD metal-binding motif (residues 124-126). A disordered region juxtaposed so closely to the highly ordered core was of interest as it suggested that these residues may be involved in substrate binding.

3.1.5 The PPHD active site

PPHD contains an active site HXD…H metal-binding motif comprised of His124, Asp126, and His183, which along with NOG and a single water molecule octahedrally coordinate Mn(II)(Figure 3.8). Similar to PHD2 (*1*), His124 and Asp126 are positioned on βII(β3) and the loop region between strands βII(β3)and βIII(β4); the 'distal' histidine, His183, originates from strand βVII(β8). The PPHD active site superimposes well with that of PHD2 and shows that NOG binds in the PPHD core between the major and minor β-sheets of the DSBH fold and has bidentate metal coordination (oxalate group of NOG) and forms a salt bridge (C-5 carboxylate of NOG) to Arg192 (Arg383 in PHD2)(Figure 3.7*B* and Figure 3.8). Further, PPHD and PHD2 share strong conservation of residues in the core DSBH: $Ala113_{PPHD}$/$Ala301_{PHD2}$, $His124_{PPHD}$/$His313_{PHD2}$, $Asp126_{PPHD}$/$Asp315_{PHD2}$, $Ser137_{PPHD}$/$Thr325_{PHD2}$, $Tyr141_{PPHD}$/$Tyr329_{PHD2}$,

Leu154$_{PPHD}$/Leu343$_{PHD2}$, His183$_{PPHD}$/His374$_{PHD2}$, Val185$_{PPHD}$/Val376$_{PHD2}$, Arg192$_{PPHD}$/Arg383$_{PHD2}$, Ser194$_{PPHD}$/Ala385$_{PHD2}$, Thr196$_{PPHD}$/Thr387$_{PHD2}$, Trp198$_{PPHD}$/Trp389$_{PHD2}$. The evident similarity between the PPHD and PHD2 structures confirmed the presence of a human PHD homologue in prokaryotes, and raised questions concerning the evolutionary relationship of the two proteins (see Chapter 6 for a detailed discussion).

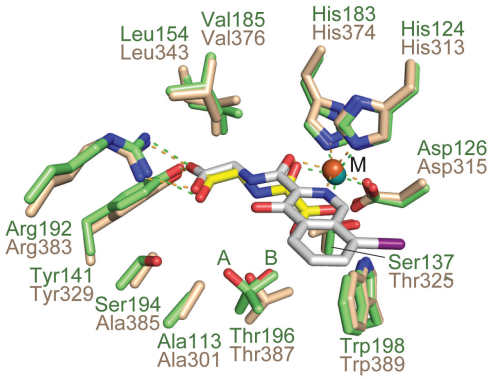

Figure 3.8. PPHD and PHD2 active site superimpositions reveal evolutionary conservation of the residues at the active site. Superimposition of PPHD(green):NOG(yellow) and human PHD2(brown):**1**(grey)[**1**: *N*-(4-hydroxy-8-iodoisoquinolin-3-yl)carbonylglycine](PDB ID: 2G1M) active sites reveals similarity in active site residues. M refers to Mn(II) (teal sphere) and Fe(II) (orange sphere). Figure and figure legend are adapted with permission from J.S. Scotti *et al*, Human oxygen sensing may have origins in prokaryotic elongation factor Tu prolyl-hydroxylation. *Proc Nat Acad Sci USA*. In press (2014).

3.1.6 Overall structural comparison of PPHD to PHD2 and collagen prolyl-4-hydroxylases

Given the clear structural homology between PPHD and PHD2, it was of interest to compare PPHD to another subfamily of prolyl-4-hydroxylases, the CP4Hs. Two structures of isolated (no substrate bound) CP4H-related proteins have been reported: the prokaryotic *Bacillus anthracis* P4H (BaP4H; PDB ID: 3ITQ)(*24*) and the algal *Chlamydomonas reinhardtii* P4H (CrP4H; PDB ID: 2JIG)(*25*).

Superimpositions of PPHD and CrP4H/BaP4H (PPHD/CrP4H r.m.s.d. 2.8 Å over 151 Cα atoms**;** PPHD/BaP4H r.m.s.d. 2.6 Å over 149 Cα atoms) reveal that PPHD is more structurally homologous to PHD2 than to the CP4Hs, and suggests that PPHD and PHD2 are members of a different structural subfamily than are CrP4H and BaP4H (CrP4H and BaP4H r.m.s.d. 2.1 Å over 172 Cα atoms)(r.m.s.d. calculated using the pairwise Dali server)(Figure 3.9, *A* and *C*)(*26*). The CrP4H and BaP4H structures both contain inserts between DSBH core β-strands that are absent in the PPHD structure. Compared to PPHD, CrP4H has insertions in i) the βIV-βV loop (8 residue insertion) that, like the PPHD βIV-βV loop, contains a 3_{10}-helix, and ii) the βII-βIII loop (11 residues), which is positioned at the active site opening analogously to the disordered region in the PPHD structure (residues 128-134), further implicating that region in PPHD substrate binding. Both CrP4H and BaP4H contain an insertion (8 residues) between βVI-βVII; 5 residues of which fold into an α-helix in the case of BaP4H. PPHD α3 (21 residues) is elongated compared to the corresponding helices of CrP4H and BaP4H (both 14 residues)(Figure 3.9, *A* and *C*).

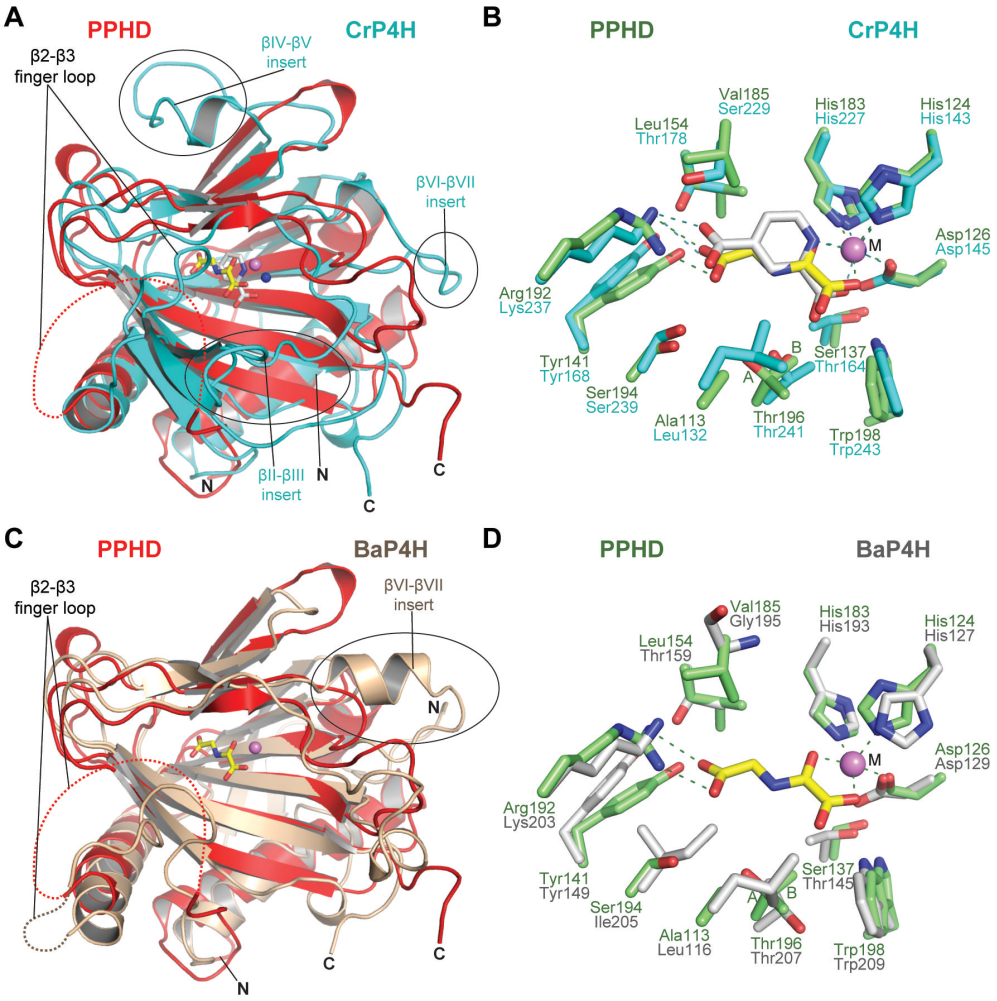

Figure 3.9. Superimpositions of PPHD and CrP4H/BaP4H reveal structural differences indicative of two distinct structural subfamilies. (**A**) Superimposition of the overall structures of PPHD(red):NOG(yellow) and CrP4H(cyan):2,4-PDCA(grey). (**B**) Superimposition of the core DSBH active site residues of PPHD(green):NOG(yellow) and CrP4H(cyan):2,4-PDCA(grey) (2,4-PDCA: 2,4-pyridine dicarboxylate). Mn(II) (pink sphere) is bound to PPHD; Zn(II) (blue sphere) is bound to CrP4H. (**C**) Superimposition of the overall structures of PPHD(red):NOG(yellow) and BaP4H(sand). (**D**) Superimposition of the core DSBH active site residues of PPHD(green):NOG(yellow) and BaP4H(grey). Mn(II) (pink sphere) is bound to PPHD; BaP4H does not contain metal or 2OG mimetic inhibitor in the active site.

The crystallised forms of PPHD and PHD2 contain an α-helix (α1) as the *N*-terminal secondary structure element, yet the first secondary structure elements in the CrP4H and BaP4H structures are 2 β-strands, respectively. Importantly, BaP4H was crystallised in its *apo* (no metal bound) form (*24*), and

additional of metal in the BaP4H metal-binding site may stabilise the DSBH core and so modulate the local secondary structure.

The region corresponding to the disordered β2-β3 finger loop in PPHD and PHD2 is ordered in CrP4H (Figure 3.9*A*), yet is positioned away from the active site in the absence of contacts with other ordered protein, suggesting that ordering of the loop in CrP4H may be due to stabilising contacts with symmetry molecules in the crystal packing. Indeed, closer inspection of the crystal packing in the CrP4H structure reveals that the apex of the β2-β3 finger loop interacts with symmetry molecules; inspection of the two other CrP4H crystal forms (PDB IDs: 2JIJ and 2V4A)(*25*) reveals the β2-β3 finger loop disordered and a lack of similar contacts between the β2-β3 finger loop and symmetry molecules. These observations reveal that the conformational flexibility of the β2-β3 finger loop is likely conserved in the PHDs and CP4Hs, suggesting that the β2-β3 finger loop plays a similar role in substrate recognition in both prolyl-4-hydroxylase subfamilies.

In contrast to the α-helical *C*-terminus of PHD2, the *C*-terminal regions of PPHD (7 residues; 201-207), CrP4H (5 residues; 247-251), and BaP4H (5 residues; 212-216) are all observed to contain loop secondary structure and extend from DSBH strand VIII (Figure 3.9, *A* and *C*).

Overall, analysis of the differences between the PHD/PPHD and CP4H prolyl-4-hydroxylase subfamilies may assist in the assignment of putative prolyl-4-hydroxylases as PHD or CP4H homologues.

3.1.7 Active site comparison of PPHD to PHD2 and collagen prolyl-4-hydroxylases

Many active site residues which are conserved between PPHD and PHD2 are not conserved between PPHD and CrP4H/BaP4H (Figure 3.9, *B* and *D*): $Ala113_{PPHD}/Leu132_{CrP4H}/Leu116_{BaP4H}$, $Leu154_{PPHD}/Thr178_{CrP4H}/Thr159_{BaP4H}$, $Val185_{PPHD}/Ser229_{CrP4H}/Gly195_{BaP4H}$, $Arg192_{PPHD}/Lys237_{CrP4H}/Lys203_{BaP4H}$, and $Ser194_{PPHD}/Ser239_{CrP4H}/Ile205_{BaP4H}$. The lack of conservation of residues in the DSBH core between PPHD/PHD2 and CrP4H/BaP4H suggests that these residues evolved divergently in response to changes in substrate preferences, and their identities are not required for the integrity of the jelly-roll fold.

3.2 The crystal structure of *P. putida* EF-Tu

3.2.1 Crystallisation trials and optimisation

In order to better understand the position of Pro54 on the EF-Tu switch I loop and to provide a foundation for comparison with a PPHD:EF-Tu complex structure, structural studies were pursued on *P. putida* EF-Tu. Purified, full-length EF-Tu was produced and purified as described (see section 2.3.5 and Figure 2.10). Crystallisation trials were pursued in the same manner as for PPHD using multiple commercial crystallisation screens at both 20 and 4 °C – i.e. the JCSG+, PACT Premier, SaltRx, Index, MIDAS, Structure, PEGION and Natrix screens (Molecular Dimensions and Hampton Research)(*8-13*). Mg(II) and GDP were added to increase EF-Tu stability. Initial rhombohedral crystals were observed in the Natrix screen well A3 (Hampton Research) in the presence of 0.1 M MgOAc, 20% MPD and 0.05 M MES pH 5.6 at 4 °C. Successful optimisation was achieved by increasing the drop and reservoir volume (10-fold, 0.4 µL drop to 4.0 µL drop) and through the use of the Additive and Detergent screens

(Hampton Research)(*14-17*); diffraction-quality 250 µm x 150 µm x 150 µm rhombohedral crystals were grown in a final condition consisting of 0.1 M MgOAc, 20% MPD, 0.05 M MES pH 5.6 and 10 mM strontium chloride hexahydrate (Figure 3.10).

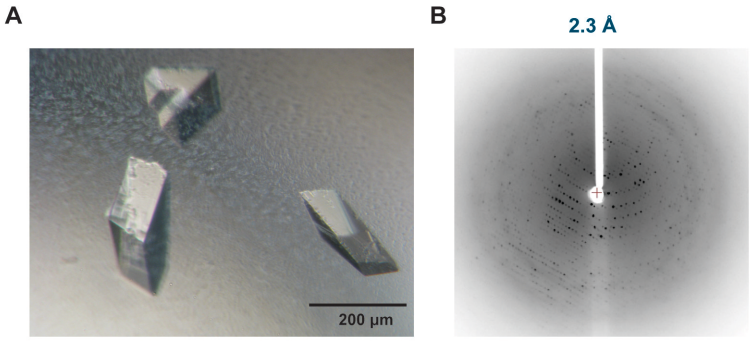

Figure 3.10. Crystallisation of *P. putida* EF-Tu. (**A**) Diffraction quality crystals of *P. putida* EF-Tu and (**B**) diffraction pattern to 2.3 Å.

3.2.2 Data collection and structure solution

A dataset of *P. putida* EF-Tu was collected to 2.3 Å resolution in monoclinic space group *C* 2 and the structure was solved using *E. coli* EF-Tu (PDB ID: 1DG1) as the search model (*27*) using the MR-PHASER (*18*) subroutine of PHENIX (*19*).

3.2.3 Overall structure of P. putida EF-Tu

Consistent with all available structures of EF-Tu, EF-Tu$_{putida}$ contains three distinct domains (Figure 3.11*A*). Mg(II) and GDP are bound to the nucleotide binding site in domain I. *P. putida* EF-Tu and *E. coli* EF-Tu have very similar overall folds (r.m.s.d. 1.5 Å over 353 Cα atoms) and Mg(II) binding sites in their inactive GDP-bound states (Figure 3.11*B*)(*27*). Domains II and III do not have any intrinsic GTP hydrolysis activity, but harbour the binding sites for

several EF-Tu targeting antibiotics, including kirromycin, enacyloxin IIA, and GE2770A (Figure 3.15*A*)(*28-32*). These antibiotics stabilise the GTP-bound conformation of EF-Tu and prevent GTP hydrolysis and concomitant departure of EF-Tu from the ribosomal A site, thus halting bacterial translation (*28, 33*).

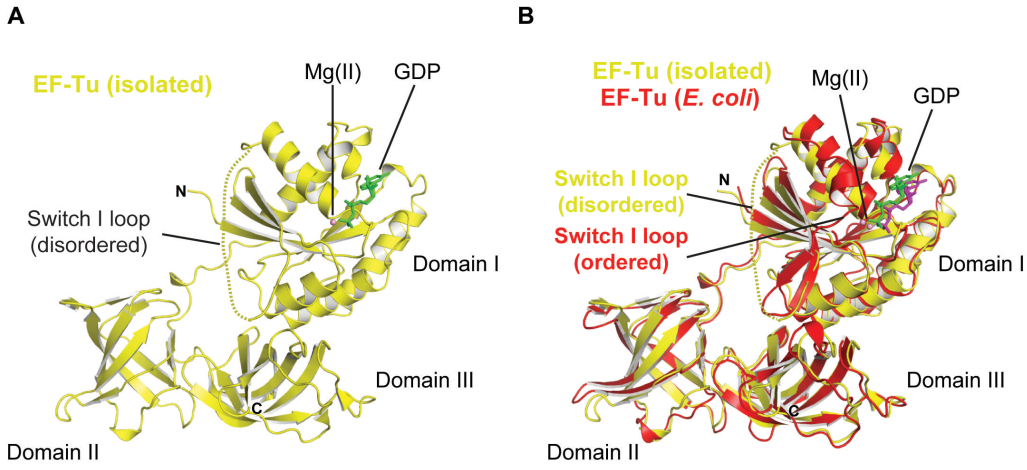

Figure 3.11. The crystal structures of *P. putida* EF-Tu and *E. coli* EF-Tu share similar overall folds. (**A**) View from an overall structure of *P. putida* EF-Tu (yellow) in its GDP-bound conformation with the switch I loop (residues 44-59) disordered. (**B**) Superimposition of *P. putida* EF-Tu (yellow) with *E. coli* EF-Tu (PDB ID: 1DG1)(red)(r.m.s.d. 1.5 Å over 353 Cα atoms). Figure and figure legend are adapted with permission from J.S. Scotti *et al*, Human oxygen sensing may have origins in prokaryotic elongation factor Tu prolyl-hydroxylation. *Proc Nat Acad Sci USA*. In press (2014).

The switch I loop of EF-Tu$_{putida}$ (residues 44-59) is disordered in the crystal structure of *P. putida* EF-Tu (Figure 3.11*A*). This is of interest because unlike the crystallisable overall EF-Tu fold, the ODD regions of HIF-α are, like the switch I loop, (at least in isolation) also disordered. The structure of EF-Tu and the location of the disordered switch I loop in space (in the absence of contacts with other ordered protein), suggests that PPHD-binding may order the switch I loop.

3.3 Purification and crystallisation of a PPHD:EF-Tu protein-protein complex

3.3.1 Purification of an intact PPHD:EF-Tu protein-protein complex

In solution binding studies on PPHD and EF-Tu demonstrated that PPHD stabilises the GDP-bound conformation of EF-Tu and PPHD:EF-Tu complexation would likely be mediated by GDP-bound EF-Tu (for discussion, see section 2.6). A crystal structure of a PPHD:EF-Tu protein-protein complex would have important implications for not only the mechanism of the PPHDs, but also for catalysis by the PHDs and collagen prolyl-4-hydroxylases. Further, a crystal structure of a prolyl-4-hydroxylase in complex with its full-length protein substrate would likely provide insight into hitherto unobserved substrate-enzyme interaction interfaces that may serve as platforms for the development of novel types of prolyl-4-hydroxylase inhibitors.

To date, there are no reported structures for a prolyl-hydroxylase, nor indeed any 2OG dependent oxygenase, in complex with a full-length protein substrate and no structures of EF-Tu in complex with protein/nucleic acid not immediately related to its translational role. To gain insight into the interactions involved in EF-Tu binding and recognition by PPHD, it was desirable to purify and crystallise this complex.

Initial attempts at PPHD:EF-Tu complex formation by mixing PPHD and EF-Tu followed by size exclusion chromatography proved unsuccessful. Therefore, purification of an intact PPHD:EF-Tu protein-protein complex was approached in light of previous results on PPHD:EF-Tu binding in solution and on the successful purification of PPHD-free hydroxylated EF-Tu. Coexpression of PPHD and EF-Tu in a single *E. coli* cell was avoided due to expected PPHD

catalysed hydroxylation of EF-Tu and consequent unlikelihood of complex formation. Further, the attachment of a bulkier affinity tag [typically glutathione *S*-transferase (GST)] to either enzyme was avoided to prevent blocking critical PPHD:EF-Tu interactions. Therefore, the chosen purification strategy began with colysis of two distinct *E. coli* cell pellets, each containing PPHD and EF-Tu produced by overexpression, respectively, both with an *N*-terminal hexahistidine tag. Purification by colysis presented an important potential problem; colysis of PPHD and EF-Tu proteins with an identical affinity tag would not result in 1:1 stoichiometry due to inevitably different levels of protein production. However, an excess of one component was thought to assist in driving the equilibrium of complex formation to completion, especially considering that 1:1 stoichiometry, indicative of ideal binding, is unlikely. Finally, both hexahistidine tagged proteins had already been purified and were known to express well in isolation.

Mg(II) and Mn(II) ions were added to the standard Ni-affinity chromatography buffer during colysis in order to stabilise EF-Tu nucleotide binding and to inhibit PPHD catalysed EF-Tu hydroxylation, respectively. Ni-affinity chromatography was pursued in the same manner as for each individual protein. SDS-PAGE revealed both PPHD and EF-Tu in the eluent. Subsequent size exclusion chromatography in a buffer containing no salt except $MgCl_2$ (to promote PPHD:EF-Tu complex formation and to maximise EF-Tu stability) revealed two significant peaks. SDS-PAGE analysis revealed that the first peak, of higher molecular weight, contained purified PPHD and EF-Tu, whereas the second contained purified PPHD alone (Figure 3.12). The size exclusion chromatogram coupled with SDS-PAGE analysis revealed that purification of a PPHD:EF-Tu complex was successful; more than 30 mg of >99% purified

PPHD:EF-Tu complex could be isolated using this method. Notably, no isolated EF-Tu was observed; all EF-Tu was found to be complexed with PPHD (Figure 3.12).

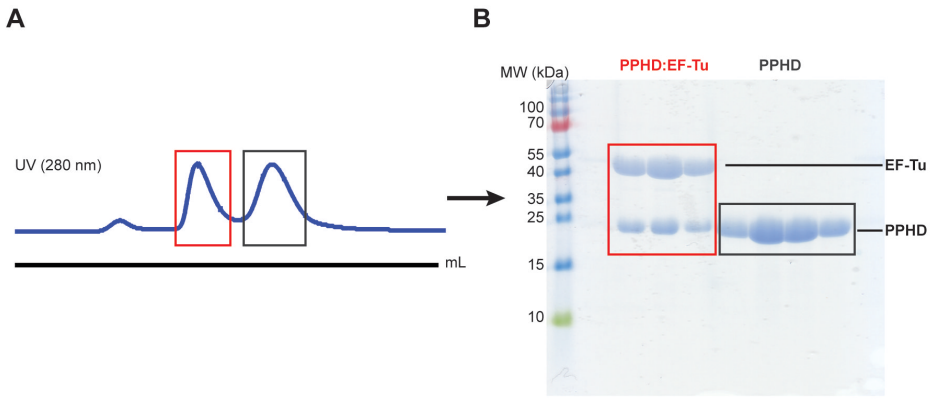

Figure 3.12. Purification of a PPHD:EF-Tu complex. Representative (**A**) size exclusion UV chromatogram and (**B**) associated SDS-PAGE gel reveal a single homogenous peak corresponding to the purified PPHD:EF-Tu complex (red box) and subsequent peak corresponding to purified uncomplexed PPHD (grey box). No peak corresponding to isolated EF-Tu was observed.

3.3.2 Crystallisation and optimisation

Crystallisation trials on the PPHD:EF-Tu complex were begun immediately with freshly purified protein from the column using multiple commercial crystallisation screens at both 20 and 4 °C – i.e. the JCSG+, PACT Premier, SaltRx, Index, MIDAS, Structure, and PEGION screens (Molecular Dimensions and Hampton Research). After two weeks small crystals of haystack morphology appeared in JCSG well B3 at 20 °C [0.1 M bicine pH 9.0, 20% (w/v) PEG 6000] and in JCSG well C4 at 4 °C [0.1 M Na HEPES pH 7.0 and 10% (w/v) PEG 6000]. Crystals from both wells were harvested and screened but no diffraction (indicating either salt or protein crystals) was observed. Therefore, optimisation of both hits was pursued in both small and large scale by varying buffer pH and PEG concentration in an effort to obtain larger, diffraction quality crystals. Despite the inconclusive evidence that those hits were indeed protein

crystals, the observation that no salt was present in either the protein or reservoir solution was promising. Unfortunately, after multiple rounds of optimisation the crystals proved irreproducible.

The purification of the PPHD:EF-Tu complex was then reproduced, but using a fresh cell pellet. The solution studies revealed that the maximal decrease in the rate of EF-Tu GTP hydrolysis was observed in the presence of PPHD, metal(II) ions, and 2OG. Therefore, crystallisation trials were approached in a similar manner as before, except that $MnCl_2$ and NOG were added to the purified complex immediately prior to crystallisation trials to stabilise PPHD and improve PPHD:EF-Tu binding. After 1 week, initial hits (300 x 20 x 20 μM long rods) were observed in JCSG well G2 [0.1 M HEPES pH 7.5, 0.1 M MgCl2, 22% (w/v) polyacrylate 5100] at 20 °C, which were screened in-house and diffracted to 5 Å, indicating that they were protein crystals (Figure 3.13*A*). Interestingly, crystals were only observed in the JCSG screen (Molecular Dimensions) and not in the identical condition in the INDEX screen (Hampton Research). Therefore, crystallisation was sensitive even to the origin of the reagents. Optimisation of the putative PPHD:EF-Tu protein-protein complex crystals began in earnest by varying the buffer, $MgCl_2$, and polyacrylate concentrations. Successful optimisation resulted in larger crystals that were then brought to the synchrotron beam line at Diamond Light Source (Figure 3.13*B*).

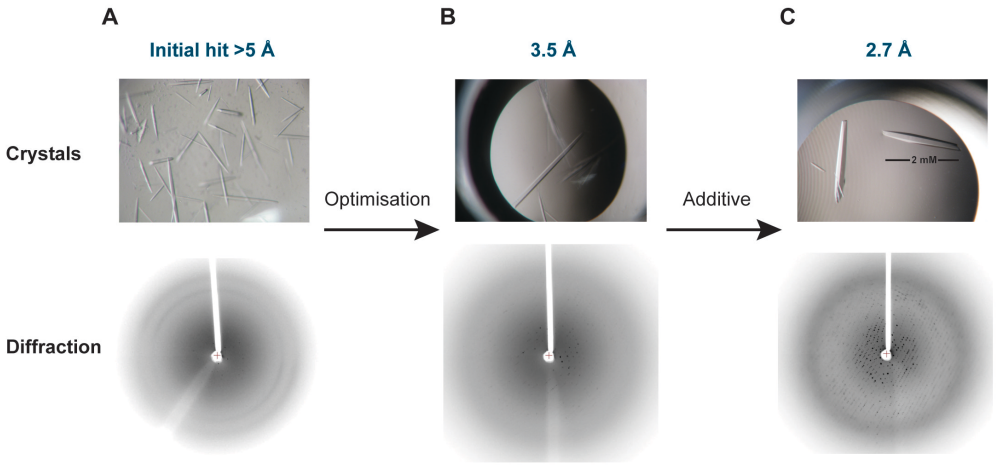

Figure 3.13. Optimisation of PPHD:EF-Tu crystallisation. (**A**) Initial hits in JCSG well G2. (**B**) Optimisation around polyacrylate 5100 concentration. (**C**) Addition of 1 mM GDP resulted in large diffraction quality crystals.

3.3.3 Data collection and structure solution

A complete dataset for the PPHD:EF-Tu crystals was collected to 3.5 Å resolution in the hexagonal space group *P* 3_1 2 1 (Figure 3.13*B*). The structure of the PPHD:EF-Tu protein-protein complex was solved by molecular replacement using the MR-PHASER (*18*) subroutine of PHENIX (*19*) using the isolated PPHD structure (PDB ID: 4J25, this thesis) and EF-Tu (PDB ID: 1DG1)(*27*) as search models. Crystal packing in the hexagonal space group *P* 3_1 2 1 revealed 2 copies of the PPHD:EF-Tu complex in the asymmetric unit (2 copies of PPHD and 2 copies of EF-Tu). Due to the low resolution, structure refinement was not pursued in favour of further crystal optimisation with the goal of obtaining higher resolution data. For the next round of optimisation, crystal drop and reservoir size were increased 100-fold and GDP was added to further stabilise EF-Tu. After one week large 2 mm x 150 µM x 150 µM hexagonal rods were observed (Figure 3.13*C*).

The fully optimised PPHD:EF-Tu complex crystals were brought to the synchrotron and a dataset complete to 2.7 Å resolution was collected in the hexagonal space group $P\ 3_1\ 2\ 1$. The structure was solved using the molecular replacement solution derived from the lower resolution data as a search model and structure refinement was pursued with the highest resolution data. For a full set of data collection and refinement statistics, see Experimental Procedures.

3.4 A crystal structure of a PPHD:EF-Tu protein-protein complex

3.4.1 Overall structure

In the PPHD:EF-Tu protein-protein complex structure (Figure 3.14*A*), EF-Tu is present in its translationally inactive GDP-bound conformation (only EF-Tu:GTP binds aa-tRNA, for details see section 2.4)(*34, 35*), consistent with the results from the solution studies that showed a PPHD-dependent inhibition of EF-Tu GTP hydrolysis. A Mg(II) ion and GDP are present in the EF-Tu domain I nucleotide binding site, as in the isolated EF-Tu structure. PPHD is located adjacent to EF-Tu domain I and sits adjacent to EF-Tu domains II/III, in a similar position to domain I of EF-Tu in its translationally active GTP-bound conformation (PDB ID: 2BVN)(Figure 3.15)(*29*).

The similar positioning of PPHD in the PPHD:EF-Tu complex and EF-Tu domain I in the structure of EF-Tu in its GTP-bound active conformation may explain the mechanism underlying the observed PPHD-dependent inhibition of EF-Tu GTP hydrolysis in solution; PPHD complexation with GDP-bound EF-Tu likely inhibits the ability of EF-Tu to adopt its GTP-bound conformation, and thus its ability to hydrolyse GTP.

Mn(II) and NOG are present in the PPHD active site, further supporting the results from the solution studies, which suggested that maximal PPHD-dependent inhibition of EF-Tu GTP hydrolysis was observed in the presence of metal(II) and 2OG (NOG).

3.4.2 Location of the EF-Tu switch I loop in the PPHD active site

In contrast to the structure of isolated EF-Tu, the majority of the EF-Tu switch I loop is ordered and positioned in the PPHD active site (Figure 3.14*B*; Figure 3.16). The unambiguous positions of most of the EF-Tu switch I loop residue backbone atoms and side chains in the electron density map were further confirmed with an $|F_o - F_c|$ OMIT map contoured to 3.0 σ (Figure 3.14*B*). Only 6 residues of the EF-Tu switch I loop are disordered (residues 43-48) in the complex, most likely due to their presence in space as a flexible tether from the PPHD active site to the rest of EF-Tu domain I and consequent dearth of contacts with other ordered protein.

Superimposition of EF-Tu in the PPHD:EF-Tu complex and isolated *E. coli* EF-Tu:GDP (PDB ID: 1DG1) (78% identity; r.m.s.d. 1.2 Å over 338 Cα atoms)(*27*) with its switch I loop ordered (*E. coli* residues 40-62) reveals little changes in overall fold (78% identity; r.m.s.d. 1.2 Å over 338 Cα atoms), yet major conformational changes in the EF-Tu switch I loop. The different positions of the switch I loop, either adjacent to the domain I nucleotide binding site in isolated EF-Tu or in the PPHD active site in complexed EF-Tu, result in the positions of the proline residues (Pro54 in *P. putida*; Pro53 in *E. coli*) to differ by 22 Å (Figure 3.14*C*). Notably, superimposition of complexed EF-Tu and isolated EF-Tu from *P. putida* with the switch I loop disordered reveal no changes in overall fold (Cα

r.m.s.d. 0.4 Å), with the exception of the ordering of the switch I loop, consistent with the superimpositions with *E. coli* EF-Tu (Figure 3.16).

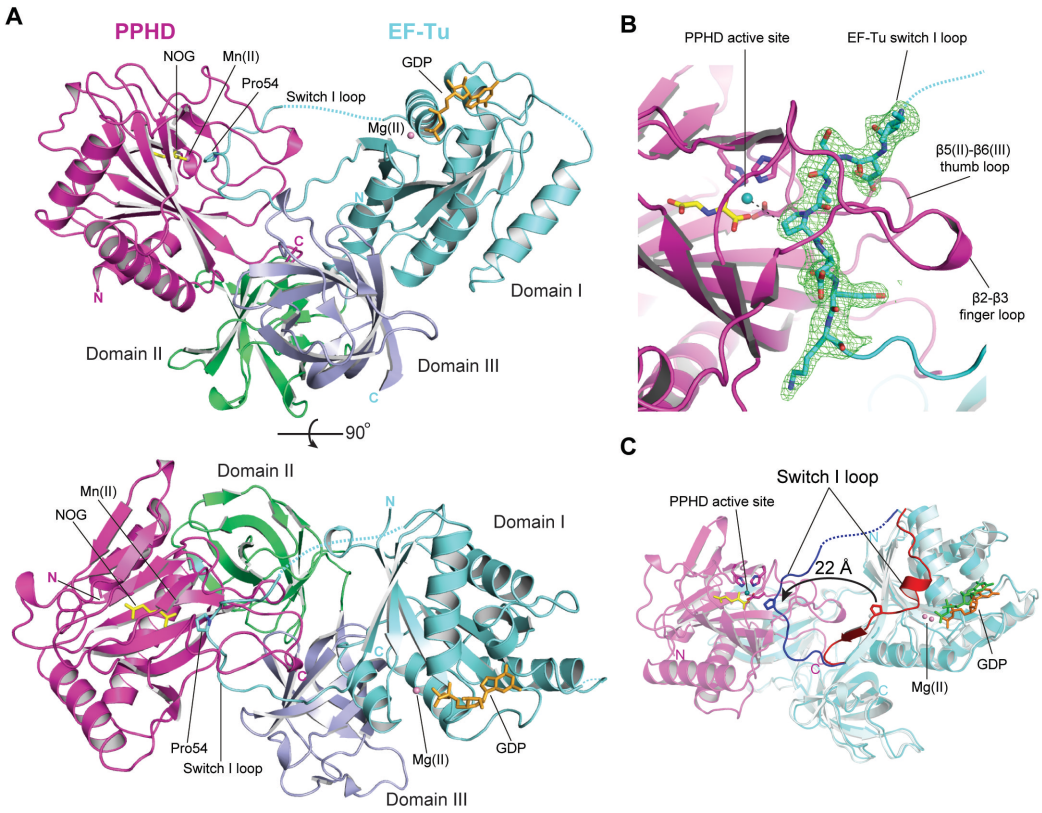

Figure 3.14. PPHD:EF-Tu complex structure. (**A**) Views from a crystal structure of a PPHD(magenta):EF-Tu(cyan) complex reveals EF-Tu in its GDP-bound inactive conformation with its switch I loop present in the active site of PPHD and EF-Tu Pro54 situated for *trans*-4-hydroxylation. (**B**) Electron density OMIT $|mF_o - DF_c|$ map (green mesh) contoured to 3.0 σ of the EF-Tu switch I loop in the PPHD active site. (**C**) Superimposition of *P. putida* EF-Tu from the PPHD:EF-Tu complex with its switch I loop (blue) positioned in the PPHD active site and *E. coli* EF-Tu (PDB ID: 1DG1) with its switch I loop (red) positioned adjacent to the nucleotide binding site reveals a 22 Å distance between Pro54 (Pro53 in *E. coli*) residues. Figure and figure legend are adapted with permission from J.S. Scotti *et al*, Human oxygen sensing may have origins in prokaryotic elongation factor Tu prolyl-hydroxylation. *Proc Nat Acad Sci USA*. In press (2014).

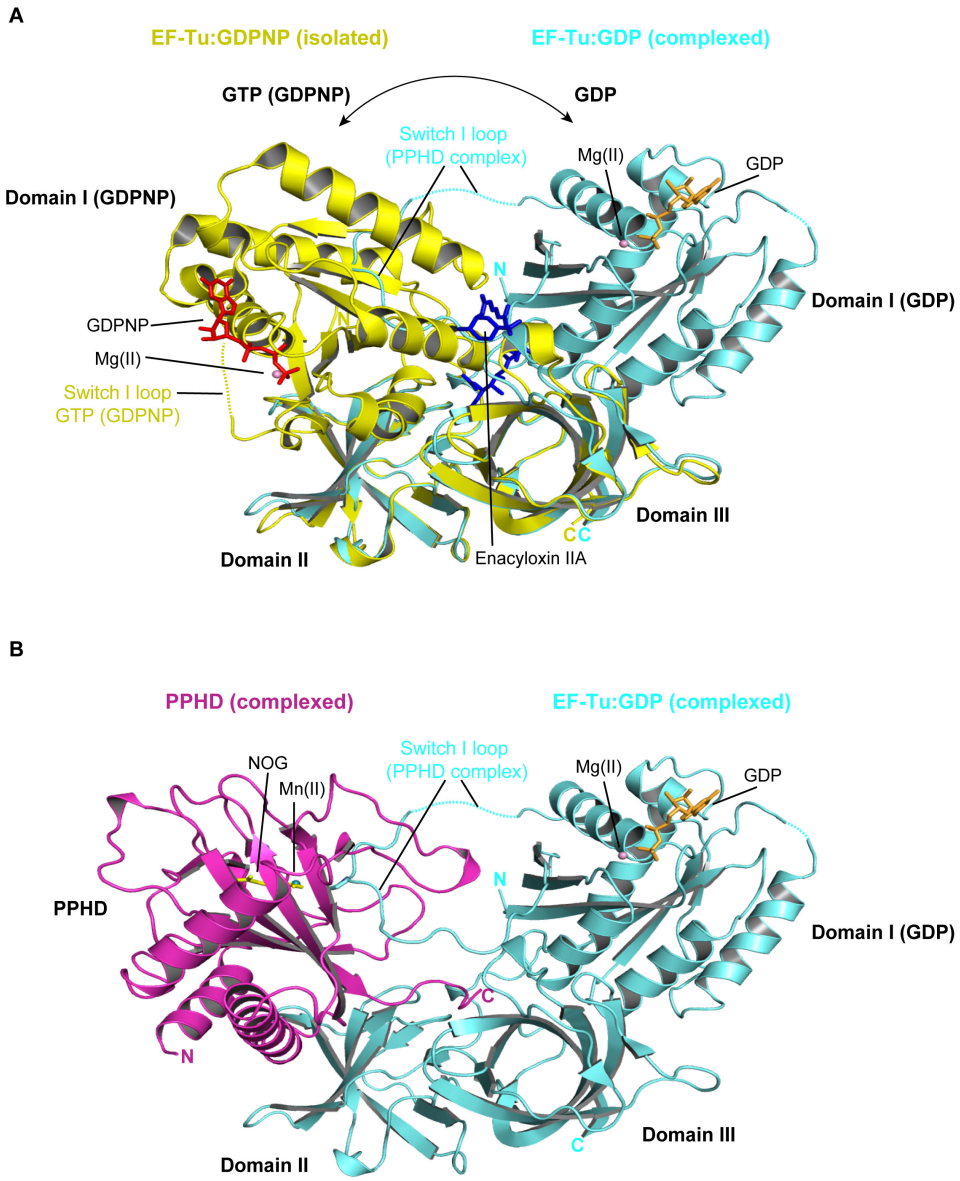

Figure 3.15. In the PPHD:EF-Tu complex, PPHD occupies a similar position relative to EF-Tu as does EF-Tu domain I in its GTP-bound active state. (**A**) Superimposition of domains II and III of *E. coli* EF-Tu (PDB ID: 2BVN)(yellow)(*29*) bound to enacyloxin IIA (blue sticks) and the non-hydrolysable GTP-analogue GDPNP (red) (GDPNP and enacyloxin IIA serve to lock EF-Tu in its GTP-bound conformation) and *P. putida* EF-Tu from the PPHD:EF-Tu complex (r.m.s.d. 0.6 Å)(PPHD not shown) reveals the large rotation in EF-Tu domain I relative to domains II and III from its GDP-bound to GTP-bound states. (**B**) View from the same orientation of the PPHD:EF-Tu complex with PPHD shown (magenta) reveals that PPHD is similarly positioned to domain I of EF-Tu bound to GTP. Figure and figure legend are adapted with permission from J.S. Scotti *et al*, Human oxygen sensing may have origins in prokaryotic elongation factor Tu prolyl-hydroxylation. *Proc Nat Acad Sci USA*. In press (2014).

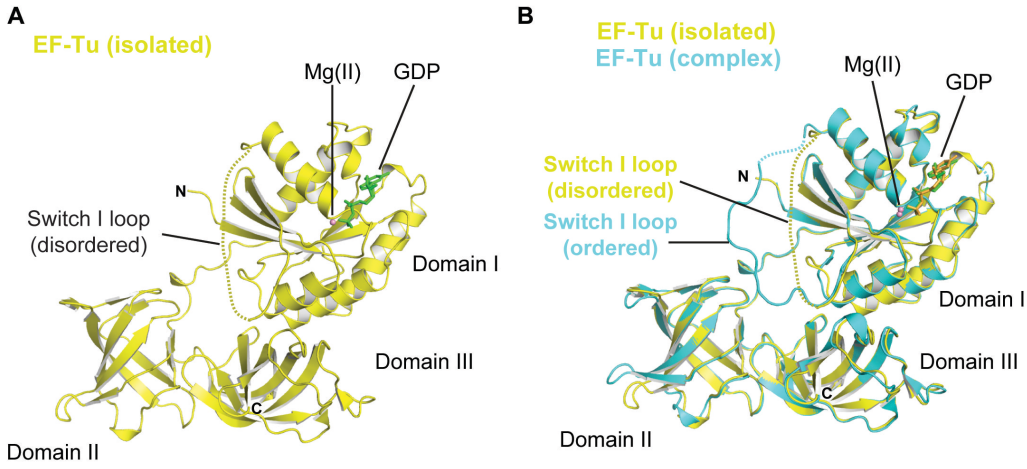

Figure 3.16. View from a crystal structure of isolated *P. putida* EF-Tu and comparison with complexed EF-Tu. (**A**) The structure of *P. putida* EF-Tu:GDP (yellow) reveals a disordered switch I loop (residues 44-59). (**B**) Superimposition of *P. putida* EF-Tu:GDP (yellow) with EF-Tu of the PPHD:EF-Tu complex (cyan) illustrates that the switch I loop is ordered upon complexation with PPHD, yet the overall EF-Tu fold remains consistent with isolated EF-Tu:GDP. Figure and figure legend are adapted with permission from J.S. Scotti *et al*, Human oxygen sensing may have origins in prokaryotic elongation factor Tu prolyl-hydroxylation. *Proc Nat Acad Sci USA*. In press (2014).

3.4.3 Conformational changes in the PPHD β2-β3 finger loop

Conformational changes in both PPHD and EF-Tu observed in the PPHD:EF-Tu complex are not limited to EF-Tu. PPHD also undergoes major conformational changes relative to its isolated state (Figure 3.17). In the PPHD:EF-Tu complex, the PPHD β2-β3 finger loop (24 residues, 51-74), which was observed to be disordered in the isolated structure, is ordered and positioned to sequester the EF-Tu switch I loop entirely within the PPHD active site (Figure 3.17 and Figure 3.19*A*). The second region observed to be disordered in the isolated PPHD structure, which corresponds to the β5(II)-β6(III) thumb loop (7 residues, 128-134), acts in concert with the β2-β3 finger loop to enclose the EF-Tu switch I loop within the PPHD active site (Figure 3.17 and Figure 3.19*A*).

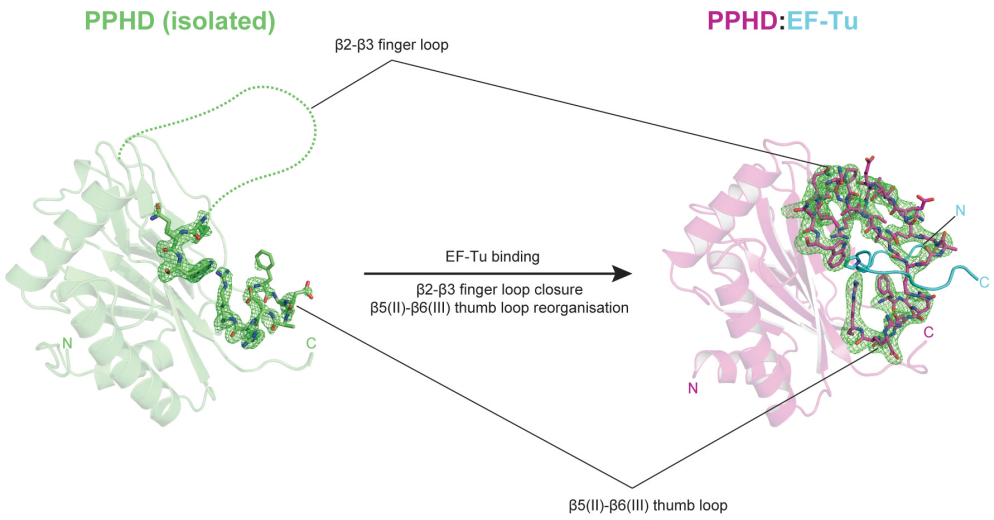

Figure 3.17. EF-Tu binding to PPHD is mediated by large conformational changes in the PPHD β2-β3 finger and β5(II)-β6(III) thumb loops. The electron density OMIT $|mF_o - DF_c|$ map (green mesh) contoured to 3.0 σ of the PPHD β2-β3 finger (residues 51-74) and the β5(II)-β6(III) thumb (residues 128-134) loops are shown. Dashed lined indicates disordered protein (no electron density observed).

The pyrrolidine ring of EF-Tu Pro54 is positioned in the C-4 *endo* conformation, such that the C-4 is positioned 4.3 Å from the Mn(II) [used as a surrogate for Fe(II) for crystallisation] apparently primed for *trans*-4-hydroxylation (Figure 3.19*B*). These observations are in agreement with the stereochemistry of Pro54 hydroxylation by PPHD determined from amino acid analyses (see Chapter 2). Interestingly, there is little variation in the positions of NOG or the residues within the PPHD active site (His124, Asp126, Leu154, His183, Val185, Arg192, Ser194, Thr196, Trp198) upon substrate binding (Figure 3.19*C*), with the more robust conformational changes stemming from movements in the β2-β3 finger and β5(II)-β6(III) thumb loop.

The β2-β3 finger loop of PPHD is composed of mostly flexible amino acids including 4 glycine (Gly54, Gly56, Gly58, Gly69) and 2 alanine (Ala53 and Ala59) residues, which may explain its disorder in the absence of substrate. The β2-β3

finger loop of PPHD forms multiple direct electrostatic interactions with EF-Tu in the active site (Table 3.18).

Table 3.18. Electrostatic interactions between the PPHD β2-β3 finger loop and EF-Tu.

β2-β3 finger loop (residues 51-74)			
PPHD residue	**EF-Tu residue**	**Distance (Å)**	**Interaction type**
Gly54 backbone oxygen	Glu55 backbone nitrogen	3.2	Hydrogen bond
Gly54 backbone nitrogen	Glu55 carboxylate	3.0	Hydrogen bond
Gly56 backbone nitrogen	Ala53 backbone oxygen	2.9	Hydrogen bond
Trp74 indole nitrogen	Glu55 carboxylate	3.4	Hydrogen bond

In the complex, the apex of the β2-β3 finger loop folds into a 3_{10} helix (residues 58-60), positioning a solitary arginine residue (Arg57), flanked by two glycine residues, to form a salt bridge with an aspartate residue (Asp130) of the β5(II)-β6(III) thumb loop, thereby 'closing' the finger and thumb and forming a channel through which the EF-Tu switch I loop is threaded (Figure 3.17 and Figure 3.19*A*).